Methods to induce polarity in constructed neuronal networks

Von der Fakultät für Mathematik, Informatik und Naturwissenschaften der Rheinisch-Westfälischen Technischen Hochschule Aachen zur Erlangung des akademischen Grades einer Doktorin der Naturwissenschaften genehmigte Dissertation

vorgelegt von

Diplom-Biologin

Tanja Decker

aus Telgte

Berichter: Universitätsprofessor Dr. Andreas Offenhäusser

Universitätsprofessor Dr. Hermann Wagner

Tag der mündlichen Prüfung: 16.05.2008

Diese Dissertation ist auf den Internetseiten der Hochschulbibliothek online verfügbar.

Round about the cauldron go;
In the poison'd entrails throw.
Toad, that under cold stone
Days and nights has thirty-one
Swelter'd venom sleeping got,
Boil thou first i' the charmed pot.

Double, double toil and trouble;
Fire burn, and cauldron bubble.

Fillet of a fenny snake,
In the cauldron boil and bake;
Eye of newt and toe of frog,
Wool of bat and tongue of dog,
Adder's fork and blind-worm's sting,
Lizard's leg and owlet's wing,
For a charm of powerful trouble,
Like a hell-broth boil and bubble.

Double, double toil and trouble;
Fire burn and cauldron bubble.

Scale of dragon, tooth of wolf,
Witches' mummy, maw and gulf
Of the ravin'd salt-sea shark,
Root of hemlock digg'd i' the dark,
Liver of blaspheming Jew,
Gall of goat, and slips of yew
Silver'd in the moon's eclipse,
Nose of Turk and Tartar's lips,
Finger of birth-strangled babe
Ditch-deliver'd by a drab,
Make the gruel thick and slab:
Add thereto a tiger's chaudron,
For the ingredients of our cauldron.

Double, double toil and trouble;
Fire burn and cauldron bubble.

Cool it with a baboon's blood,
Then the charm is firm and good.

Mac Beth, Act 4, Scene 1, William Shakespeare

Abstract

This work focused on the control of neuronal polarity in geometrical patterned neuronal networks. Two different approaches were taken in order to direct polarity within a neuronal network. The first strategy was to chemically pattern two proteins with distinct effects on neurite growth. Aligned two-step microcontact printing (2-step μCP) was developed for accurate aligned printing of two complementary protein patterns under visual control. Netrin-1, laminin-1 and ECM-gel were chosen as axon-guiding proteins, while poly-D-lysine (PDL) was printed as neutral protein. The protein transfer during 2-step μCP and the effect of the second printed pattern on the primary ones was characterized by fluorescence microscopy, ellipsometry and atomic force microscopy (AFM) using manual 2-step μCP substrates. Each method showed, that the first printed pattern consisting of polylysine was not blurred or removed by printing of the second pattern. Moreover, the transfer of ECM-gel, laminin-1 and netrin-1 onto the substrates was inhomogeneous, characterized by a lower protein transfer at areas with preprinted polylysine. A highly irregular protein surface was observed for all proteins by ellipsometry and AFM measurements. Additionally, AFM measurements showed a mesh-like structure in some areas of the transferred laminin pattern. Cell culture experiments on the manual 2-step μCP substrates showed that E18 rat striatal neurons cultured on ECM/PDL substrates and on laminin/PDL had a similar good morphology and viability as neurons cultured on PECM-grids, while on netrin/PDL substrates the amount of dead cells was increased. Electrophysiological measurements showed that E18 rat cortical neurons cultured on the aligned ECM/PDL substrates possessed similar electrophysiological properties as neurons cultured on PECM grid patterns except for the AP-frequency, which was significantly lower in comparison to the neurons on the PECM substrates. Further patch-clamp experiments are required in order to test if neuronal growth on aligned 2-step μCP substrates is guided by the complementary patterns of axon-guiding and neutral proteins.

As second strategy for the induction of a defined polarity in neuronal networks the reconstruction of the natural polarity between cortex and striatum in cell culture was chosen. For coculture cell culture of E18 rat striatal neurons was established at the Institute for Bio-and Nanosystems based on the already existing cortical cell culture. About 70 % of the cells could be identified as striatal neurons by

expressing striatum-specific G-protein coupled receptor-RNA-transcripts. The striatal neurons in monoculture had similar electrophysiological properties as described in literature, except for a significantly higher membrane time constant. For coculture a microstructured coculture chamber was reversibly sealed on glass substrates using activation by UV/ozone plasma and subsequent chemical hydrophilization by sodium hydroxide. Cell culture experiments in the coculture chambers showed, that 25 % of the chambers contained viable cortical and striatal neurons at DIV 3. By removing the coculture chamber at DIV 3 and increasing the cell density, neurons in 14 % of these chambers could survive up to DIV 11. Electrophysiological analysis at DIV 10-11 showed no significant differences between the electrophysiological properties of the cocultured striatal neurons in comparison to striatal neurons in monocultures. The cocultured cortical neurons showed a significant lower FLHM compared to cortical monocultures on PECM-grids. By double patch-clamp measurements a synapse between two cocultured striatal neurons could be measured, confirming the ability of the cocultured neurons to form synaptic contacts. Further patch-clamp experiments are required in order to test if the natural polarity between cortex and striatum could be reconstructed in cell culture.

Zusammenfassung

Diese Arbeit war auf die Kontrolle neuronaler Polarität in geometrisch strukturierten neuronalen Netzwerken fokussiert. Dabei wurden zwei unterschiedliche Ansätze verfolgt: Die erste Strategie war die chemische Strukturierung von zwei Proteinen mit gegensätzlichen Effekten auf das Neuritenwachstum. „Aligned two-step microcontact printing“ (aligned 2-step µCP) wurde für das genau aufeinander ausgerichtete Drucken von zwei komplementären Proteinmustern unter optischer Kontrolle entwickelt. Netrin-1, Laminin-1 und ECM-Gel wurden als Axon-leitende Proteine ausgewählt, während Poly-D-Lysine als neutrales Protein gedruckt wurde. Der Proteinübertrag während des 2-step µCP wurde durch Fluoreszenzmikroskopie, Ellipsometrie und Rasterkraftmikroskopie (atomic force microscopy, AFM) von manuell gestempelten 2-step µCP Substraten charakterisiert. Dabei zeigte sich, daß das zuerst gestempelte Polylysine-Muster durch das Drucken des zweiten Proteinmusters weder verwischt noch entfernt wurde. Der Übertrag von Netrin-1, Laminin-1 und ECM-Gel auf die Substrate war inhomogen, was durch einen geringeren Proteinübertrag auf die Gebiete mit vorgestempelten Polylysine charakterisiert wurde. Bei Ellipsometrie- und AFM-Messungen wiesen alle Proteine eine sehr unregelmäßige Oberfäche auf. Ausserdem wurde bei AFM-Messungen eine netzähnliche Strukturierung in einigen Gebieten des gedruckten Laminin-1 beobachtet. In Zellkulturexperimenten auf manuell gestempelten 2-step µCP Substraten stellte sich heraus, das die Morphologie von striatalen E18 Nervenzellen aus der Ratte auf ECM/PDL und Laminin/PDL ähnlich gut wie auf PECM-Gittern war. Im Vergleich dazu war der Anteil toter Zellen auf den Netrin/PDL Substraten erhöht. Bei elektrophysiologischen Messungen zeigten kortikale E18 Nervenzellen aus der Ratte, die auf ECM/PDL Substraten kultiviert wurden, ähnliche elektrophysiologische Eigenschaften wie kortikale Nervenzellen auf PECM-Gittern. Allerdings war die AP-Frequenz der Nervenzellen auf ECM/PDL im Vergleich zu den Kontrollen signifikant niedriger. Weitere Patch-Clamp-Experimente sind notwendig, um zu testen, ob das Wachstum von Nervenzellen auf aligned 2-step µCP Substraten durch die komplementären Muster von Axon-leitenden und neutralen Proteinen gesteuert wird.

Die zweite Strategie zur Induktion einer gerichteten Polarität in neuralen Netzwerken beinhaltete die Rekonstruktion einer natürlichen Polarität zwischen

Kortex und Striatum in der Zellkultur. Für die Kokultur wurde die Kultur von striatalen E18 Nervenzellen aus der Ratte ausgehend von der bereits existierenden kortikalen Zellkultur am Institut für Bio- und Nanosysteme etabliert. Etwa 70 % der Nervenzellen expremierten m-RNA-Transkripte eines Striatum-spezifischen G-protein gekoppelten Rezeptors und konnten so als striatale Nervenzellen identifiziert werden. Abgesehen von einer signifikant höheren Membranzeitkonstanten ähnelten die elektrophysiologischen Eigenschaften der striatalen Nervenzellen in Monokultur den in der Literatur angegebenen Werten. In der Kokultur ermöglichten eine Oberflächenaktivierung durch UV/Ozone-Plasma und eine anschließende chemische Hydrophilisierung die reversible Bindung einer mikrostrukturierten Kokulturkammer an Glas-Substrate. In Zellkulturexperimenten enthielten 25 % der Kokulturkammern nach 3 Tagen in Kultur vitale striatale und kortikale Nervenzellen. Durch das Entfernen der Kokulturkammern an Tag 3 und die Erhöhung der Zelldichte konnten Nervenzellen in 14 % dieser Kammern 11 Tage lang kultiviert werden. Bei elektrophysiologischen Messungen an Tag 10-11 in Kultur zeigten die elektrophysiologischen Eigenschaften der kokultivierten striatalen Nervenzellen keine signifikanten Unterschiede im Vergleich zu den Eigenschaften der striatalen Nervenzellen in Monokultur. Die kokultivierten kortikalen Nervenzellen hatten eine signifikant niedrigere halb-maximale AP-Breite im Vergleich zu kortikalen Nervenzellen auf PECM-Gittern in Monokultur. Durch Doppel-Patch-Clamp-Messungen konnte eine Synapse zwischen zwei striatalen Nervenzellen in der Kokultur gemessen werden. Dies bestätigt die Fähigkeit der kokultivierten Nervenzellen, synaptische Kontakte auszubilden. Weitere Patch-Clamp-Experimente sind erforderlich, um zu testen, ob die natürliche Polarität zwischen Kortex und Striatum in der Zellkultur rekonstruiert wurde.

Table of contents

1. Introduction 7

1.1 Chemical patterning of proteins 8
1.2 Reconstruction of a natural polarity 11
1.3 Aim of this work 13

2. The mammalian nervous system 14

2.1 Glial cells 14
2.2 Neurons 16
2.2.1 Neuronal Polarity 17
2.2.1.1 Axonguiding and development of neuronal networks 17
2.2.2 Polarity in the CNS 23
2.2.2.1 The corticostriatal pathway 23
2.3 Electrophysiological properties of neurons 26
2.3.1 Resting potential 26
2.3.2 Action potential 28
2.3.3 Synapses 31
2.3.3.1 Electrical synapses 31
2.3.3.2 Chemical synapses 32
2.3.3.3 Synaptic plasticity 34

3. Materials and methods 36

3.1 Microcontact printing 36
3.1.1 Waferstructures 39
3.2 Production and sealing of the microstructured coculture chamber 42
3.3 Cell culture 44
3.3.1 Preparation of substrates 44
3.3.2 Cortical cell culture 45
3.3.3 Striatal cell culture 47
3.4 Immunofluorescence 48
3.5 Electrophysiologal measurements in patterned neuronal cell culture . 50
3.5.1 Patch-clamp technique 50

3.5.2 Experimental set-up for patch-clamp experiments 53
3.5.2.1 Procedure for Double patch-clamp measurements 55
3.5.2.2 Membrane time constant tau 57
3.5.2.3 Current density / voltage relations 58
3.5.2.4 Synaptic delay 58
3.5.2.5 Patch solutions 60
3.6 Ellipsometry 61
3.7 Atomic force microscopy 63

4. Two-step microcontact printing for directed growth of neurons 66

4.1 Manual two-step microcontact printing 67
4.1.1 Improved printing of hydrophilic protein “inks” with low viscosity 68
4.1.2 Analysis of pattern transfer by fluorescence microscopy 70
4.1.3 Characterization of substrates with ellipsometry and with atomic force microscopy 72
4.1.3.1 Quantification of ECM/PDL; laminin/PDL and netrin-1/PDL protein thickness with the ellipsometer 72
4.1.3.2 Quantification of protein homogenity of ECM/PDL, laminin/PDL and netrin-1/PDL patterns by atomic force microscopy 81
4.1.4 Comparison of ellipsometer- and AFM-results 84
4.1.5 Cell culture on manual two-step microcontact printing substrates 85
4.2 Aligned two-step microcontact printing with the Fineplacer 87
4.2.1 Cell culture on aligned two-step microcontact printing substrates 91
4.2.2 Electrophysiology on aligned two-step microcontact printing substrates 92

5. Coculture system 93

5.1 Mechanical coculture 94
5.1.1 Striatal cell culture 94
5.1.2 Mechanical coculture system 98
5.2 Microstructured coculture chamber 101
5.2.1 Sealing of the microstructured coculture chamber 102
5.2.2 Cell culture in the microstructured coculture chamber 104
5.2.3 Electrophysiology of cocultured neurons 109

6. Discussion 111

6.1 Two-step microcontact printing 111
6.2 Coculture system 116

7. Summary 121

8. Outlook 124

9. Literature 126

10. Appendix 137

10.1 List of materials and devices 137
10.2 List of figures 141
10.3 List of tables 143
10.4 List of abbreviations 144
10.5 Publications 146
10.6 Curriculum vitae 147
10.7 Danksagung 149

1. Introduction

The greatest challenge of neural science is to understand how the brain encodes complex human behaviour like moving, thinking and learning. The human brain contains about 10^{11} individual neurons which possess the same basic architecture. Complex behaviours depend widely on the formation and activity of precise networks between individual neurons. These networks detect, store and transmit information.

Information processing in the brain can be analyzed by various *in vivo* imaging techniques such as functional magnetic resonance or positron emission tomography, allowing to monitor brain activities as they occur (Levy *et al.*, 1997; Abdullaev *et al.*, 1998; Yoo *et al*., 2002). Extracellular recording electrodes enable the recording of small groups of neurons in freely moving rats (Bhalla *et al.,* 1997; Chang *et al*., 1998). The spatial resolution of such methods is too low to investigate the contribution of single neurons to the network activity. The use of sharp microelectrodes in acute brain slices (Calabresi *et al*., 2001) and in cocultures of slices obtained from adjacent brain areas (Plenz *et al*., 1996a; 1996b) enables the analysis of single neurons, but still cannot exclude unknown interference from other areas within the slice.

Another approach to analyze signal processing in neuronal networks is the culture of dissociated neurons derived from a certain brain area, e.g. cortex or hippocampus. These neurons formed randomly organized functional networks and electrical signals from single neurons and synapses can be obtained in the network (Dichter *et al.*, 1978; Dichter *et al.*, 1983; Laiwand *et al*., 1992). In multiple whole cell recordings from such networks, long term depression (Fitzsimonds *et al.*, 1997) as well as long term potentiation (Tao *et al*., 2000) can be investigated. Such studies allow a deeper understanding of network behaviour and the development of correlated activity patterns. Nevertheless, these randomly organized networks are still too complex to investigate single synapses in a precisely controlled environment.

The next step towards artificially designed neuronal networks with less complexity is the culture of dissociated neurons on geometrical patterned substrates (Wheeler *et al.,* 1999; Scholl *et al.*, 2000). The geometrical pattern and the low amount of

neighboured neurons allows investigation of signal transduction between two synaptically connected neurons nearly without interfering influence from other neurons. Based on previous findings on rat cortical neurons, inherent features of neuronal behaviour appear to be undisturbed by patterned growth (Vogt *et al.*, 2003; 2005a, 2005b). In addition, protein patterns printed on multi-electrode-arrays (MEAs) and field-effect-transistors (FETs) enable the growth of small neuronal networks on extracellular recording devices which allows noninvasive signal recording (Lauer *et al.* 2001; Cohen *et al.*, 2004; James *et al.*, 2004). Except for the geometry, these neuronal networks are still randomly organized. It is not possible to stimulate and record synapses within these networks without any interfering signals from surrounding neurons. For more detailed information about the impact of different connectivity patterns on network behaviour it is of main interest to control the direction of signal processing (polarity) and the type of synapses (excitatory/ inhibitory) within the neuronal network. This control also enables the determination of single synapse behaviour due to defined electrical stimuli without random inputs from other neurons. Moreover, the interpretation of results gathered from a defined network is more reliable than from a randomly organized neuronal network.

In this work, two different approaches were taken in order to induce directed polarity within a neuronal network. The first strategy was to chemically pattern two proteins with distinct effects on neurite growth. As second strategy, the reconstruction of a natural polarity *in vitro* was chosen.

1.1 Chemical patterning of proteins

Dotti *et al.* (1988) used primary rat hippocampal neurons to study neuronal polarity in cell culture. After plating hippocampal neurons undergo maturation and develop a single axon and several shorter dendrites within 7 days *in vitro* (DIV). The polarization of cultured neurons in the uniform environment of a cell culture dish shows that axonal fate is specified by intrinsic factors (Dotti *et al.*, 1988). On the other hand extracellular guiding cues play a crucial role in axon formation *in vivo* and *in vitro* (Song *et al.*, 2001; Dickson, 2002). Moreover, these extracellular guiding cues direct growing axons to their targets either by attraction or repulsion

(Song *et al.*, 2001). Short-range guidance is mediated by proteins of the extracellular matrix or within the cell membrane of neighboured cells (Kandel *et al.*, 2000). The axon can also navigate along gradients of cell surface molecules or of secreted soluble molecules by chemotaxis (Kandel *et al.*, 2000). In cell culture these gradients can be mimiced by embedding a brain explant which secrets axon-guiding proteins and cortical explants in a hydrogel (Metin *et al.*, 1997; Richards *et al.*, 1997). An alternative method is a spatially separated coculture of dissociated neurons which express axon-guiding cues and cortical tissue explants, both embedded in a hydrogel (Metin *et al.*, 1997). However, hydrogel embedding of neurons and brain explants does not allow patch-clamp measurements. Instead, intracellular recordings require the production of an immobilized protein gradient on glass. For the production of such a gradient McKenna *et al.* (1988) filled molten agarose into a chamber consisting of two glass coverslips and a U-shaped silicon gasket. After cooling a laminin solution was layered on top of the agarose gel. Laminin diffused into the agarose layer and simultaneously adsorbed to the glass coverslips, thereby forming an immobilized laminin gradient. A more defined protein gradient can be produced by using microfluidic channels: These microfluidic channels generate immobilized protein gradients in stripes of 45 µm width which consist of a pattern of parallel stripes with different concentrations (Dertinger *et al.*, 2001; Jiang *et al*., 2005). The protein was attached on glass either by direct physical adsorption or by covalent bonding of biotinylated proteins on previously patterned avidin-gradients (Dertinger *et al.*, 2001; Jiang *et al*., 2005). Although this method allows axon guiding, the large stripe width of 45 µm does not allow a precise geometrical control of neurite growth. Grid patterns of laminin, ECM or polylysine with a line width of 2 µm or 4 µm enable this geometrical control but do not induce a directed polarity within a patterned neuronal network (Vogt, 2003a; Vogt *et al*., 2005a). Similar results were obtained on partially interrupted grid patterns (Vogt *et al*., 2004; fig. 1-1). The design and development of these patterns based on the assumption, that the longest neurite matures into an axon (Dotti *et al*., 1988). After attaching of neurons on the nodes of the pattern, the neurite outgrowth should be favoured on the continuous protein line, while the growth in the other directions is constrained due to the interruptions in the protein lines, resulting in a specific neuronal polarity in one direction.

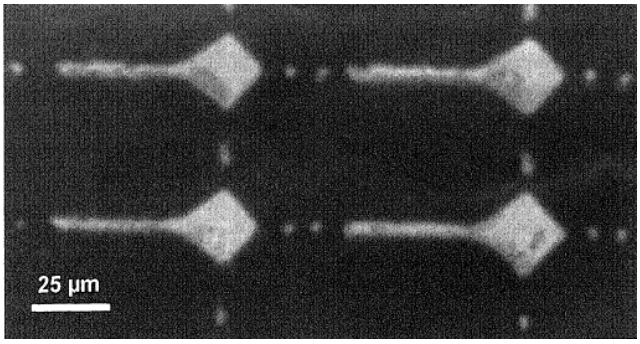


Fig. 1-1: Fluorescence image of a partially interrupted grid pattern consisting of PECM (mixture of polylysine (10 µg/ml) and ECM (8-12 µg/ml). The protein solution was mixed with 10 µg/ml sulforhodamine for visualization (from Vogt *et al.*, 2004).

For the chemical patterning of two proteins with distinct effects on neurite growth, several proteins were selected due to their axon-guiding properties *in vivo* and *in vitro*: Laminin is a kationic glycoprotein and part of the extracellular matrix (Bruch *et al.*, 1989; Chen *et al*., 1998). In an *in vitro* assay of poly-L-lysine stripes, alternating with stripes of either laminin or neuron-glia cell adhesion molecule (NgCAM), hippocampal neurons preferentially formed axons on contact with laminin and NgCAM stripes (Esch *et al*., 1999). Moreover, if immature neurites contacted laminin coated beads, the neurite which touched the bead first developed rapidly into an axon (Menager *et al*., 2004). Dertinger *et al.* (2002) showed that rat hippocampal neurons grow along a laminin gradient towards increasing laminin concentrations, while Matzuzawa *et al.* (1998) observed a directional axon outgrowth of rat hippocampal neurons cultured on lines of a decapeptide (RDIAEIIKDI) derived from the neurite outgrowth domain of the γ1 chain of mouse laminin-1. This directional axon outgrowth did not require a molecular gradient.

Netrins are a class of soluble axon-guiding proteins, which are homologous to the γ1-chain of laminin-1 (Tessier-Lavigne *et al*., 1988). They have been shown to be secreted by the floor plate cells in the developing spinal cord of mice and to be involved in guidance of the commissural axons towards the ventral midline (Tessier-Lavigne *et al*., 1988; Serafini *et al*., 1994; Tessier-Lavigne *et al.*, 1996). In explant cocultures netrin-1 has been demonstrated to be an axon-guiding cue for cortical neurons (Metin *et al.*, 1997; Richards *et al*., 1997).

As third approach for axon-guiding ECM-gel (ECM) was chosen. ECM is a mixture of extracellular matrix proteins derived from a mouse sarcoma, which contains mainly laminin, but also other components as collagen type IV, heparan sulfate proteoglycan, entactin and other minor components (distributors description). Due to the high laminin content (60%) it may also act as axon-guiding cue.
Polylysine was selected for chemical patterning in order to achieve a contrast to the axon-guiding proteins. It is a kationic protein and commonly used for coating of substrates in neuronal cell culture in either L-or D-conformation with a molecular weight > 30 kDa (Jacobson *et al.*, 1977). Although polylysine promotes cell attachment and neuronal outgrowth, it seems to be neutral and possesses no axon-guiding effects (Oliva *et al.*, 2003).

1.2 Reconstruction of a natural polarity

The central nervous system receives information through several periphal sensory systems. Sensory afferents in the periphery project to one or several regions in the spinal cord, brainstem and thalamus. The thalamus transmits this information to the primary sensory cortex from which the information is further projected to other areas of the cerebral cortex (Kandel *et al.*, 2000). Informations are conveyed from one brain area to another by axon bundles which project together in a so-called pathway to the next stage of signal transmission. These pathways often cross the midline of the nervous system (Kandel *et al.*, 2000). The axons forming these pathways are guided to their defined target by different guiding mechanisms (see 1.1 and 2.2.1.1). Moreover, these pathways possess a determined polarity (Kandel *et al.*, 2000).
In this work a coculture system was tested for the reconstruction of a natural polarity *in vitro*. The corticostriatal pathway was chosen, because it has a defined polarity (Graybiel *et al.*, 1994; Wickens *et al.*, 2003) and both brain areas have already developed to a size sufficient for preparation in 18 days old (E18) rat embryos (Altman et al., 1994). While cortical afferents provide direct input to the striatum, signalling from the striatum to the cortex occurs only indirect via the thalamus (McGeorge *et al.*, 1989). This natural polarity between cortex and striatum was also observed *in vitro* in organotypic cocultures of striatal and cortical

brainslices (Plenz *et al.*, 1996a; 1996b). Segal *et al.* (2003) observed no spontaneous excitatory postsynaptic currents (EPSCs) in a pure rat striatal cell culture, while EPSCs were recorded from striatal neurons cocultured with mouse cortical neurons was provided. The authors interpreted this result as an effect of cortical input to striatal neurons. Unfortunately they did not investigate, if there was also input from striatal to cortical neurons. For coculturing of dissociated striatal and cortical neurons Segal *et al.* (2003) combined cultures of mouse and rat neurons. They plated green-fluorescence protein expressing cortical cells derived from postnatal (P1) mice onto 3 day-old striatal cultures prepared from E19 rats. The coculture of immature neonatal striatal neurons with more mature P1 cortical neurons may alter the electrophysiological properties of the striatal neurons (Snyder-Keller *et al.*, 2004).

The reconstruction of the *in vivo* situation of cortex and striatum in cell culture and the analysis of functional polarity between cortical and striatal neurons by patch-clamp experiments requires a spatial separation of both neuron types. Taylor *et al.* (2003) developed a microfluidic multicompartment system for the spatial separation of neurons. It is possible to culture rat cortical neurons neurons up to 6 days in this coculture chamber (Rhee *et al.*, 2005). Due to the irreversible seal the coculture chamber cannot be removed, thereby this system would not be appropriate for subsequent analysis by patch-clamp measurements. Furthermore, in a cell culture of dissociated neurons synapse formation is observed earliest on DIV 7 (Dotti *et al*., 1988) and nascent synapses continue to mature for several days up to 2 weeks (Garner *et al.*, 2006). Since during this time synapses become more stable (Garner *et al*., 2006), the dissociated neurons in coculture should be cultured at least up to DIV 10 before analyzing their electrophysiological properties.

1.3 Aim of this work

This work focuses on the control of neuronal polarity. Partially interrupted grid patterns of PECM (fig. 1-1) did not induce a specific polarity within geometrical patterned neuronal networks (Vogt *et al.*, 2004). In this work the contrast between axon-guiding and neutral regions should be achieved not simply by interrupting a grid pattern but by printing complementary patterns of proteins with different effects on axon outgrowth. Therefore, a printing technique has to be developed, which allows accurate aligned printing of two complementary protein patterns under visual control (aligned two-step microcontact printing). Because the protein transfer of low-viscosity hydrophilic proteins like poly-D-lysine with microcontact printing was not proved as satisfactory as the transfer of high-viscosity proteins like ECM (Vogt, 2003a), different pretreatments of the stamp surface should be tested in order to achieve a similar transfer for each protein by microcontact printing. The protein transfer during two-step microcontact printing and the effect of the second printed pattern on the primary patterns are characterized using ellipsometry, atomic force microscopy and fluorescence microscopy. The functionality of the previously described aligned two-step microcontact printing patterns is tested in cell culture and by patch-clamp experiments on the cultured neurons.

In parallel a coculture system for the reconstruction of the natural polarity between cortical and striatal neurons in cell culture is tested as second approach. In order to achieve a physiological synapse formation, neurons from the same species and the same developmental age are used for the coculture of striatal and cortical neurons. In this work, a coculture-system which allows to remove the coculture device should be established in order to enable subsequentially electro-physiological measurements. Moreover, neurons cultured in the coculture system should survive 10 DIV or longer to allow synapse maturation. The electro-physiological properties of the cocultured striatal and cortical neurons are tested using patch-clamp experiments.

2. The mammalian nervous system

There are two major groups of cells in the mammalian nervous system: Neurons and glial cells. Neurons form precise neuronal networks which can trigger different actions depending on the type of connection with each other or with sensory receptors and muscles. Glial cells act as supporting cells and provide a structurally and chemically stable environment. Both cell types can be further divided into different sub-categories depending on their function and location in the nervous system.

2.1 Glial cells

Glial cells in the vertebrate nervous system can be divided into microglia and macroglia. Microglia form the immune system of the central nervous system. They are activated after injury, infection or disease and develop from macrophages outside the nervous system. Microglia are thought to be key elements in the neuroinflammatory responses involved in various chronic neurodegenerative diseases including Parkinson´s disease and Alzheimer´s disease (Streit *et al.*, 2004).

There are three types of macroglia: Astrocytes, oligodendrocytes and Schwann cells. Oligodendrocytes are small cells with few processes which are found in the central nervous system. In the white matter they insulate up to 15 axons by wrapping layers of myelin around them. In the grey matter perineural oligodendrocytes surround and support the cell bodies of neurons (fig. 2-1A). Schwann cells provide myelin insulation to axons in the peripheral nervous system. Each schwann cell can cover about 1 mm² of an axon which requires hundreds of them to insulate an axon completely (fig 2-1B). The intervalls between the myelin sheats are called “Nodes of Ranvier”. They permit saltatory conduction of action potentials which greatly speeds up signal transmission and saves energy (Kandel *et al.*, 2000).

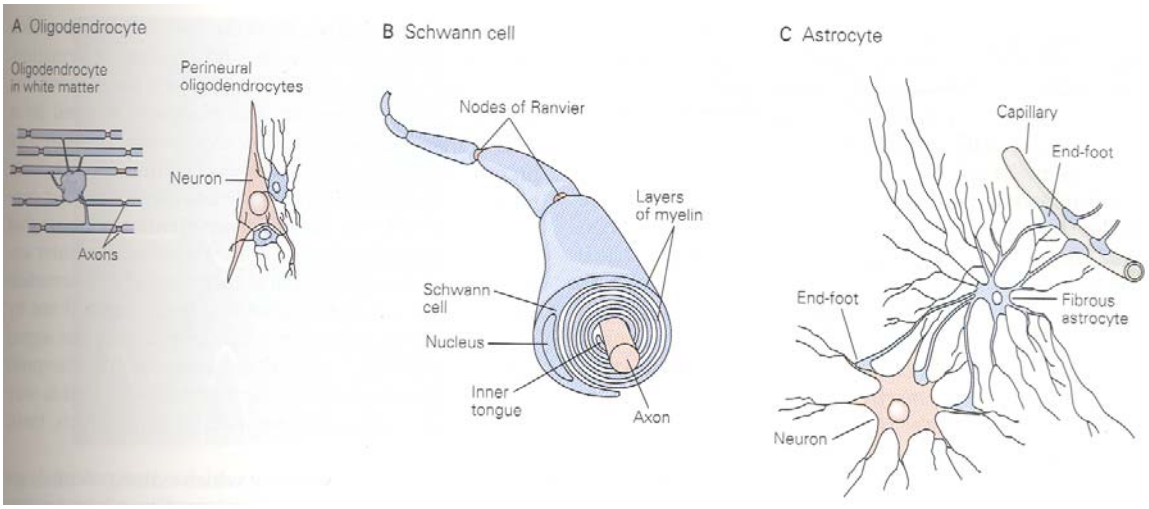


Fig 2-1: Types of glial cells in the mammalian nervous system. A: Oligodendrocytes insulate up to 15 axons in the white matter. In the grey matter perineural oligodendrocytes surround and support the cell bodies of neurons. B: Schwann cells insulate single axons in the periphal nervous system. They wrap myelin sheats around an area of about 1 mm². C: Astrocytes are characterized by their star-like shape and broad end-feet on their processes. Astrocytes provide nutrion, structural support and a chemically stable environment for neurons (Kandel *et al.*, 2000).

Most glial cells are astrocytes, roughly star-shaped cells with long processes (fig. 2-1C). Some astrocytes form broad end-feet on the surfaces of neurons in the brain and the spinal cord. They give structural support and provide nutrients for the neurons. Furthermore, astrocytes help to maintain a stable chemical environment for the neurons due to their high permeability to potassium and their ability to take up neurotransmitters after release (Parpura *et al.*, 2000; Piet *et al*., 2004). In response to ATP-release from electrically active neurons the astrocytes secrete the cytokine leukemia inhibitory factor (LIF), a regulatory protein that promotes the myelinating activity of oligodendrocytes (Ishibashi *et al*., 2006). Recent studies have shown that astrocytes can modulate heterosynaptic transmissions between neurons by rapid changes in their morphology (Piet *et al*., 2004). Heterosynaptic transmissions depend on glutamate release into the extracellular space and its diffusion to the neighbouring synapses. Astrocytes act as physical barrier against diffusion in the extracellular space (Piet *et al*., 2004). Piet *et al.* (2004) showed that reduced astrocytic coverage of magnocellular neurons occurring in the supraoptic nucleus of lactating rats enhanced glutamate diffusion.

Some astrocytes place end-feet on blood-vessels and serve as intermediaries in neuronal regulation of blood flow (Parri *et al*., 2003). In the brain they support the formation of tight juctions by endothelial cells of blood vessels, resulting in the blood-brain barrier.

2.2 Neurons

Neurons are the main signaling units of the nervous system. Most neurons consist of three morphologically defined regions: The cell body, dendrites and the axon (fig. 2-2).

Axons and dendrites are two structurally and functionally distinct compartments

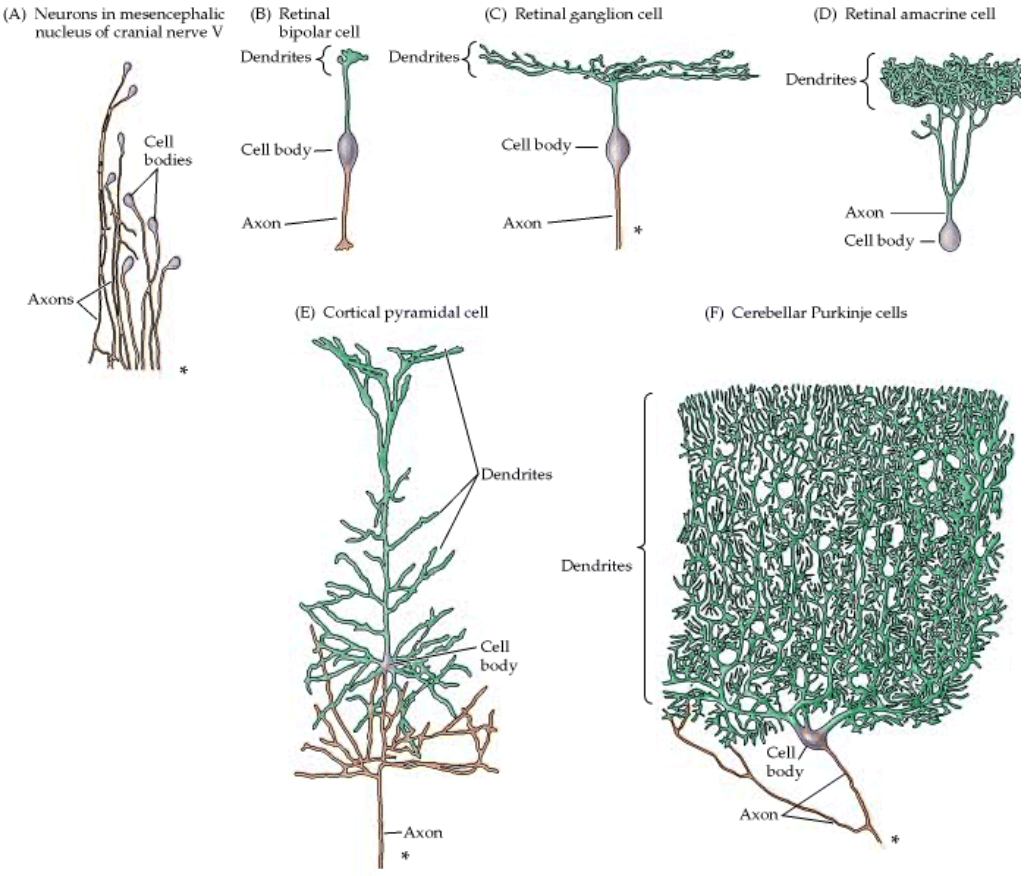


Fig. 2-2: Examples (A—F) of the rich variety of nerve cell morphologies found in the human nervous system. Most neurons consist of three morphologically defined regions: The cell body, dendrites and the axon. Asterisks indicate that the axon runs on much farther than shown. The drawings are not all at the same scale (Purves *et al.*, 2004).

which enable neurons to transmit and receive electrical signals.

Axons are long and thin and branch perpendicular to the cell body. They contain neurotransmitters in synaptic vesicles and release them at axon terminals due to electric signals from the cell body (Craig *et al.*, 1994; Fukata *et al*., 2002). Their microtubule system has an uniform polarity (Mattson, 1999). Proteins specific for axons are tau proteins which are microtubuli associated proteins controlling tubulin polymerization (Binder *et al.*, 1986) and a neuron specific growth-associated protein named GAP-43 which is selectively distributed to the axonal domain in developing neurons (Goslin *et al.,* 1988; 1990).

Dendrites are relatively short in comparison to axons. They appear thick at their base but become thinner with increasing distance from the cell body and branch in Y-shape (Craig *et al*., 1994; Fukata *et al*., 2002). They form dendritic spines, membraneous protusions from the neuronal surface which contain receptors for neurotransmitters and signalling systems like the postsynaptic density complex (Nimchinsky *et al.*, 2002). In contrast to axons the microtubuli of dendrites possess a random polarity (Mattson,1999). Proteins specific for dendrites are the microtubule-associated protein 2 (MAP-2) (Caceres *et al.,* 1986; Craig *et al.*, 1993) and the glutamate receptor subunit GluR1 (Caceres *et al.,* 1986; Craig *et al.*, 1993).

The strict morphological and functional separation of cell body, axons and dendrites is called neuronal polarity (for further details see 2.2.1).

2.2.1 Neuronal Polarity

2.2.1.1 Axonguiding and development of neuronal networks

Neuronal polarization

Dotti *et al.* (1988) used primary rat hippocampal neuronal cell culture to study neuronal polarity. After plating cultured hippocampal neurons undergo maturation and develop a single axon and several shorter dendrites. The differentiation process can be divided into five morphologically different stages (Dotti *et al.*, 1988; fig. 2-3): After attachment to the substrate a neuron forms lamellipodia, short cytoskeletal actin projections (stage 1), which develop into 4-5 short immature

neurites (stage 2). Within a day one immature neurite rapidly elongates and becomes the axon (stage 3). The neurites which elongate slowlier acquire dendritic characteristics after DIV 3 (stage 4). Axon and dendrites continue to mature and develop synaptic contacts. The polarization is complete at DIV 7 (stage 5) (see 2.2 for details on axonal and dendritic characteristics).

Axon formation is the first step in neuronal polarization. Enhanced neurite/axon outgrowth requires increased reorganization of actin filaments and microtubules (Fukata *et al.*, 2002). Most rearrangements during neurite elongation occur at the tip of growing axons (Bradke *et al.*, 2000; Baas *et al.*, 2004). Application of actin-depolymerizing cytochalasin D to immature stage 2 neurons leads to neurons with multiple axon-like neurites (Bradke *et al.*, 1999).

Microtubule growth in the neurite depends on the transport of microtubule polymers and on their assembly at the plus ends of the microtubules (Baas, 1997). This happens in the cell body and the growth cone (Brown *et al.*, 1992; 1993).

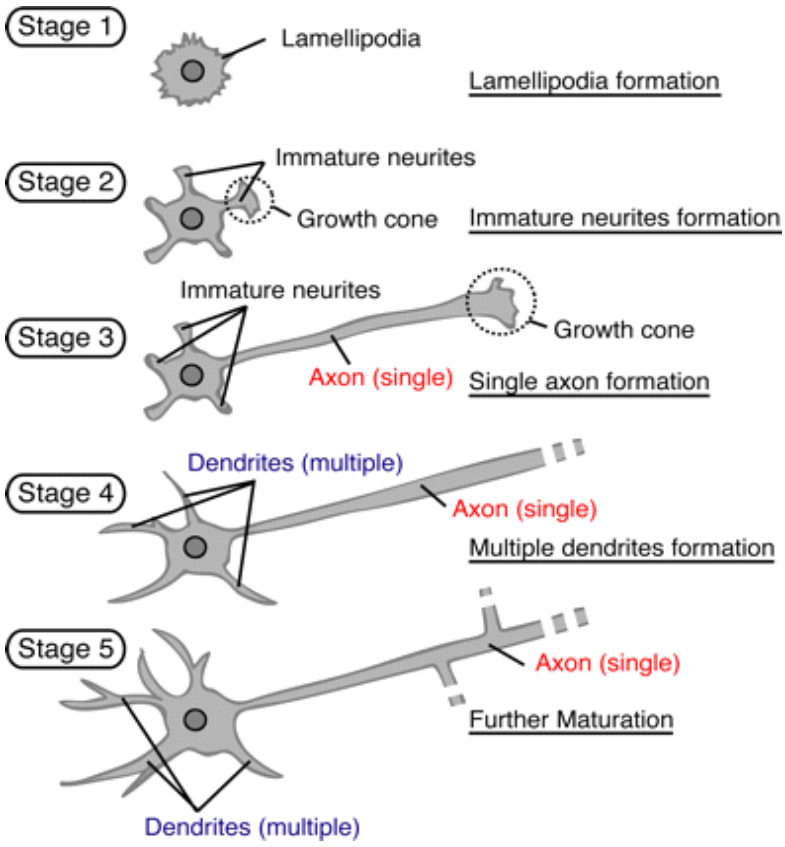


Fig. 2-3 : Processes of neuronal polarization in cultured hippocampal neurons. Cultured pyramidal neurons from a rat hippocampus acquire their characteristic polarized morphology in five well defined stages (Dotti *et al.*,1988).

Depolymerization of actin-filaments seems to enhance polymerization and transport of microtubules leading to enhanced neurite outgrowth and axon formation (Bradke *et al.*, 1999).

Axon guiding

The polarization of cultured neurons in the uniform environment of a cell culture dish shows that axonal fate is specified by intrinsic factors (Dotti *et al.*, 1988). On the other hand extracellular guiding cues play an important role in axon formation *in vivo* and *in vitro.* The tip of elongating axons is broadened and is called the growth cone. It has a central core which contains a lot of microtubules and other organelles. Projecting from the body are long and thin extensions called filopodia. Between the filopodia are the shorter and broader lammellipodia. Both are motile, contain high amounts of actin and lead to a ruffled appeareance of the growth cone (Forscher *et al.*, 1988). The filopodia contain receptors which interact with extracellular guiding cues. Depending on the signal the growth cone either advances, retracts or turns (Rehder *et al.*, 1996). Different mechanisms have evolved in order to guide growing axons to their targets even if great distances have to be traversed (fig. 2-4). Short-range guidance is provided by proteins of the extracellular matrix or within the cell membrane of neighboured cells. In some cases the first axon reaches the target region during early development when the embryo is small and the distance is short. This first axon acts as pioneer neuron in later development. Other axons attach themselves to the pioneer and grow along the predetermined path (fasciculation). The axon can also navigate along gradients, either of cell surface molecules or of secreted solube molecules, by chemotaxis. Both short-range and long-range guiding cues can either act repulsive or attractive (Kandel *et al.*, 2000).

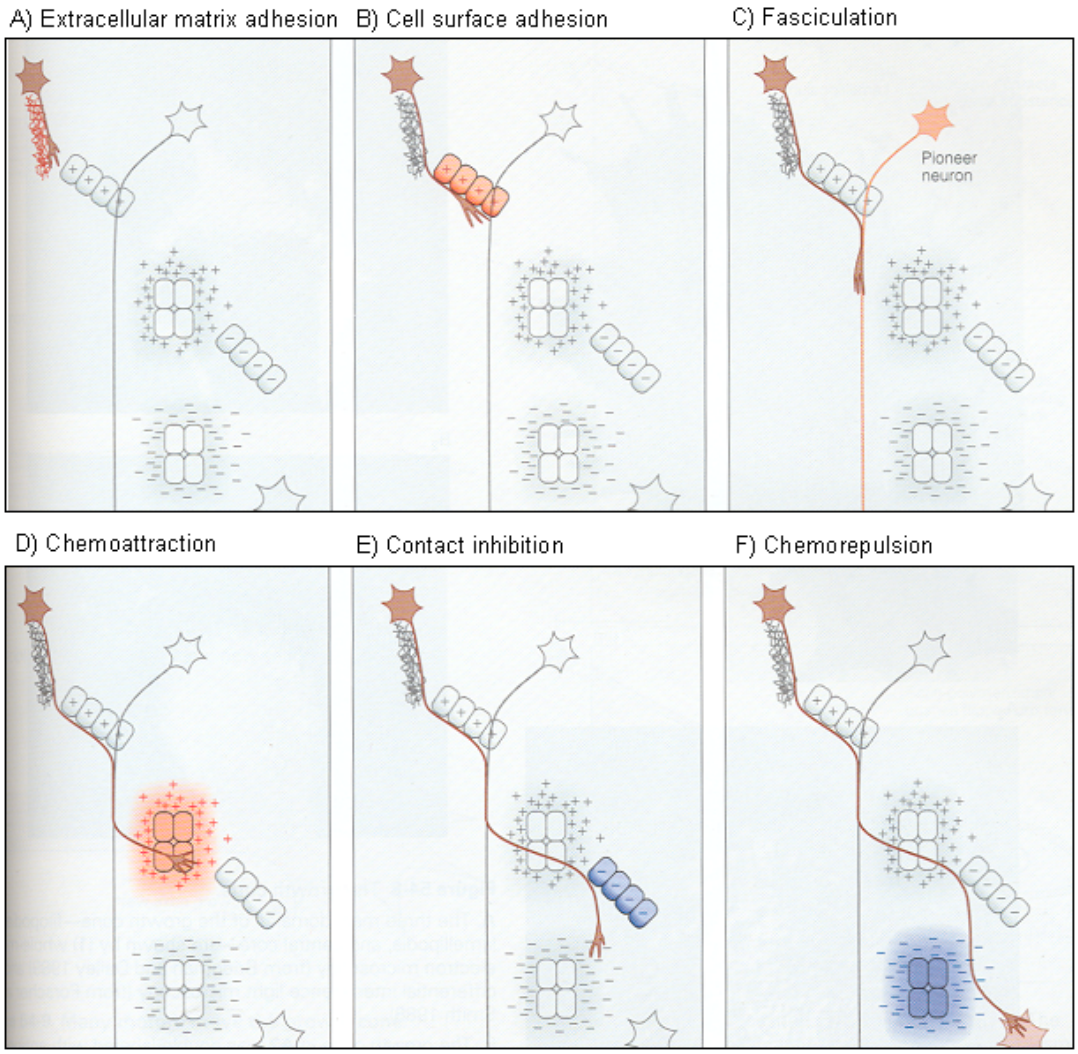


Fig. 2-4 : Mechanisms for axon guiding. A growth cone is guided by different guiding cues to the target region. The diagrams illustrate them arrayed into a single hypothetical pathway. A: The axon interacts with growth promoting molecules in the extracellular matrix *en route* to its synaptic target. B: Adhesive cell surface molecules on neuroepithelial cells promote the axon´s growth. C: The axon encounters another axon and fasciculates with it. D: A soluble chemoattractant molecule directs the axon. E: An intermediate target bears a repellent cue on its surface, which makes the axon turn. F: A soluble inhibitory molecule biases the axon´s trajectory to the right. Finally, after contact with the synaptic target the growth cone stops elongating and begins to form a terminal arbor (adapted from Kandel *et al.*, 2000) .

There are several main families of guiding cues. Ephrins and ephrin kinases are membrane-bound proteins. Ephrin kinases are present on the growth cone while ephrins are bound to cell membranes of neuronal and non-neuronal tissues. Both can be divided into two subfamilies: Ephrin A molecules are linked to glycosyl phosphatidyl inositol (GPI) and bind preferentially to ephrin A kinases. Ephrin B molecules are membrane-spanning proteins that bind preferentially to ephrin B

kinases. Binding of ephrins activates the ephrin kinase and inhibits axon outgrowth in the rat retinotactal pathway. It also promotes the fasciculation of rat cortical axons (Flanagan *et al.*, 1998; O´Leary *et al.*,1999).

Another class of inhibitory guiding cues are the semaphorins. This class includes membrane-bound and soluble molecules. Key receptors for the semaphorins in rats are immunoglobin superfamily proteins called neuropilins and a family of proteins that show structural similarities to the semaphorins called plexins (Püschel, 1996).

Neurothrophins like neural glia factor (NGF) and brain derived neurothrophic factor (BDNF) can promote axonal outgrowth and act as chemoattractant for retinal ganglion cells in frogs and fish (Cohen-Cory, 2004). In addition, they modulate synapse formation in the central nervous system. They bind to two kinds of receptors: The tyrosine kinase receptors (TrkA, TrkB, TrKC) and a common neurothrophin receptor (Cohen-Cory, 2004).

Some molecules of the extracellular matrix like laminins and cell adhesion molecules of the cadherin and immunoglobin superfamilies (e.g. neuron cell adhesion molecule; L1 and neuron-glia cell adhesion molecule) promote axonal outgrowth. Esch *et al.* (1999) cultured rat hippocampal neurons on substrates patterned with stripes of poly-L-lysine and either laminin or neuron-glia cell adhesion molecule (NgCAM). The axons were preferentially formed on contact with laminin and NgCAM although the immature neurons attached on poly-L-lysine and either laminin or NgCAM equally. If the neurons were already polarized into an axonal and a dendritic compartment contact with laminin or NgCAM enhanced axon elongation. Menager *et al.* (2004) cultured rat hippocampal neurons in the presence of laminin-coated beads. They observed rapid axon formation when an immature stage 2 neurite reached a laminin-coated bead. Matsuzawa *et al.* (1998) observed in a stripe-assay that a decapeptide (RDIAEIIKDI) derived from the neuron outgrowth domain of the B2 chain of laminin is sufficient to promote axon guiding of rat hippocampal neurons. Recent studies in rat hippocampal neurons have shown that local contact of immature neurites with the extracellular matrix activates PI3 kinase and leads to the accumulation of PI(3,4,5)P3 at the tip of the neurite. PI3 kinase inhibitors affect axon formation and elongation, thus delaying the development of immature stage-1-neurons to polarized stage-3-neurons (Shi

et al., 2003; Menager *et al.*, 2004). This suggests that the signal cascades which are triggered by the contact of extracellular matrix molecules (e.g. laminin and Ng-CAM) with adhesion signalling receptors in the cell membrane, like integrins, initiate neurite growth and axon formation. Similar results have been observed by Oliva *et al.* (2003). Patterned substrates with poly-L-lysine lines crossing lines of the cell adhesion molecule L1 were produced without denaturing the proteins. In cell culture rat cortical axons preferentially grew on the L1-lines while the dendrites remained unaffected.

Netrins are bifunctional soluble guiding cues that can trigger either attraction or repulsion of an axon. First studies were done in *Xenopus.* The response of an axon to netrin-1 depends on the composition of netrin receptors on the surface of the growth cone. Members of the Deleted in Colorectal Cancer (DCC) family (DCC and neogenin in vertebrates) usually mediate attraction while the vertebrate Unc5a-Unc5d receptors mediate repulsion (Huber *et al.*, 2003). DCC can also lead to repulsive axon guidance due to the netrin-induced association of DCC and Unc5 in the cytoplasm (Stein *et al.*, 2001; Hong *et al.*, 1999). Another important switch between attraction and repulsion is the internal Ca^{2+} concentration in the growth cone. Hong *et al.* (2000) converted netrin-mediated attraction to repulsion by blocking the Ca^{2+} influx or the Ca^{2+} release from internal reservoirs.

Netrin-1 attracts growing rat cortical axons in explant cocultures (Metin *et al.*, 1997; Richards *et al.*, 1997) and promotes the axon branching (Dent *et al.*, 2004). The link to intracellular signal cascades is the activation of focal adhesion kinase (FAK) and src-kinase due to netrins (Li *et al.*, 2004; Liu *et al.*, 2004; Meriane *et al.*, 2004; Ren *et al.*, 2004). This leads to the activation of the ERK2-MAPK cascade (Forcet *et al.*, 2002). It has also been shown that netrin-1 activates local protein synthesis in vitro (Campbell *et al.*, 2001) which requires MAPK-activity (Campbell *et al.*, 2003). In additon it activates the calcineurin-dependent nuclear factor NFAT (Graef *et al.*, 2003). Blocking of these pathways prevents netrin-induced axonal outgrowth (Campbell *et al.*, 2001; Graef *et al.*, 2003) and axon-turning (Forcet *et al.*, 2002; Campbell *et al.*, 2003).

2.2.2 Polarity in the CNS

The central nervous system receives information through several periphal sensory systems. Signal transmission is organized serially in so-called relays. Sensory afferents in the periphery project to one or several regions in the spinal cord, brainstem and thalamus. The thalamus transmits this information to the primary sensory cortex from which the information is further projected to other areas of the cerebral cortex. Two functional classes of neurons have been identified: Interneurons are local neurons which exclusively transmit information within their stage of the relay. Projection neurons convey information to the next stage of the relay by axon bundles which project together in a pathway to the next stage. These pathways often cross the midline of the nervous system (Kandel *et al.*, 2001). The axons forming these pathways are guided to their defined target by different guiding mechanisms (for details see 2.2.1.1).

2.2.2.1 The corticostriatal pathway

The most important pathway for learning and memory is the corticostriatal pathway. The striatum is the major structure of the basal ganglia which controls motor and cognitive functions (Graybiel *et al.*,1994; Wickens *et al.*, 2003). Medium spiny neurons represent 95% of the striatum and modulate the output signals of the basal ganglia by interaction with several subclasses of interneurons (Tepper *et al.*, 2004; Kawaguchi *et al.*, 1995). The striatum plays an important role in reward-related learning (McDonald *et al.*, 1993; Packard *et al.*, 2002). Neurons which are active after the presentation of food or liquid rewards and stimuli that predict reward (Mirenowics *et al.*, 1994; Mirenowics *et al.*, 1996) project mainly to the dorsal striatum and release dopaminergic reward signals (Bouyer *et al.*, 1984; Freund *et al.*, 1984; Smith *et al.*, 1990; fig. 2-5). The striatum can integrate these dopaminergic reward signals with sensory cues from corticostriatal and thalamostriatal afferents and generate motor commands. The striatum is located directly underneath the cortex (Altman *et al.*, 1994; Mizushima *et al.*, 2000; see striatum preparation 3.3.3) and receives input from all areas of the cortex and parts of the thalamus. This was shown by retrograde transport of horseradish peroxidase from the striatum to the cortex (McGeorge *et al.*, 1989; fig. 2-5). The

corticostriatal axons release glutamate into the striatum (Divac *et al.*, 1977; Perschak *et al.*, 1990) and form synapses to the medium spiny neurons (Somogyi *et al.*, 1981; fig. 2-5).

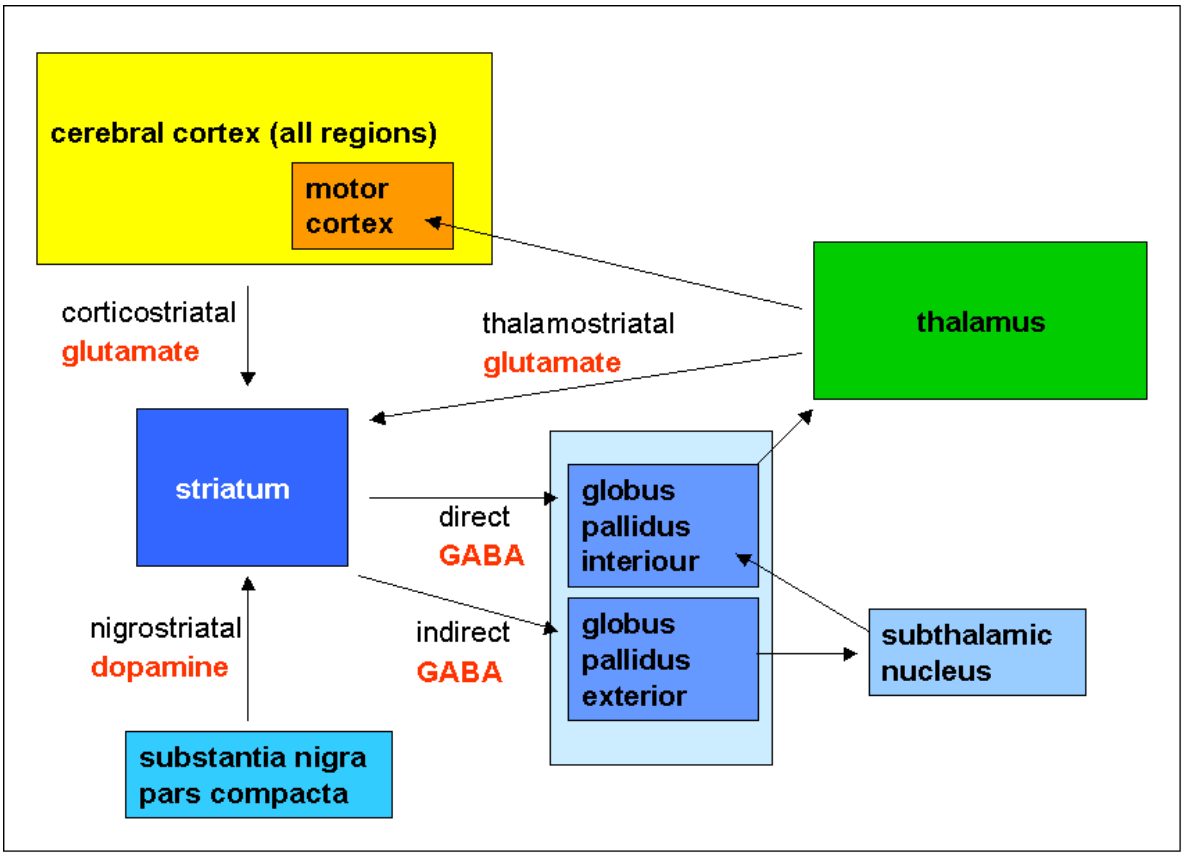


Fig. 2-5: A diagram showing the connections of the striatum and basal ganglia output nuclei with the cerebral cortex and substantia nigra pars compacta. Reward-related dopamine pulses released in the striatum are proposed to facilitate the selection of particular pathways through various basal ganglia to the motor cortex, and hence of particular actions, according to past and anticipated rewards. The involved neurotransmitters are dopamine, glutamate and γ-amino-butyric acid (GABA) (modified from Wickens *et al.*, 2003).

In vivo striatal neurons show spontaneous fluctuations of the resting membrane potential (V_{rest}). The neurons switch between a hyperpolarized "down" state and a depolarized "up" state. In anaestized adult rats the "up" state showed a mean V_{rest} of –66 ± 8 mV, while the average V_{rest} in the "down" state was –85 ± 7 mV (Reynolds *et al.,* 2000). Interestingly, compared to silent medium spiny neurons the average V_{rest} of spontaneously firing medium spiny neurons in the "up" state is significantly higher (-51 ± 7 mV compared to –62 ± 5 mV; Wickens *et al.*, 1998). These differences in V_{rest} depend on excitatory input from cortical afferents. Synchronous firing of several cortical afferents induces the "up" state in striatal

neurons which is characterized by inactivation of the Mg^{2+} block of N-methyl-D-aspartate (NMDA) receptors (Wilson *et al.*, 1996; Stern *et al.*, 1998; Wickens *et al.*, 1998). Thus action potentials are usually triggered in the "up" state (Stern *et al.,* 1997). Depending on the V_{rest} of striatal neurons and the dopamine release from nigrostriatal neurons a high frequency stimulation either induces long term potentiation (LTP) or long term depression (LTD). Strong dopamine release due to a reward stimulus combined with repetetive stimulation from cortical afferents and an "up" state leads to LTP (Schultz, 2002; Reynolds *et al.*, 2001) while LTD induction requires a low dopamine release and a striatal "down" state during HFS stimulation (Mahon *et al.*, 2004; Schultz, 2002).

The polarity between cortical and striatal neurons can also be observed in organotypic cultures of cortical and striatal slices obtained from newborn rats (P0-P2). After 3 weeks *in vitro* cortical neurons with projections to the striatum showed similar morphological characteristics to corticostriatal projections *in vivo* while no projections from striatum to cortex were found. Cortical and striatal neurons respectively show similar electrophysiological properties in organotypic coculture compared to *in vivo* conditions (Plenz *et al.*, 1996a; 1996b). The "up" state in the cocultured striatal neurons is induced by a strong synaptic input. Striatal neurons receive about 800 synaptic inputs per second during the "up" state compared to 10–40 inputs per second during "down" states (Blackwell *et al.*, 2003).

Segal *et al.* (2003) tested the effect of cortical afferents on striatal neurons in low density neuronal cell culture. The authors cocultured P1 cortical cells with E19 striatal cells. No spontaneous signal transduction (characterized by excitatory postsynaptic currents, EPSCs) was observed in a pure rat striatal cell culture while EPSCs were recorded when input from cocultured mouse cortical neurons was provided. It was not tested if action potentials induced in the striatal neurons triggered action potentials in the cortical neurons. It was demonstrated in slice cultures that the age of the cortical slice determines the innervation pattern of corticostriatal connections (Snyder-Keller *et al*., 2004). Therefore the results of Segal *et al.* (2003) do not represent the physiological situation.

In this work a coculture of dissociated cortical and striatal neonatal rat neurons with a spatial separation was developed. In this system the neurons are not only

taken from the same species, they are also taken at the same stage of development. As the coculture is a low density culture it allows to observe the polarity and synaptogenesis of corticostriatal synapses on a single-cell level.

2.3 Electrophysiological properties of neurons

2.3.1 Resting potential

The cell membrane is a lipid bilayer which blocks diffusion from the extracellular to the cytoplasmic side and *vice versa*. In neurons negative and positive charges are separated across the cell membrane: At V_{rest} the extracellular side of the cell membrane is charged positive while the cytoplasmic side is negative. Two factors influence V_{rest}: First the different concentrations of ions on each side of the membrane and second the transport of ions from one side to the other due to ion channels.

Sodium, chloride and calcium are present in high concentrations outside of the cell while potassium is strongly enriched within the cell. These concentration gradients are created by membrane integral ion pumps, e.g. the Na^+-K^+ pump. The Na^+-K^+ pump exchanges 3 intracellular Na^+ ions for 2 extracellular K^+ ions under the consumption of ATP. This prevents the equilibration of the ion gradients and maintains a constant charge separation across the cell membrane over time (Kandel *et al*., 2000).

The cell membrane contains a large variety of channel proteins that are passively permeable to different ion species. Most of these channels are regulated, but some are also open in the resting state. The majority of them are selectively permeable to potassium. At V_{rest} potassium flows out of the cell along the concentration gradient, resulting in a loss of positive charge from the cell. In addition, sodium flows into the cell due to a small amount of sodium channels open at rest. The permeability for sodium is far lower than that for potassium, resulting in a negative potential within the cell which can hold back potassium ions through electrostatic forces. The third type of channels open at rest is selective for chloride, which again contributes to the negative membrane potential by flowing

into the cell (Kandel *et al*., 2000). Each ion is influenced by the electrical driving force depending on the electric potential difference and the chemical driving force depending on the concentration gradient across the membrane. The equilibrium potential is the potential at which the electrical driving force exactly balances the chemical driving force. It can be calculated for single ion species using the Nernst-Equation:

$$E_{ion} = \frac{R \times T}{z \times F} \ln \frac{[Ion]_{out}}{[Ion]_{in}} \qquad \text{(Equ. 2-1)}$$

E_{ion} = Equilibrium Potential for the ion species

R = Gas constant

T = Absolute temperature

z = Valence of the ion

F = Faraday's constant

$[Ion]_{out}$ = Concentration of ions outside the cell

$[Ion]_{in}$ = Concentration of ions inside the cell

The Nernst-Equation can be used for calculation of the equilibrium potential if the cell membrane is permeable for only one ion species at V_{rest}, as e.g. in glial cells. Their cell membrane is only permeable for K^+ ions and their V_{rest} equals the equilibrium potential of K^+ (-75 mV). If the cell membrane is permeable for more ion species, the Goldmann-Equation is used for the calculation of V_{rest} (Kandel *et al*., 2000):

$$V_{rest} = \frac{R \times T}{F} \ln \frac{P_K[K^+]_{out} + P_{Na}[Na^+]_{out} + P_{Cl}[Cl^-]_{in}}{P_K[K^+]_{in} + P_{Na}[Na^+]_{in} + P_{Cl}[Cl^-]_{out}} \qquad \text{(Equ. 2-2)}$$

V_{rest} = Resting membrane potential

$P_{K/Na/Cl}$ = Relative permeability of the membrane for the $K^+/Na^+/Cl^-$

2.3.2 Action potential

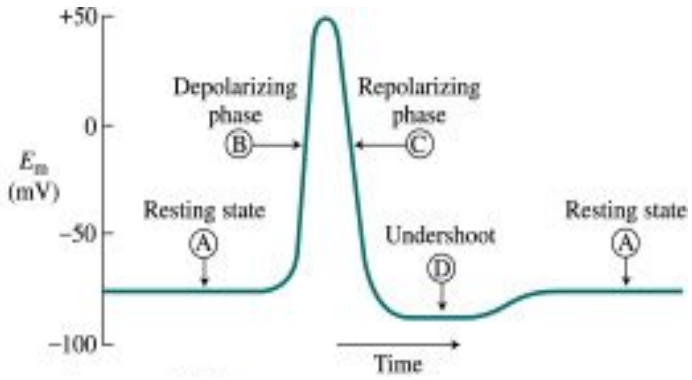


Fig. 2-6: Scheme of an action potential (adapted from Matthews, 2001).

Action potentials (APs) are produced by passive flow of ions across the cell membrane through voltage-gated ion-channels. An influx of Na^+ depolarizes the cell membrane. After depolarization over the threshold for APs (all- or-nothing behaviour) voltage-gated Na^+ ion channels open and the membrane potential depolarizes rapidly towards the equilibrium potential of Na^+ (2-6 B). This gradually inactivates the Na^+ ion channels and activates K^+ ion-channels. The resulting outflow of K^+ ions repolarizes the cell membrane (2-6 C). The AP is followed by the so-called “undershoot” (2-6 D). During this time the membrane potential is slightly hyperpolarized because it takes 20-30 milli-seconds (ms) until all voltage-gated K^+ channels (so-called delayed rectifier with a slower kinetic) have switched back to the closed state. After an AP there is a short time of diminished excitability (about 1 ms). This refractory period is caused by the inactivation of Na^+-channels and the increased opening of K^+-channels. Upon repolarization the Na^+-channels return to the resting state while the K^+channels are closed. This ensures that the cell returns to resting potential (2-6 A) and prevents a running down of the chemical gradient due to overstimulation. During the refractory period the Na^+-K^+ pump restores the chemical gradient by exchanging 3 intracellular Na^+ ions for 2 extracellular K^+ ions (Kandel *et al*., 2000; Matthews, 2001).

The AP can be propagated along an axon without a loss in signal amplitude. The AP induced at point A depolarizes the cell membrane in the neighbourhood due to passively flowing current (electrotonic conduction). This leads to the opening of voltage-gated Na^+channels at a point B and induces an AP. Backpropagation of the AP is prevented by the refractory period of voltage-gated Na^+-channels. In myelinated axons the myelin isolates the internodal membrane and the current

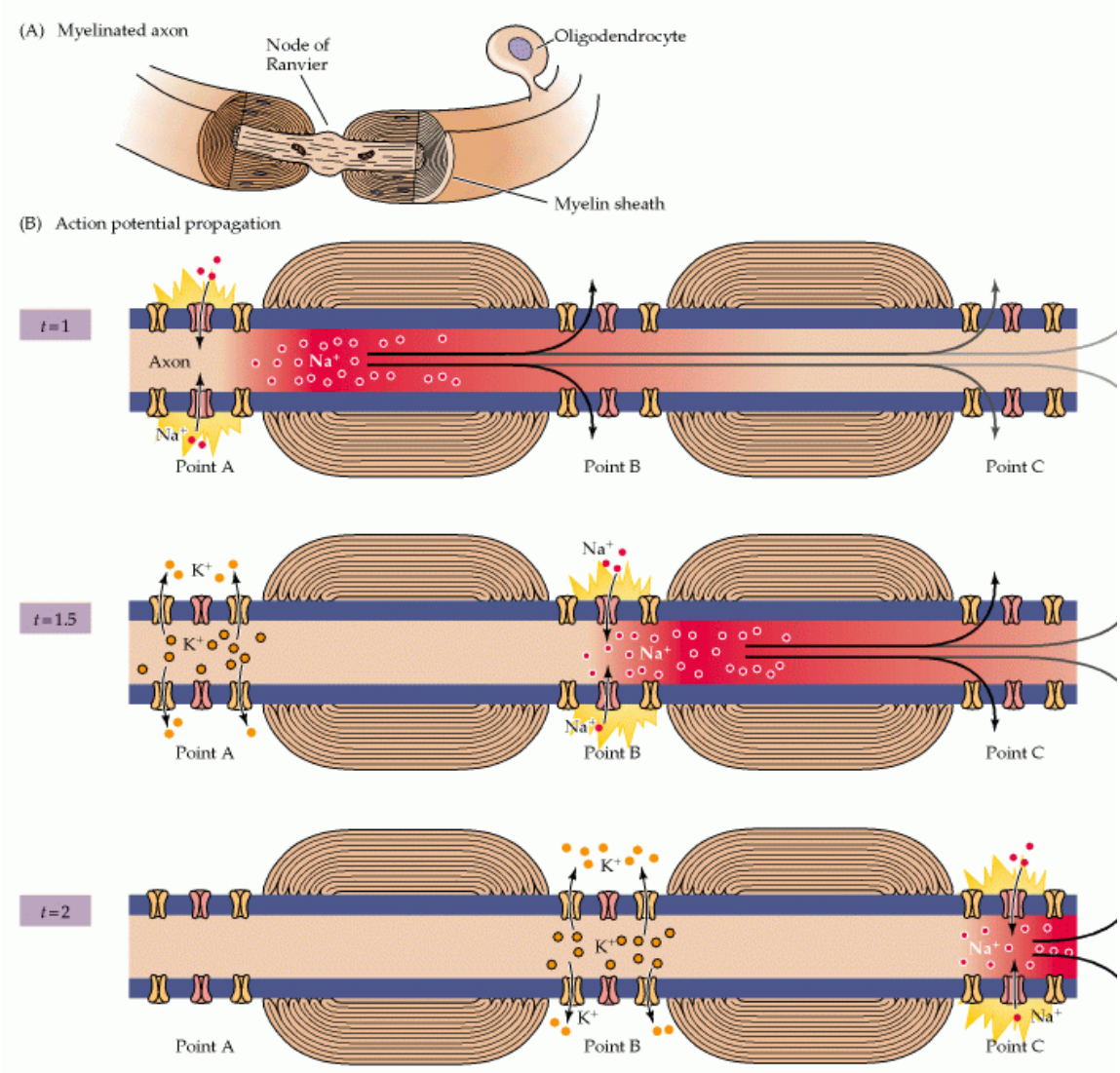


Fig. 2-7: Saltatory action potential conduction along a myelinated axon. (A) Diagram of a myelinated axon. (B) Local current in response to action potential initiation at a particular site flows locally. However, the presence of myelin prevents the local current from leaking across the internodal membrane; it therefore flows farther along the axon than it would in the absence of myelin. Moreover, voltage-gated Na^+ channels are present only at the nodes of Ranvier. This arrangement means that the generation of active, voltage-gated currents need only occur at these unmyelinated regions. The result is a greatly enhanced velocity of action potential conduction (adapted from Purves *et al.*, 2004).

flows farther. In addition, voltage-gated Na^+ channels are only expressed at the nodes of Ranvier. This leads to a faster signal propagation than in unmyelinated axons (saltatory signal propagation) (Purves *et al.*, 2004; fig. 2-7). At the end of the axon the signal is passed to the next cell through a synapse.

2.3.3 Synapses

2.3.3.1 Electrical synapses

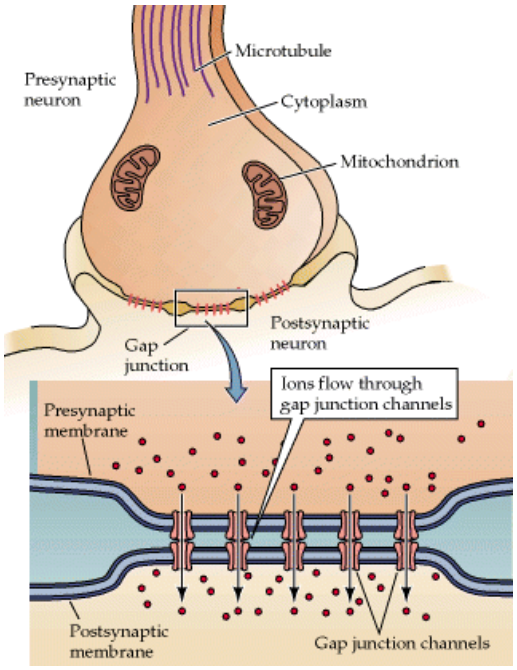


Fig. 2-8: Electrical synapse. Two adjacent neurons are directly connected by gap junctions. Current flows directly from one neuron to the other. (adapted from Purves, 2004).

Adjacent neurons can be connected directly by gap junction channels which form electrical synapses. These channels consist of two hemichannels, the so-called connexons. Each connexon has six identical subunits (connexins). The channels have a diameter of 1.5 nm and connect the cytoplasms of the pre- and postsynaptic neuron. This allows the diffusion of small intracellular metabolites (fig. 2-8).

Transmission along electrical synapses is a passive flow of current from one neuron to the other. APs in the postsynaptic neuron are generated nearly without any time delay. This allows synchronous firing of large groups of neurons (Kandel *et al.*, 2000; Purves *et al.*, 2004).

2.3.3.2 Chemical synapses

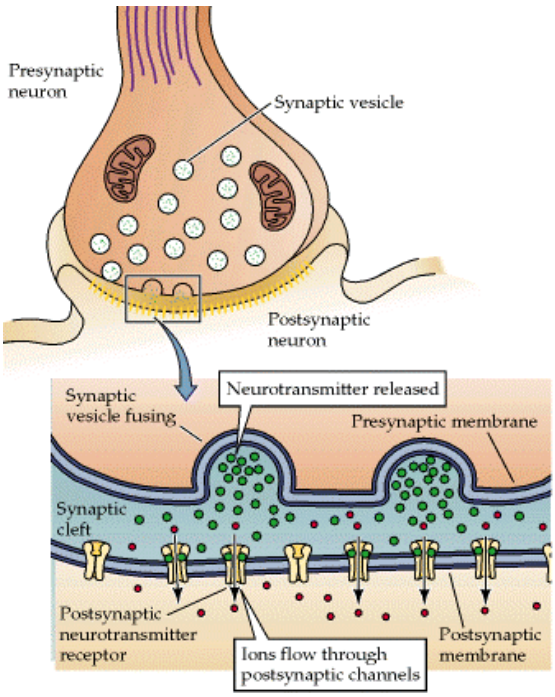


Fig. 2-9 : Chemical Synapse. Due to the incoming action potential neurotransmitter are released into the synaptic cleft. The activation of postsynaptic neurotransmitter receptors leads to a depolarization of the postsynaptic cell membrane and the generation of action potentials (adapted from Purves *et al.*, 2004).

Chemical synapses consist of the presynaptic membrane and the postsynaptic membrane (fig. 2-9). Both are separated by the 20-40 nm wide synaptic cleft. In the presynaptic membrane incoming APs trigger an influx of Ca^{2+}-ions through voltage-gated ion channels. The increase in Ca^{2+} leads to the fusion of neurotransmitter containing synaptic vesicles with the presynaptic membrane. Neurotransmitters are thereby released into the synaptic cleft, diffuse to the postsynaptic membrane and bind to their specific receptors. This leads to an opening of voltage-gated ion-channels and to the depolarization of the postsynaptic membrane resulting in the generation of a postsynaptic AP or excitatory postsynaptic potential (EPSP). The synaptic delay between the incoming presynaptic and the generated postsynaptic AP is 0.3 to several milliseconds long. Only one or two neurotransmitter molecules are sufficient to activate a postsynaptic receptor. Thus the release of thousands of transmitter molecules released by one vesicle activates many postsynaptic receptors and amplifies the signal. Ionotropic receptors (in contrast to metabotropic receptors which activate intracellular signalling pathways and are not considered here) change their conformation upon transmitter binding and open. This leads to an ion influx and changes in the membrane potential. Depending on the postsynaptic receptors the synapse has an excitatory or inhibitory function.

γ-aminobutyric acid (GABA) usually acts as inhibitory transmitter in the CNS by activating two receptors : The $GABA_A$ receptor is a Cl^- channel while the $GABA_B$ receptor activates a second messenger system which opens a K^+ channel.

Another inhibitory receptor is the glycine-receptor which is also permeable for Cl^- ions. The opening of these channels leads to an influx of Cl- ions and an efflux of K^+ ions, respectively. The resulting hyperpolarization of the cell membrane prevents AP initiation (Kandel *et al.*, 2000; Purves *et al.*, 2004).

Another important neurotransmitter in the CNS is glutamate. Glutamate receptors are ion channels which are permeable for Na^+ and K^+ with nearly the same permeability. They can be divided in ionotropic and metabotropic receptors. While the metabotropic glutamate receptors can either act inhibitory or excitatory, the ionotropic glutamate receptors always lead to an excitation of the neuron. The three major subtypes of these receptors are named according to their synthetic agonists that activate them.

The NMDA-receptor is selectively blocked by 2-amino-5-phosphonovaleric acid (APV). The NMDA-receptor has several special characteristics: First, it requires extraxcellular glycine as cofactor (normal concentration of glycine in extracellular fluid is sufficient). Second, NMDA-receptors are blocked by a Mg^{2+} ion on the extracellular side at V_{rest}. Only depolarization of the cell membrane lifts the Mg^{2+} block due to electrostatic repulsion of Mg^{2+} from the channel. In addition, the channel opens and closes relatively slowly after binding of glutamate and contributes to the late phase of EPSPs. The NMDA-receptor is not only permeable for Na^+ and K^+, but also for Ca^{2+}. The influx of Ca^{2+} activates calcium dependent enzymes and second messenger systems which are important for triggering long lasting modifications of synapses (see 2.3.3.3).

α-amino-3-hydroxy-5-methylisoxazole-4-propionic acid (AMPA) and kainite receptors are the so-called non-NMDA-receptors. They can be blocked by cyano-7-nitroquinoxaline-2,3-dione (CNQX) (Kandel *et al.*, 2000; Purves *et al.*, 2004).

2.3.3.3 Synaptic plasticity

Long lasting modifications of synapses occur through a variety of mechanisms depending on the type of synapse, the developmental age of the neurons and the experimental stimuli (Lynch *et al.*, 2004; Malenka *et al.*, 2004). Since the first strengthening of synapses (long term potentiation or LTP) was observed in the hippocampus (Bliss *et al.*, 1973) most research on synaptic plasticity was done in this area of the brain. LTP can be achieved by trains of high frequency presynaptic stimulation (1 s duration), brief high frequency stimulations (short 10 ms pulses with 1 s pause) or more natural theta burst stimulation in hippocampal slices (Bliss *et al.*, 1973;Staubli *et al.*, 1987; Abraham *et al.*, 1997, Abraham *et al.*, 2002; fig. 2-10). Low-frequency stimulation over a long time period (1 Hz, 900 pulses) induces a weakening of synapses (long term depression or LTD) (Mulkey *et al.*, 1992; Kirkwood *et al.*, 1994). In cortical low density cultures on patterned substrates low frequency stimulation (1 Hz, 5 Hz and 10 Hz) lead to short term depression of synapses (Vogt, 2003a). In hippocampal cell culture LTP was induced by simultaneous stimulation of pre- and post-synaptic neurons. Due to the observation that strong synapses remained unaffected by stimulation protocols for LTP induction, only weak glutamatergic synapses were stimulated (Bi *et al*., 1998). In addition, a spike-time dependent plasticity was observed: LTP only occurred, if the postsynaptic neuron fired an AP within 10 ms after the presynaptic AP. LTD was induced when the temporal order was reversed or when the postsynaptic neuron fired more than 10 ms after the presynaptic AP (Markram *et al.*, 1997; Magee *et al.*, 1997; Debanne *et al.*, 1998; Bi *et al.*, 1998). These spike-time dependent

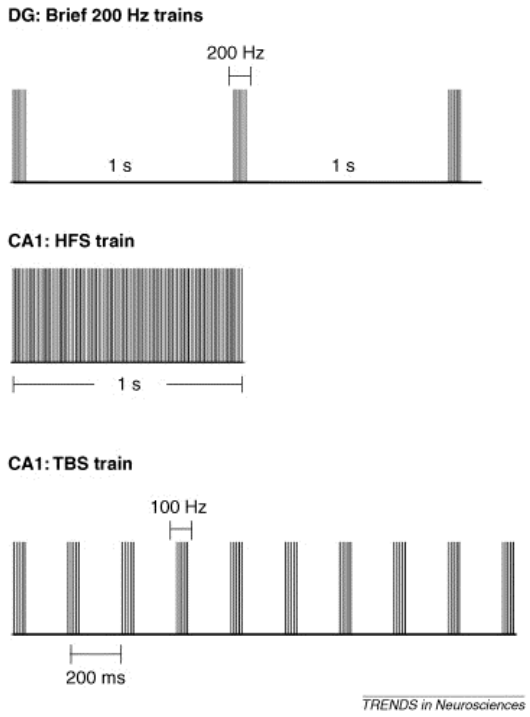


Fig. 2-10 : Common electrical stimulation protocols used to induce LTP (DG : dentate gyrus ; CA1 : CA1-region of the hippo-campus ; HFS : high frequency stimulation ; TBS : theta burst stimulation; Raymond, 2007).

plasticity was also shown in the cortex (Egger *et al.* 1999; Feldman, 2000; Sjostrom *et al.*, 2001).

Depending on the LTP-decay time-constants, three different forms of LTP can be distinguished in rat hippocampal slices (Abraham *et al.*, 1991) : LTP 1 is short-lived (hours *in vivo*) and involves posttranslational modifications of synaptic proteins. LTP 2 lasts several days *in vivo* and depends on protein synthesis, but not on gene expression. LTP 3 is the long-lasting form (hours *in vitro* and weeks or months *in vivo*) of LTP and requires transcription of genes.

Each form of LTP is induced by a high-frequency stimulation of presynaptic neurons. The resulting glutamate release depolarizes the postsynaptic neuron by activation of non-NMDA-receptors. This leads to a removal of the Mg^{2+} block on the NMDA-receptor and an Ca^{2+} influx (Lynch *et al.*, 2004).

Three different effector mechanisms can be distinguished depending on the form of triggered LTP: post-translational modification, dendritic protein synthesis and gene transcription. LTP1 is a rapidly decaying LTP induced by weak stimulation. It could be maintained by phosphorylation of postsynaptic receptors, e.g. AMPA receptors (Boehm *et al.*, 2005). This leads to an increased opening probability of the receptor and thus a stronger depolarization after presynaptic glutamate release. The most important protein kinase is the serine/threonine kinase Ca^{2+}/calmodulin-dependent kinase II (CaMKII) (Bliss *et al.*, 1993; Lismann *et al.*, 2002).

LTP 2 is characterized by an intermediate duration and requires dendritic protein synthesis without gene transcription due to the parallel activation of NMDA- and metabotropic glutamate receptors (Nakamura *et al.*, 2002; Rae *et al.*, 2000; Raymond *et al.*, 2000).

LTP 3 depends on strong stimulation protocols (Nguyen et a., 2003; Abraham *et al.*, 2003) and the activation of NMDA- and L-type VDCC-receptors (Morgan *et al.*, 2001; Raymond *et al.*, 2006) which lead to morphological changes in the synapse. After LTP induction the growth of new dendritic spines, the enlargement of existing spines and their postsynaptic densities (PSD) and the splitting of one functional synapse into two can be observed (Yuste *et al.*, 2001; Abraham *et al.*, 2003; Matzuzaki *et al.*, 2004).

3. Materials and methods

This chapter describes the methods used in this work. A list of all materials and devices and of all abbreviations is in the appendix.

3.1 Microcontact printing

Patterned neuronal cell culture decreases the number of neurons within the neuronal network. This simplifies the identification of morphologically connected neurons used for double patch-clamp experiments. Microcontact printing was originally developed by Kumar and Whitesides (1993). For patterned neuronal cell culture cell adhesion molecules were printed on a repellent substrate with an elastomeric PDMS-stamp using microcontact printing. This created a surface with a high contrast between the repellent and adhesive areas and achieves a high accuracy of the pattern (fig. 3-1). Primary vertebrate neurons cultured on such chemical patterns had comparable electrophysiological properties to primary vertebrate neurons cultured on unstructured substrates (Lauer *et al.*, 2004; Vogt *et al.*, 2003b; Vogt *et al.*, 2005).

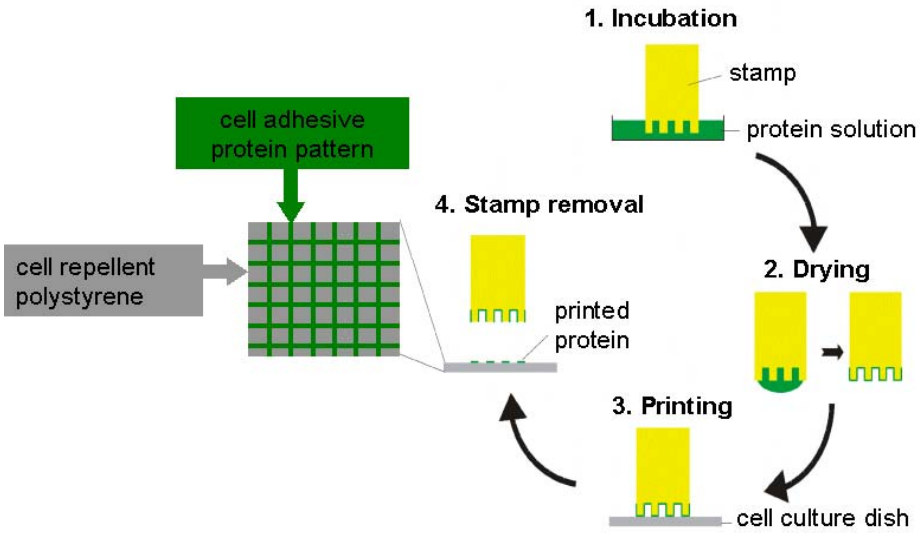


Fig. 3-1: Principle of Microcontact printing. A PDMS stamp is incubated in a protein solution. After removing the stamp from the solution a drop of protein solution sits on top of the stamp. This drop is dried with nitrogen. For printing the stamp is put on a cell culture dish. After the stamp removal the printed protein pattern remains. Incubation times in protein solution and on the cell culture dish depend on the applied protein.

Casting of the PDMS-stamp:

A siliconoxide wafer produced by electron beam lithography was used as template. The structured wafer was silanized with 1H,1H,2H,2H-Perfluoro-octyltrichlorosilane. The silanization resulted in a higher hydrophobicity of the template surface and allowed an easy removal of cured polydimethylsiloxane (PDMS) without damaging the master or deforming the stamp (Dissertation D. Schwaab, 2007). After rinsing with Milli Q the template was dried with nitrogen and clamped into the casting form. Two ml Eppendorf tubes with bottom and lid cut away were placed upside down onto the wafer. Each tube covered about 1 cm² of the desired structure. Curing agent and base agent of PDMS (Sylgard 184) were mixed thoroughly in a 1:10 ratio (volume per volume). Air bubbles were removed by storing it over night at -20 °C. 500 µl of the PDMS mixture were poured into the Eppendorf tubes. The stamps were cured for 2 h at 60 °C. For identification of the stamp pattern a small piece of paper with the pattern number was put onto the cured PDMS. The stamps were filled up with 1 ml of the PDMS mixture and cured over night at 60°C. Then the Eppendorf tubes with the PDMS-stamps were removed from the template. After cutting away the Eppendorf tubes the stamps were baked upside down in a closed glass petri dish for 1 h at 110°C.

Microcontact printing:

The PDMS-stamp was dipped into 70% ethanole p.A. for 3 seconds in order to remove fat residues and was dried with nitrogen afterwards. For printing proteins with a high viscosity like ECM-gel (mixture of extracellular matrix proteins) the stamp was incubated in the protein “ink” for at least 10 minutes. A drop of protein “ink” remained on the top of the stamp which was carefully dried with nitrogen without pushing it from the stamp surface. The dried stamp was placed on the middle of a polystyrene culture dish (8 cm²) or a hydrophilized glass coverslip (8 cm²) (see 3.2.1) for 10 – 15 minutes. Hydrophilic protein “inks” with a low viscosity (poly-D-lysine, netrin-1, laminin) required a preincubation of the PDMS-stamp in 10% sodium dodecyl sulfate (SDS) for 5 minutes (Chang *et al.*, 2005). SDS improved the wetting of the stamp and increased the amount of adsorbed protein. Before incubation in the protein “ink” the stamp was dipped into Milli Q to remove excess SDS and dried with nitrogen. The incubation time in the protein solution was increased onto 20 minutes.

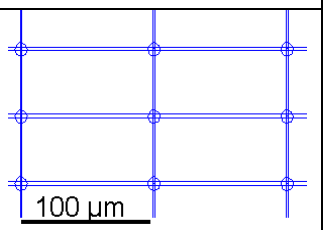
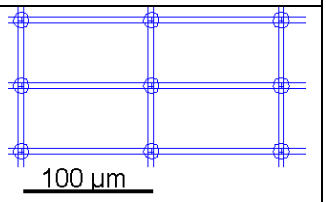
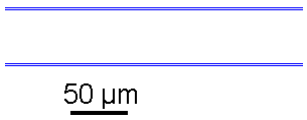
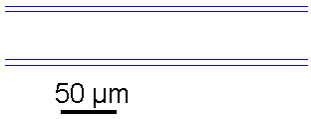
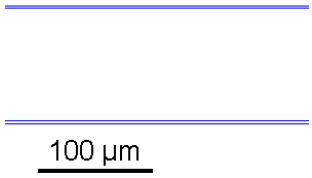
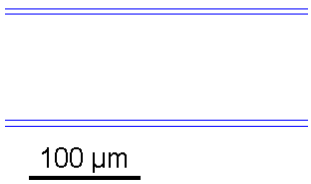
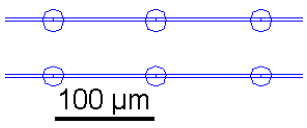
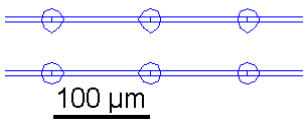
Proteins were used as described in tab. 3-1:

protein	concentration (µg/ml)	solvent
poly-D-lysine (PDL)	25	Hanks balanced salt solution ($HBSS^-$)
poly-L-lysine, fluorescin-isothiocyanate conjugated (FITC-PLL)	50	
netrin-1	5	Phosphate buffered saline (PBS) + 0.1% bovine serum albumin (BSA)
ECM-gel	80-120	$HBSS^-$
PECM	PDL:10; ECM: 80-120	$HBSS^-$
laminin	25	$HBSS^-$

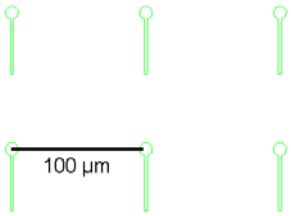
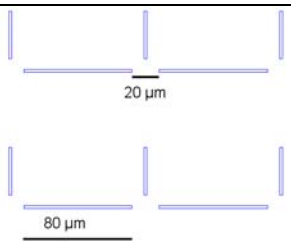
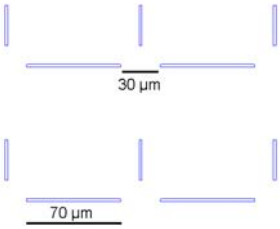
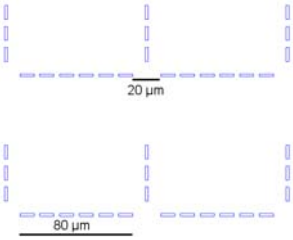
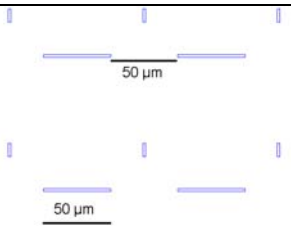
Tab. 3-1: Concentrations of proteins used for microcontact printing.

3.1.1 Waferstructures

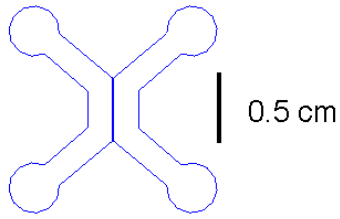
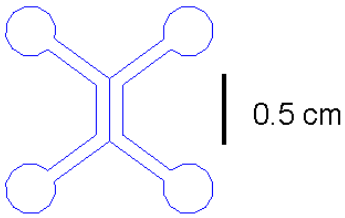
Structures for manual microcontact printing:

Stamp	Structure description	Structure
2-10	Grid with 2 µm lines and nodes with a diameter of 10 µm.	
4-12	Grid with 2 µm lines and nodes with a diameter of 10 µm.	
2-50	2 µm lines; distance: 50 µm.	
4-50	4 µm lines; distance: 50 µm.	
2-100	2 µm lines; distance: 100 µm.	
4-100	4 µm lines; distance: 100 µm.	
2-20-L	2 µm lines with 20 µm nodes; distance: 50 µm.	
4-22-L	4 µm lines with 22 µm nodes; distance: 50 µm.	

Structures for aligned two-step microcontact printing:

Stamp	Structure description	Structure
0	Short line with node	
1	Complementary lines to structure 0	
2	Complementary lines to structure 0	
3	Complementary lines to structure 0	
4	Complementary lines to structure 0	

Structures for microstructured coculture chamber:

Coculture chamber	Structure description	Structure
Microstructured coculture chamber 2 mm	The growth channels have a breadth of 2 mm. The microfluidic channels are 50 or 100 µm long. A = 0.79 cm²	
Microstructured coculture chamber 1 mm	The growth channels have a breadth of 1 mm. The microfluidic channels are 50 or 100 µm long. A = 0.65 cm²	

3.2 Production and sealing of the microstructured coculture chamber

The microstructured coculture chamber was produced with slight modifications according to the protocol of Taylor *et al.* (2003). The chamber had two growth channels (1 mm broad, 100 µm high, area 0.325 cm²/growth channel or 2 mm broad, 100 µm high, area 0.395 cm²/growth channel). These growth channels were connected by microfluidic channels (3 or 5 µm broad, 50 or 100 µm long and 10 µm high). The filling holes for the growth channel had a diameter of 4 mm (scheme see 3.1.1).

Production:

In order to cast coculture chambers a silanized silicondioxide-wafer (dissertation D. Schwaab, 2007) which contained 16 templates of the microstructured chambers was cleaned with Milli Q and dried with nitrogen. The cleaned wafer was clamped into a casting form and 7 ml of a PDMS-mixture were cast onto the wafer. After curing for 2 h at 60°C the cured PDMS was peeled off and cut into the single

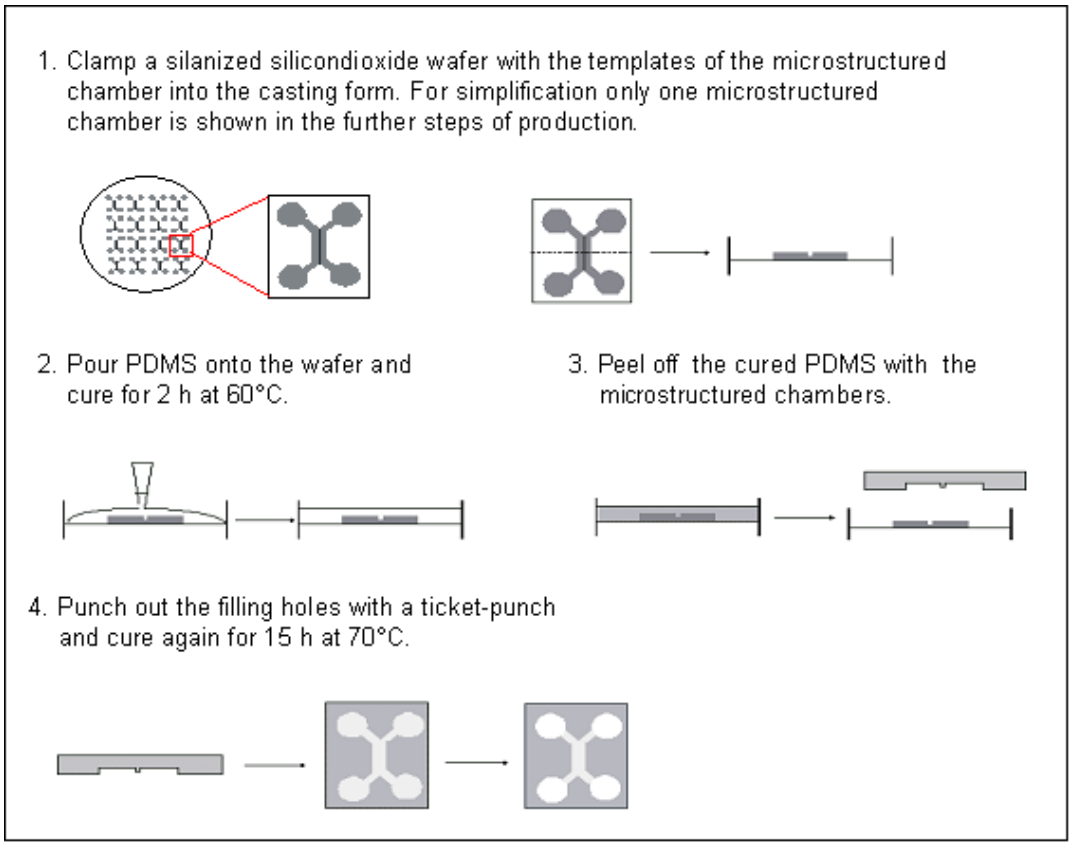


Fig. 3-2: Production of microstructured coculture chambers (scheme).

chambers. The filling holes of each chamber were punched out with a ticket-punch (fig. 3-2). The coculture chambers were placed upside down in a sterile glass petri dish and cured for 15 h at 70°C (Rhee *et al.* , 2005).

Glass coverslips (8 cm²) were hydrophilized with 20 % H_2SO_4 for 20 minutes at 80°C, washed 10 times with MilliQ and sterilized with the flame of a Bunsen burner. Then they were put into culture dishes and dried. Depending on the strength of hydrophilization the microstructured coculture chambers could be sealed either reversible or irreversible to hydrophilized glass coverslips.

For irreversible sealing the chambers were plasma-activated with a O_2-plasma oven (30 sec at 1.1mbar with 40 Watt). Before plasma-activation the O_2-concentration in the reaction chamber was increased by evacuation for 5 minutes and influx of O_2 for 1 minute (repeated 3 times). The plasma-activated chambers were directly sealed to hydrophilized glass coverslips, sterilized with UV-light for 20 minutes and coated for 1 h at room temperature with a mixture of poly-D-lysine (10 µg/ml) and ECM gel (80-120 µg/ml) (PECM) in $HBSS^-$. After washing the growth channels and microfluidic channels three times with neurobasal medium the microfluidic coculture chambers were stored at room temperature (RT) until preparation at the next day.

For reversible sealing coculture chambers were treated 6 minutes with a UV/ozone cleaner and incubated for 2 h in 0.1 M NaOH. The chambers were washed 10 times with MilliQ, dried with nitrogen and sealed directly to the glass coverslips under the clean bench. In order to remove excess NaOH in the microfluidic channels they were additionally washed with neurobasal medium 8x5 minutes at 37°C. After further incubation over night the chambers were washed twice with neurobasal medium. Over night the hydrophilization of the glass surface decreased. The sealed coculture chambers were rehydrophilized with O_2 -plasma to enable coating with PECM as described above.

3.3 Cell culture

3.3.1 Preparation of substrates

Sterilized glass coverslips (baked for 4 h at 180°C) were freshly hydrophilized by pulling them through the blue oxygen rich flame of a Bunsen burner and coated immediately. Polystyrene dishes (8 cm²) and hydrophilized glass coverslips (8 cm²) for normal cell culture and 4.91 cm² for culture in 24-well plates) were coated homogenously with a mixture of poly-D-lysine (10 µg/ml) and ECM gel (80-120 µg/ml) (PECM) in $HBSS^-$. Substrates with micropatterned proteins (see 3.1) were coated with 500 µl PECM around the pattern in order to increase the number of neurons in cell culture by providing a larger adherence area for the plated neurons. After incubation at room temperature for 1 h the substrates were washed 2 times with $HBSS^-$. The dried substrates were stored over night at RT or stored up to 6 weeks at 4°C.

For coculture, coverslips (8 cm²) were cut in half. Small glass “feet” (1 cm length) were cut from pasteur pipettes and glued onto each half coverslip with a drop of PDMS. The glass feet provided a distance of 3 mm between coverslip and culture dish and prevented crushing of the neurons. For curing and sterilization the coverslips were baked for 4 h at 180°C (fig. 3-3). Hydrophilization and coating were performed as described above.

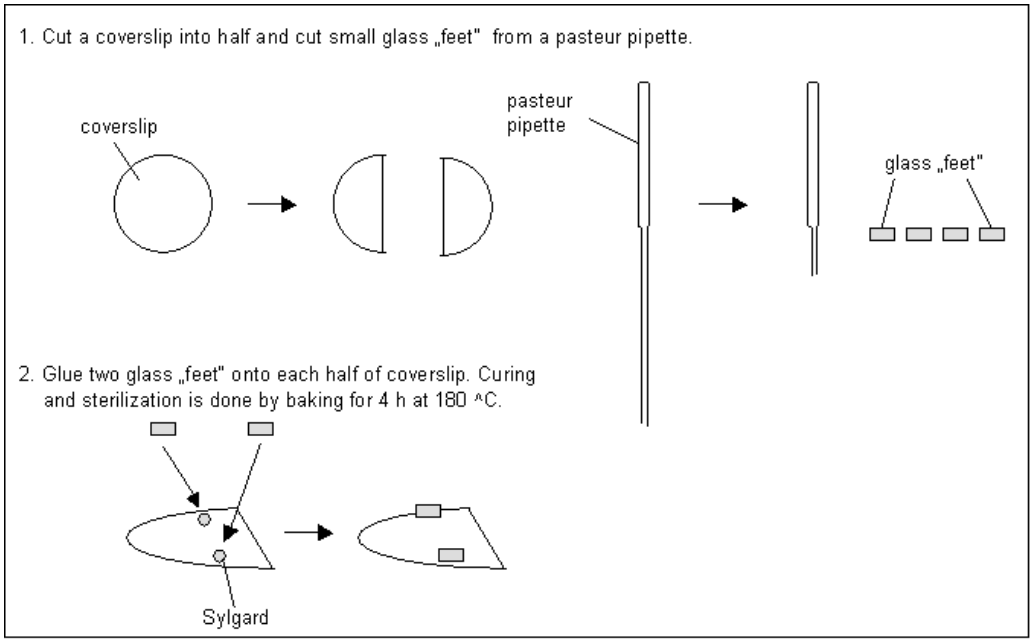


Fig. 3-3: Production of coverslips with glass feet.

3.3.2 Cortical cell culture

Brewer *et al.* (1993) established a serum–free neuronal cell culture. Instead of serum a mixture of serum-free supplements (B 27) and a defined medium, the neurobasal medium, provide optimized concentrations of several hormones, amino acids, vitamins and antioxidative agents. The serum-free, B 27 containing cell culture medium reduces glial cell proliferation and enables a low density neuronal cell culture (Brewer *et al*, 1993). For culturing cortical neurons (dissertation of A. Vogt, 2003) 18 days old rat embryos (E 18) taken from pregnant Wistar rats (Charles River) were removed from uterus and amnion. Each step of preparation was performed in 1 ml ice-cold, sterile $HBSS^-$. One embryo was taken per preparation and placed in a culture dish filled with $HBSS^-$. The head was removed using dissection scissors and transferred to a second culture dish with $HBSS^-$, where the brain was first dissected and then placed into a fresh culture dish with $HBSS^-$. Meninges and hippocampus were removed from the cortical tissue. The cortex was stored in 15 ml $HBBS^-$ in a falcon tube on ice. Further tissue preparation was carried out as described in fig. 3-4: After removing excess $HBSS^-$ the tissue was triturated with a silanized, fire-polished pasteur-pipette in

1 ml $HBSS^-$. Two ml of $HBSS^+$ were added carefully to the suspension and stored vibration-free for 3 minutes. This allowed non-dispersed tissue to settle down at the bottom of the tube. The clear supernatant was transferred into a fresh 15 ml falcon tube and centrifugated for 2 minutes at RT at 200g. The pellet was resuspended in 1 ml neurobasal medium supplemented with 2% B27 and 0.5 mM glutamine (further abbreviated as NB-medium). For determining the number of vital cells 20 µl cell suspension and 40 µl medium were mixed with 20 µl tryphan

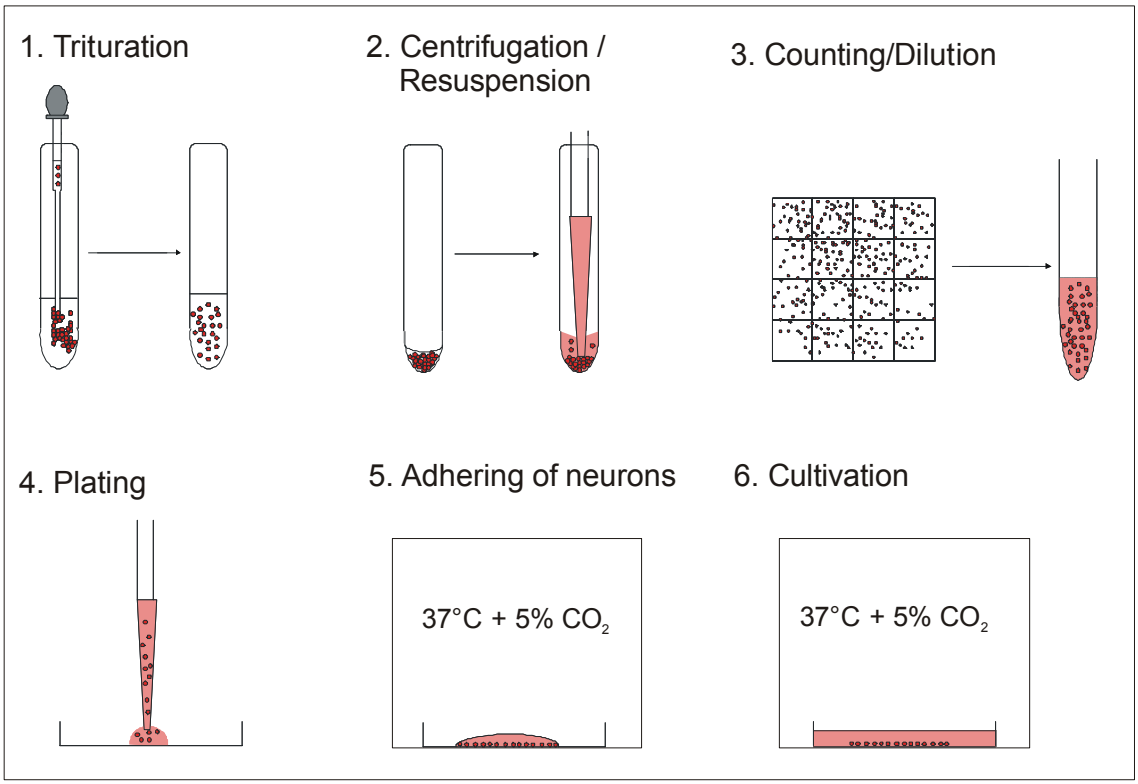


Fig. 3-4 : Scheme of neuronal tissue preparation and cell culture.

blue and counted using a Neubauer counting chamber. Living cells appear bright in phase-contrast while dead cells are stained blue. Cortical neurons were plated with a density of $1.6x10^4$ cells/cm² on completely coated cell culture dishes and half coverslips with glass feet for coculture. On micropatterned substrates $0.8x10^4$ cells/cm² were used. After 1 h incubation at 37°C and 5 % CO_2 excess medium was removed and the culture dishes were filled up with 1.6 ml fresh medium. In the 24-well plates the wells were filled up with 500 µl fresh medium. Half of the medium was changed every 3-4 days.

3.3.3 Striatal cell culture

The protocol for the striatal cell culture was established with slight modifications to the existing cortical cell culture protocol (see 3.3.2). Cortical neurons were dissected from 18 days old rat embryos and cultured in neurobasal medium supplemented with 2% B 27 and 0.5 mM L-glutamine (NB-medium). The protocol differs only in the dissected part of the embryonic brain. Striatum of 18-19 days old embryos (E18-19) is localized in the first anterior third of the brain hemispheres (Altman *et al.*, 1994; Mizushima *et al.*, 2000; fig. 3-5). Striatal tissue from 4-5 embryos was collected and triturated in 1 ml $HBSS^-$. The preparation yielded 1.5 -2 x 10^6 cells, depending on the size of the dissected embryos.

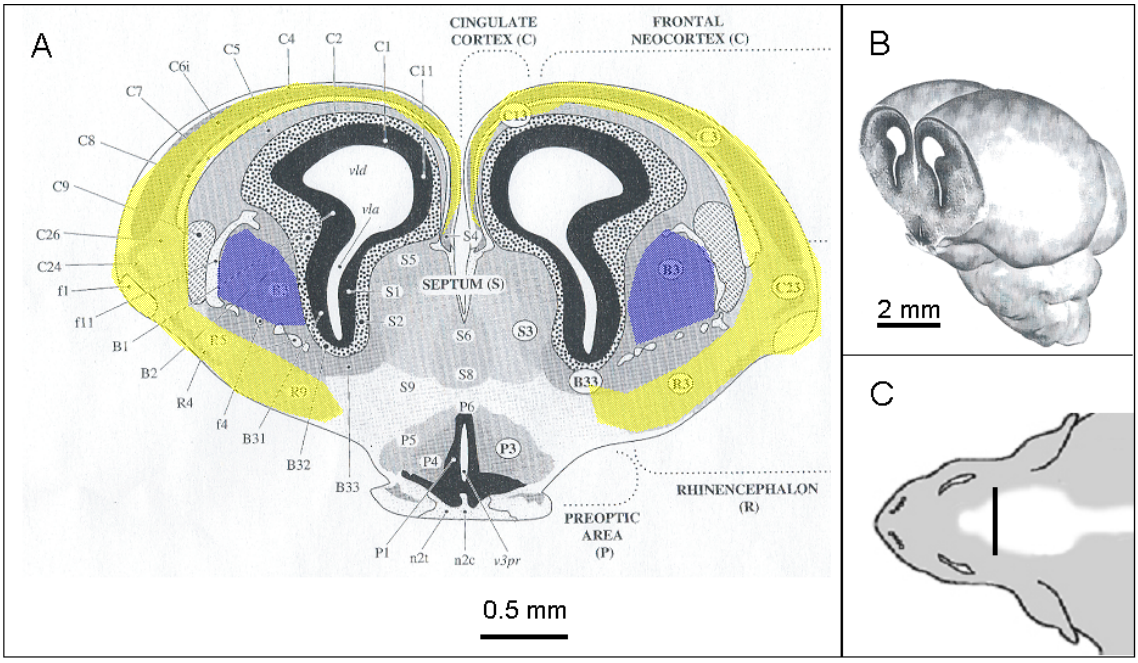


Fig. 3-5: Localization of striatum and cortex in rat E19 brains. A: scheme of a coronal section through the first third of the hemispheres. The dissected striatum is marked blue, while the dissected cortical area is marked yellow. B: three-dimensional image of a rat brain with a coronal section through the first third of the hemispheres. C: localization of the coronal section shown in A and B in the rat brain (modified from Altman *et al.*, 1994).

3.4 Immunofluorescence

For antibody staining cultures were prepared at DIV 10-14 as follows: After removing the medium cultures were washed twice with prewarmed (37°C) phosphate-buffered saline (PBS). The neurons were fixed with 4°C cold, freshly made 4% paraformaldehyde in PBS, pH 7.4, for 7 min. After washing 3x7 minutes with PBS unspecific binding sites were blocked with 2% bovine serum albumin (BSA) and 4% goat serum in PBS for 1h at room temperature. The cells were permeabilized with 0.1 % Triton-X 100 in PBS containing 2% bovine serum albumin (BSA) and 4% goat serum for 15 minutes and washed three times for 7 minutes with PBS. The coverslips were placed upside down onto a drop of antibody solution sitting on a piece of parafilm. For 8 cm² coverslips 100 µl were necessary, for 1.13 cm² coverslips 25 µl. First, antibodies were diluted in PBS and applied for 60 minutes in a humid chamber at RT. After washing three times for 3 minutes with PBS, secondary antibodies were also diluted in PBS and applied for 30 minutes in a humid chamber at RT. After washing three times for 3 minutes with PBS the coverslips were dipped into Milli Q in order to reduce the salt concentration. Excess water was carefully removed by setting the coverslip onto a paper tissue. Furthermore, a drop of mounting medium was placed onto a glass slide. The coverslip was put upside down and excess mounting medium was carefully wiped away. After 1-2 h at RT the mounting medium was cured, then the samples were stored at 4°C protected from light until analysis (up to 1 week). The samples were visualized with an Axiovert 200 (Zeiss) equipped with a mercury vapour lamp (IX-FLA, Olympus) and an appropiate filter set. Pictures were taken with an AxioCam color (Zeiss). For pictures with a higher resolution a Laser scanning microscope (Zeiss) was used.

In this thesis the following antibodies were used:

antibody	specificity	host		dilution	Cat.-number	Distributor
anti-microtubuli associated protein 2 (MAP2)	neuron-specific	rabbit	polyconal	1:1000	AB5622	Chemicon
anti-tau	axon-specific up to DIV 5	mouse	monoclonal	1 :200	MAB3420	Chemicon
anti-glial fibrillary acidic protein (GFAP)	glia-specific	mouse	polyclonal	1:100	MAB3402	Chemicon

Tab. 3-2: Primary antibodies.

antibody	fluorophor	host		dilution	Cat.-number	Distributor
anti-rabbit	TRITC (tetramethyl rhodamine isothiocyanate)	donkey	polyconal	1:100	711-166-152	Dianova
anti-mouse	FITC (fluorescein isothiocyanate)	donkey	polyclonal	1 :100	715-096-150	Dianova
anti-rabbit	Alexa 568	goat	polyclonal	1:1000	A11011	Molecular probes
anti-mouse	Alexa 488	goat	polyclonal	1:1000	A11001	Molecular probes

Tab. 3-3: Secondary antibodies.

3.5 Electrophysiologal measurements in patterned neuronal cell culture

Patch-clamp measurements provide very detailed information about electrically active cells. Neuronal cell culture allows electrophysiological measurements of single neurons by recording APs in the current clamp mode and by measuring ionic currents across the membrane in the voltage clamp mode. In addition to single cell analysis, double patch-clamp measurements can be performed. In patterned neuronal cell culture it is further possible to characterize single synapses and the direction of signal transmission (polarity). Moreover, changes in synaptic strength due to high or low frequency stimulations can be observed.

3.5.1 Patch-clamp technique

The patch clamp technique was invented in order to measure small currents from ion channels (Neher *et al.*, 1976). Small membrane patches were isolated electrically by pressing the tip of a very fine, fire polished glass pipette on the cell membrane. This tight seal to the cell membrane is called Gigaseal according to the pipette resistance which rises to 1 or more Gigaohm. Starting from a Gigaseal four possible configurations can be reached: In the cell-attached configuration (fig. 3-6) a glass pipette is attached and sealed to the membrane. Currents flowing between the cytoplasma and the extracellular bath solution through the trapped ion channels can be measured. In the whole-cell configuration the cell membrane under the pipette is ruptured resulting in a direct contact between pipette solution and cytoplasma (fig. 3-6). Gradually the cytoplasma is replaced by the intracellular pipette solution which thereby has to be isoosmotic to the cytoplasma and should contain similar concentrations of cytoplasmic ions. In this configuration electrical signals of the whole cell are recorded. Starting from the cell-attached configuration two other configuration can be reached. In the inside-out configuration the pipette is pulled back from the cell. As a result a membrane patch sticks to the pipette tip and the interiour side of the membrane now faces the extracellular bath solution (fig. 3-6). By using different bath solutions the effect of certain compounds on the ion channels in the patch can be observed. In the outside-out configuration the

membrane ruptures and the free ends reseal due to gently pulling back of the pipette. The exteriour side of the membrane faces the extracellular bath solution (fig. 3-6).

The whole cell configuration includes two different measurement modes: In the voltage-clamp (VC) mode the membrane potential is clamped to defined values. Changes in membrane potential such as APs are prevented by injecting an equal current of opposite direction into the membrane. Stepwise hyper- or depolarizing

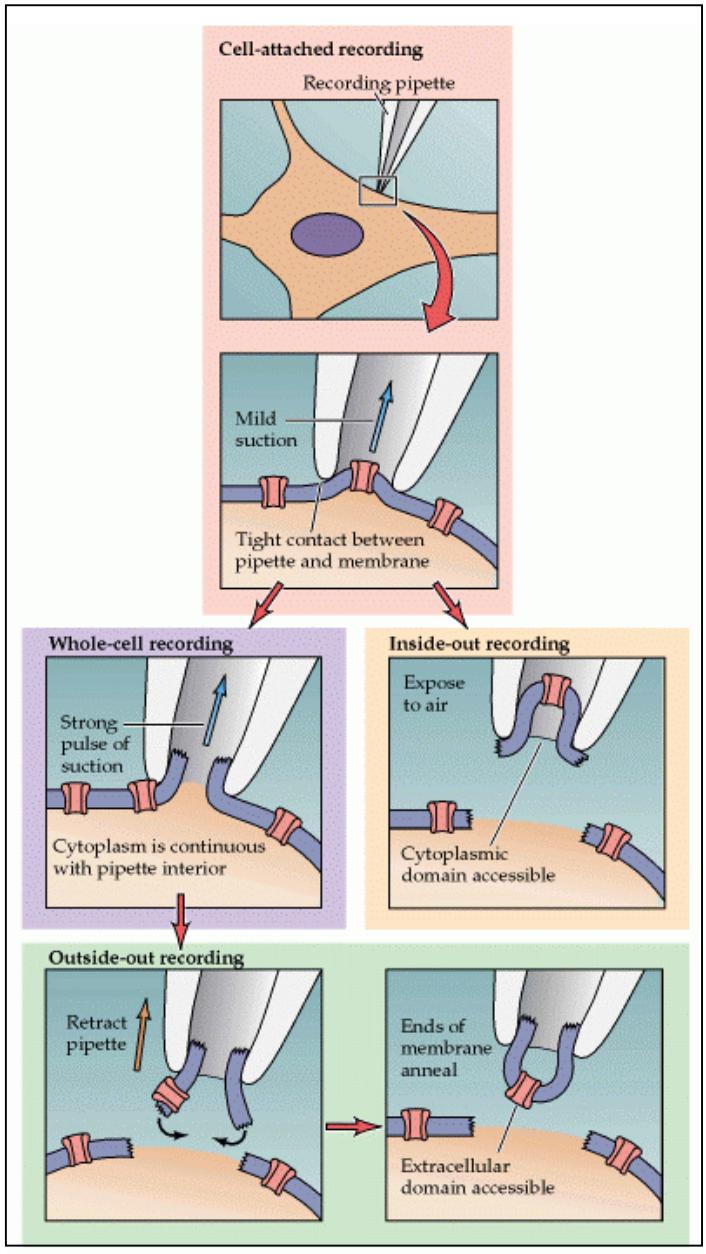


Fig. 3-6: The four possible configurations of a patch clamp measurement: Cell attached mode; whole cell mode; inside out mode and outside out mode (Purves *et al.* , 2004)

voltage pulses are applied. At a certain threshold, voltage-sensitive ion channels open and the resulting inward or outward currents are recorded. Inward membrane currents are considered negative, while outward membrane currents are displayed as positive (Hille, 2001).

A typical VC-measurement is shown in fig. 3-7.

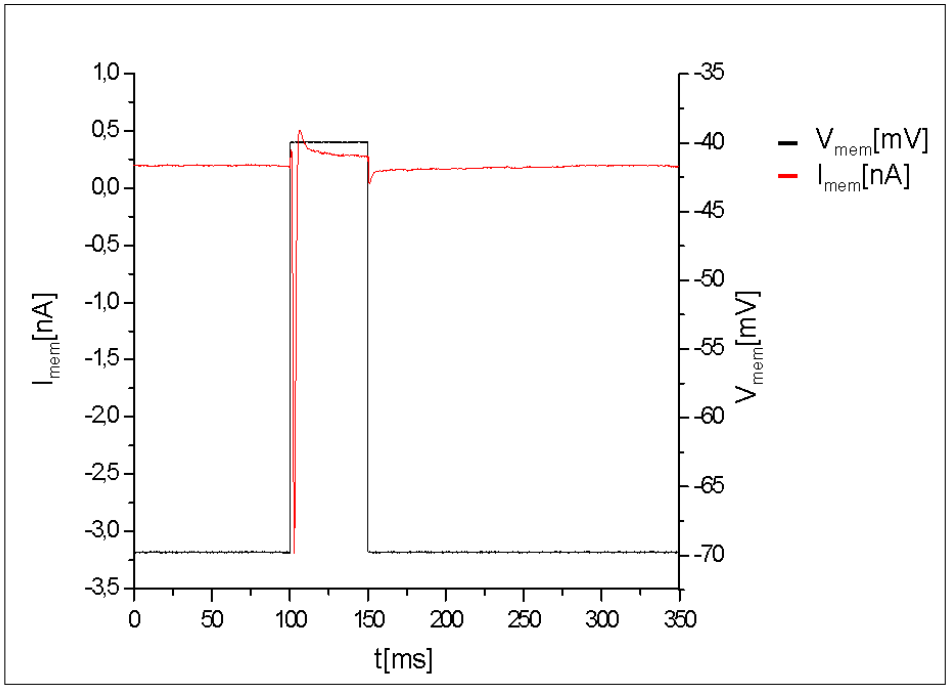


Fig. 3-7: Typical voltage-clamp measurement. A rectangular depolarizing voltage pulse leads to a depolarization of the cell membrane above the threshold for voltage-gated sodium channels. This results in a strong inward current. Shortly afterwards the sodium channels close while voltage-gated potassium channel open resulting in an outward current.

In the current-clamp (CC) mode the cell is clamped to a constant current. Stepwise applied depolarizing current pulses lead to a depolarization above firing threshold and APs can be recorded. The resting potential of a neuron can be measured by applying no current. A typical CC – measurement is shown in fig. 3-8.

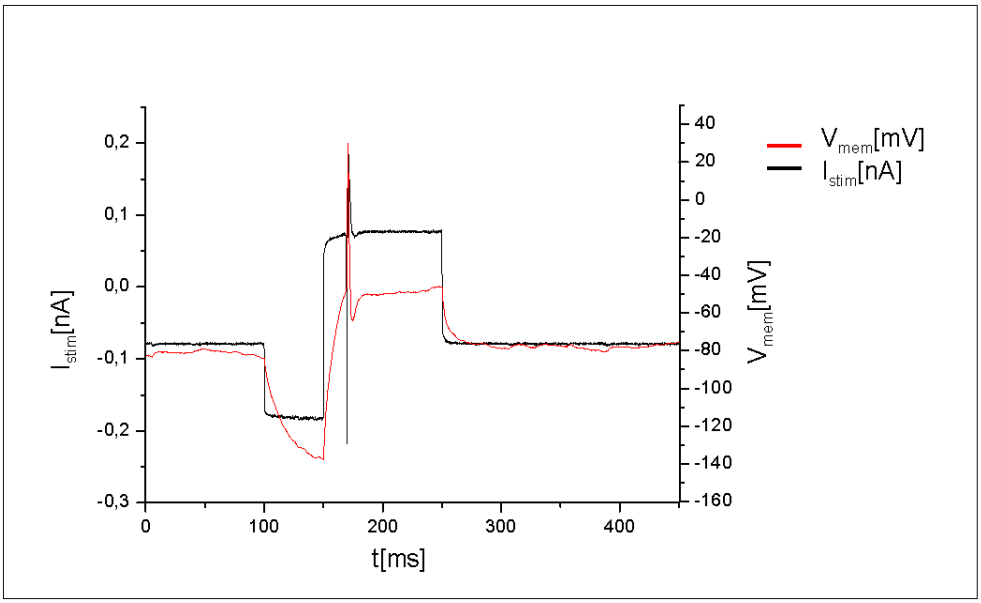


Fig. 3-8: Typical current clamp experiment. A current pulse first hyperpolarizes the cell membrane in order to close all channels. The cell membrane is depolarized until the membrane potential reaches the firing threshold. The opening of voltage-gated sodium channels evokes an action potential. The deviation from the rectangular pulse in the current trace results from the fact that the amplifier does not compensate the changes in membrane conductance fast enough.

3.5.2 Experimental set-up for patch-clamp experiments

For patch-clamp experiments, the following electrophysiological set-up was used (fig. 3-9): Neurons were recorded and stimulated with an EPC-9/3 patch-clamp amplifier (HEKA Elektronik, Germany) operated by TIDA 5.0. Three micro-manipulators (Luigs & Neumann GmbH, Germany) allowed movement of the patch pipettes in µm-range. Each micromanipulator consisted of three motors for movements in x-, y- and z-direction. It is connected to an amplifier head which holds the patch pipette. A silicon tube connected with the patch pipette allowed the application of negative pressure or overpressure . The petridish with neurons was placed onto an inverted transmitting light microscope (Olympus IX50, Zeiss, Germany) which was equipped with phase contrast and mounted on a vibration-free, air cushioned table (Newport, USA). The microscope was provided with a fluorescence illumination and an appropriate filter set for fluorescein and rhodamine. A digital video camera (Sony XC-333 P, Sony International Europe

GmbH) allowed better visual control during pipette approach to a neuron and image acquisition.

An Ag/AgCl electrode was used as ground contact. Therefore, a silver wire was chlorinated for 30 s in 1 M HCl by biassing it with 3 V.

In order to reduce interference due to electrical noise the setup was shielded by a Faraday cage.

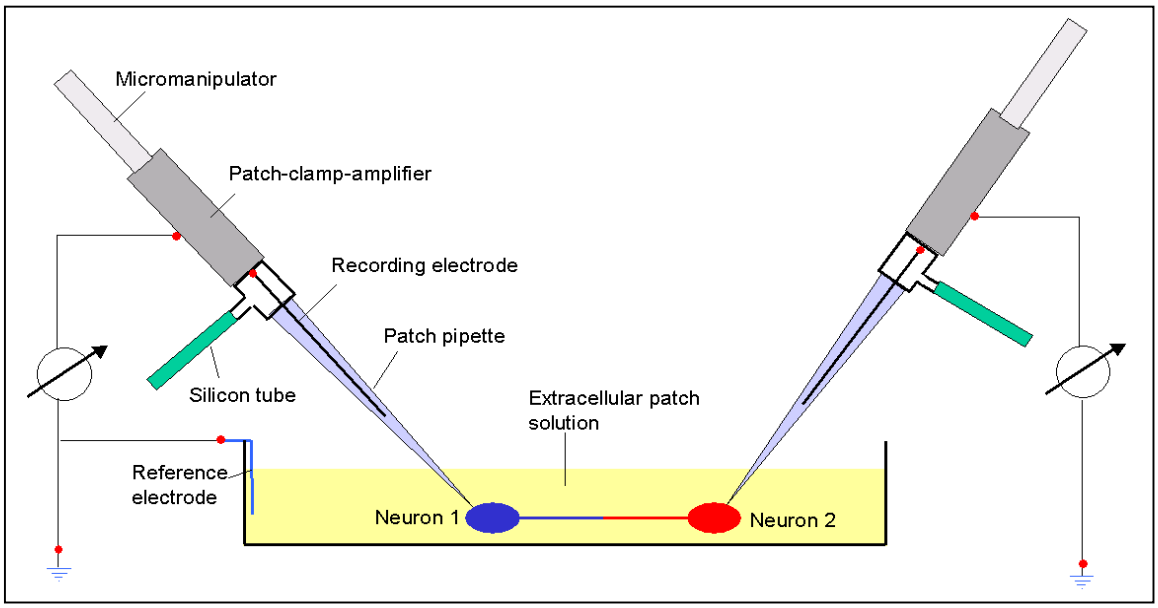


Fig. 3-9: Patch-clamp-setup for double-patches (scheme). A silver/silver chloride electrode is inserted into a patch pipette filled with intracellular patch solution. The electrode is mounted onto an amplifier head which in turn is fixed to a micromanipulator unit. This unit allows to move the pipette with a high precision. The tip can be closely approached to the cell membrane and a Gigaseal can be obtained. Through a silicon tube, over- or underpressure can be applied to the pipette. A reference electrode in the bath solution closes the electrical circuit. While stimulating neuron 1 the second neuron is recorded simultaneously and *vice versa.*

3.5.2.1 Procedure for Double patch-clamp measurements

One aim of this thesis was the control of polarity within a neuronal network. Thus double patch-clamp measurements were performed in whole-cell configuration to record synaptic transmission between two morphologically connected neurons. Synaptic connections were identified by alternate stimulation of both neurons. The presynaptic neuron was held in the CC-mode at resting potential or at –70 mV in order to evoke APs while the postsynaptic neuron was held in the VC-mode and clamped down to –70 mV. Alternatively, both neurons could be held in either in VC-mode or CC-mode. If the presynaptic APs or currents generated a postsynaptic current or potential a synaptic connection was confirmed. The type of synapse, emitted neurotransmitters and postsynaptic receptors could be determined using the postsynaptic response, synaptic delay, reversal potential and the direction of the synapse. For inducing APs or extracellular postsynaptic currents (EPSCs) first a hyperpolarizing pulse (50/100 ms, - 200 pA) was applied in order to close all voltage-gated ion-channels. Then stepwise depolarizing pulses (- 200 to 300 pA , 50/100 ms) lead to a depolarization above the firing threshold. The weakest pulse which induced an AP was given 10 times and the recordings were averaged. In the following, the experimental procedures will be explained in detail.

1. Culture medium was replaced by an extracellular patch solution (EP; see 3.5.2.5). This garanties the same ionic concentrations, osmolarity and pH in each experiment.
2. An intracellular patch solution (IP, see 3.5.2.5) was filled into borosilicate glass pipettes (R_{pip} 8-10 MOhm). A positive pressure was applied to the pipette by a silicon tube connected with the pipette. This leads to a constant flow of IP out of the pipette tip and prevents blocking of the pipette tip by particles. The voltage offset due to different ionic concentrations and strengths of EP and IP was corrected during data analysis and added to the measured resting potential V_{rest} of the membrane.
3. The pipettes were immersed into the bath solution and positioned near two morphologically connected neurons. The offset potential due to an electrochemical potential between chlorinated silver wire electrodes and the used patch solutions was adjusted to zero. During approach the resistance

of the pipette (R_{pip}) was calculated by applying a small voltage pulse (10 mV) and measuring a proportional current. The optimal distance for sealing could be determined by an increase of R_{pip} of about 0.5-1 Megaohm and a dark half-moon forming around the pipette tip in phase-contrast microscopy. This dark half-moon is a dent in the membrane and caused by the efflux of IP. Release of the positive pressure at the pipette along with slight negative pressure achieved sealing.

4. V_{mem} was set to –50 mV and the capacitance (C_{fast}) of the pipette was compensated. Electrical contact to the neuron was achieved by opening the membrane with a brief suction. V_{mem} was set to –70 mV and the series resistance R_{ser}, resting potential V_{rest}, membrane capacitance C_{mem} and leak conductance were measured. For further experiments C_{mem} (C_{slow}), R_{ser} and leak conductance were compensated in order to obtain only recordings resulting of induced changes of the membrane conductance.

A good seal is marked by a resting potential under – 50 mV (offset potential added) and a leak conductance smaller than 5 nS. In addition to the described steps, for the measurement of synapses each neuron was clamped to –70 mV in the VC mode in order to get current/voltage relations. The duration of the AP at the half maximum amplitude (“full length at half measurement” (FLHM)) was determined from recordings of APs which were induced by a current pulse of 150 pA. AP frequency was determined from the same recordings; APs with an amplitude lower than 30 mV were counted as 0.5 APs. A low FLHM and a high amount of APs are a criterion for fit neurons either due to ion channels with a fast kinetic or a high amount of ion channels in the cell membrane.

3.5.2.2 Membrane time constant tau

The membrane time constant tau (τ) describes the passive properties of the cell membrane due to the diffusion of ions through open ion channels and the function of the cell membrane as lipid bilayer. This constant can be determined with three different methods:

a) Tau is defined as product of the measured membrane resistance R_{mem} and the membrane capacitance C_{slow}.

$$C_{slow} \times R_{mem} = \tau \qquad \text{Eq 3.2}$$

b) Calculation of τ by solution of the equation

$$V(t) = V_0 \times e^{-(t_0 - t)/\tau} \qquad \text{Eq 3.3}$$

with V_0 = offset voltage, t = time of repolarization to V_{rest}, t_0= end of hyperpolarizing current pulse and τ = decay time.

c) Approximate solution of the equation 3.3 by graphical evaluation of current-clamp data to a hyperpolarizing current pulse. τ is equal to the time, in which V_{mem} repolarizes to $1/e^{-1}$ (~63%) of the original value (fig. 3-10).

In this thesis τ was determined by graphical evaluation on decaying hyper-polarizations due to 100 pA current pulses.

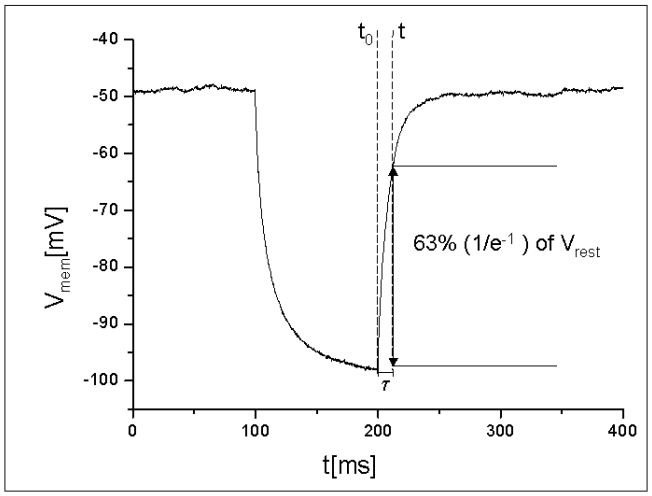


Fig. 3-10: Illustration of τ determination. It was calculated by measurement of the decay time to $1/e^{-1}$ (~63%) of $V_{rest.}$

3.5.2.3 Current density / voltage relations

Current density/voltage relations provide information about the kinetics of voltage-gated ion-channels. In a voltage-clamp-measurement with stepwise depolarization the maximum resulting currents, representing the membrane conductance, were measured as illustrated in fig. 3-11. The maximum amplitude of inward currents I_{in}(max) and the amplitude of sustained outward currents I_{out}(sus) are measured and plotted against the V_{mem} induced by the associated voltage step. The resulting graph shows at which membrane potential the voltage-gated ion channels open.
In addition, it was a criterion for the fitness of neurons. Neurons with slowly increasing outward currents or slowly decreasing inward currents were excluded from analysis.

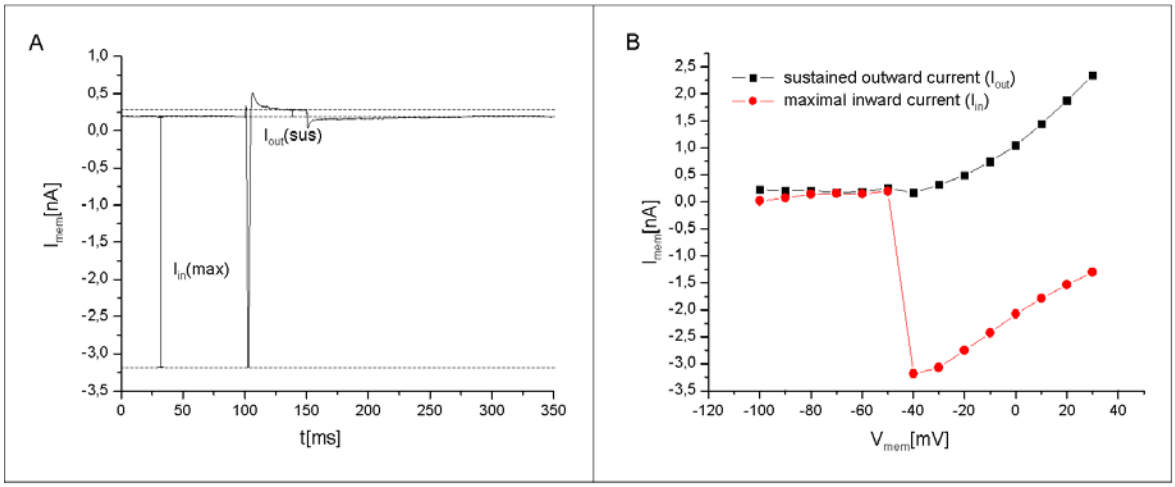


Fig. 3-11: Exemplary illustration of the analysis for current-voltage relations. A: Whole-cell patch-clamp recording (voltage-clamp mode) of a striatal neuron (V_{rest} –70,7mV; DIV 20). The amplitudes of the maximum inward current I_{in}(max) and the sustained outward current I_{out}(sus) were determined by measuring their differences to the current at membrane potential. B: Plot of a current-voltage relation. Measured currents were plotted against the applied voltage step.

3.5.2.4 Synaptic delay

Synaptic delay is a criterion for discrimination between chemical and electrical synapses. Electrical signals which are propagated by electrical synapses have a time delay < 0.3 milliseconds (ms), whereas release of neurotransmitters, their diffusion across the synaptic cleft and generating electrical signals by gating of postsynaptic channels takes at least 0.3 ms, usually 1-5 ms or longer (Kandel *et al.*, 2001).

Fig. 3-12 shows a current-clamp recording of two morphological connected neurons. The presynaptic neuron (red) was held at resting potential in CC-mode while the postsynaptic neuron was clamped to –70 mV in VC-mode. Synaptic delay was defined as the time Δt between the peak of an AP and the onset of the postsynaptic response.

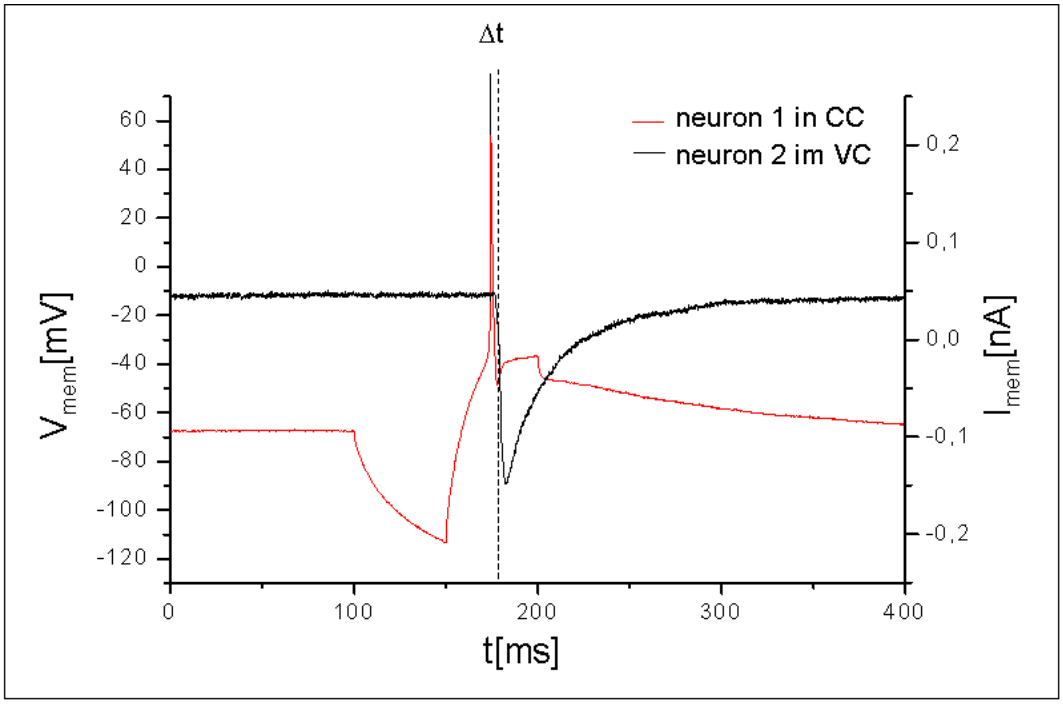


Fig. 3-12 : Double patch-clamp measurement of two cortical neurons at DIV 11. The presynaptic neuron 1 (red) was held at resting potential in CC-mode while the postsynaptic neuron 2 (black) was clamped to –70 mV in VC-mode. Synaptic delay was defined as the time Δt between the peak of an AP and the onset of the postsynaptic response.

3.5.2.5 Patch solutions

Extracellular patch solutions (EP) should have a similar osmolarity as the culture medium of neurons in order to prevent hypo- or hyperosmolar neurons. The intracellular patch solution (IP) has a slightly higher osmolarity than the extracellular patch solution. Experiments were done with the patch solutions described in tab. 3-4. A high-potassium (IP 1) and a low-potassium (IP 2) intracellular patch solution were tested. Low potassium-concentrations allow precise measurement of chloride-currents, but no significant differences were observed in patch-clamp experiments with IP 1 compared to patch-clamp experiments with IP 2. Thus data from these experiments were pooled.

	Extracellular bath solution [mM]	IP 1 [mM]	IP 2 [mM]
K-gluconate	-	116	112
NaCl	130	-	-
KCl	3	20	20
$MgCl_2$	1	1	1
$CaCl_2$	2	0.1	0.1
HEPES	10	10	10
EGTA	-	0.2	5
Mg-ATP	-	4	4

Tab. 3-4: Composition of extra- and intracellular patch solution.

The pH was adjusted to 7.3 by 1 M NaOH (EP) or 1 M KOH (IP) and 1 M HCl. The osmolarity of the EP was measured with an osmolarimeter and was about 270 mosmol/kg. The osmolarity of the IP 1-2 was measured and was about 275 mosmol/kg. The liquid junction potential was calculated with the junction potential calcultor program (copyright © 1996 Peter H. Barry (School of Physiology and Pharmacology, The University of New South Wales, Sydney, Australia) and Axon Instruments, Inc. (Foster City, CA, USA). It is 14.0 mV for IP 1 and 14.1 mV for IP 2.

3.6 Ellipsometry

Ellipsometry is a very sensitive optical method for the characterization of surfaces (Matacotta *et al.*, 1995). It uses changes in the polarization state of light due to reflection at a surface in order to calculate a layer thickness on a reflective surface. In general the state of the light polarization is elliptic. Ellipsometry is often used in thin film analysis since the entire system substrate/film influences the change in polarization. Thus it is possible to acquire information about the film properties, e.g. the film thickness.

Light can be considered as an electromagnetic wave. The electric field E of a plane wave is described by:

$$E(r, t) = E_0 * e^{i(kr-\omega t)}$$

Plane waves are typically referenced to a local coordinate system (x, y, z) where z is the propagation direction and x and y are directions parallel (p) and perpendicular (s), respectively, to the plane of incidence. Now the E vector can be described by two harmonic oscillations along x and y with the same frequency but different amplitude and phase. As a result, at a fixed point in space the E vector moves along an ellipse. If the phase of the x and y oscillation is equal, the resulting ellipse transforms into a straight line. If the phase difference is +/-90° and the amplitudes are equal, the ellipse becomes a circle. Thus, linear and circular polarization are the limiting cases of the general elliptical state. For all other phase differences, a „true“ ellipse evolves. In an ellipsometric measurement

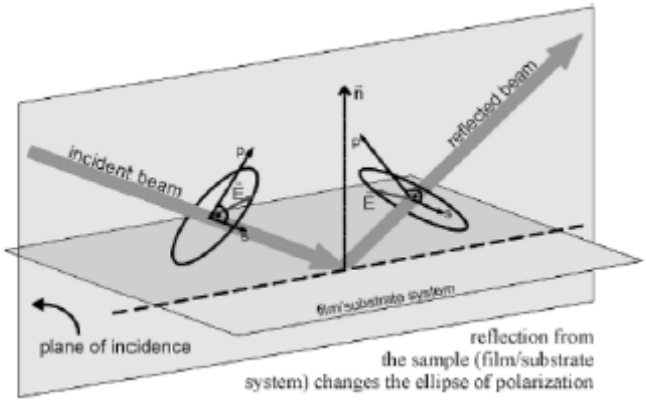


Fig. 3-13: Schematic process of ellipsometry (Nanofilm GmbH, EP3 operation instructions).

monochromatic, polarized light is reflected at the surface of a sample (fig. 3-13). The electromagnetic wave interacts with the sample to finally form the reflected light wave with an altered state of polarization. The known state of polarization x^i is transformed into x^0 after reflection according to:

$$\rho = \frac{x^0}{x^i} = \frac{r_p}{r_s}$$

where r_p and r_s are complex reflection coefficients for p- and s-polarized light, respectively. The complex reflection ratio ρ can also be represented by the angles Ψ and Δ:

$$\rho = \tan\Psi * e^{i\Delta}$$

The meaning of Ψ is an angle whose tangent gives the ratio of amplitude change for the p and s component, while Δ denotes the relative phase shift of the p and s component upon reflection.

Nulling Ellipsometry: In general, a linearly polarized light beam has an elliptical state of polarization after reflection by a substrate. The same elliptical state of polarization (but with reversed direction of rotation) incident on the surface will generate a linearly polarized reflection. This linear polarization can be detected by using a second polarizer as an analyzer in the reflected beam. Due to the fact that two linear polarizers at an angle of 90° („crossed polarizers“) do not transmit light it is possible to extinguish a linear polarized light beam by setting the second polarizer to a 90° position with respect to the axis of the linear polarization. Doing this is called „finding the Null“ or „nulling“. In this position the ellipsometer is most sensitive to changes in the polarization state of light caused by reflection on a thin film.

Measurement Setup: The typical setup of Ellipsometry is shown in fig. 3-14. The

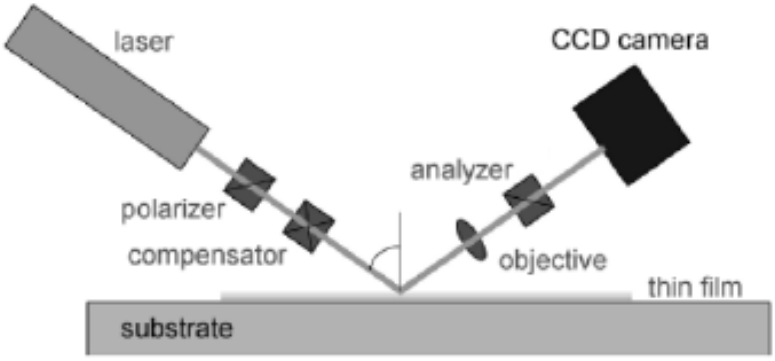


Fig. 3-14: Schematic setup of ellipsometry (Nanofilm GmbH, EP3 operation instructions).

light beam is usually produced by a Laser and polarized by a polarizer. The compensator leads to an elliptical state of polarization of the light beam. After reflection by the sample the light beam is linearly polarized. Afterwards, the electromagnetic wave is led through an analyzer and into the detector. As detector a CCD_5 camera can be used. The ellipsometer does not give absolute values of protein film thickness but provides the averaged protein thickness over an area.
Layer thicknesses were determined using a Nanofilm EP_3 ellipsometer with a Nd:YAG Laser (λ= 532 nm) and EP_3 View 2.05 software. With the mapping function it was possible to measure the thickness in an area of 1000x1000 µm. The angle of incidence was usually 42°. Substrates with an artificial SiO_2 surface layer of about 7.5 nm fabricated by dry oxidation were used for ellipsometric analysis. Calculations of film thicknesses were always carried out with the refractive index of silicon dioxide (n = 1.6678; k= 0.001; both calculated from a four-angle measurement). The thickness was calculated in the range between 0 and 80 nm.

3.7 Atomic force microscopy

The atomic force microscope (AFM) is a very high-resolution type of scanning probe microscope, with a demonstrated resolution of below an Angstrom, more than 1000 times better than the optical diffraction limit.
The AFM consists of a microscale cantilever with a sharp tip (probe) at its end that is used to scan the sample surface. The sample is attached to fine piezoelements for carefully pressing it against the tip.The cantilever is typically made of silicon or silicon nitride with a tip radius of curvature on the order of nanometers. When the tip is brought into proximity of a sample surface, forces between the tip and the sample lead to a deflection of the cantilever according to Hooke's law. Typically, the deflection is measured using a laser spot reflected from the top of the cantilever into an array of photodiodes (fig. 3-15).

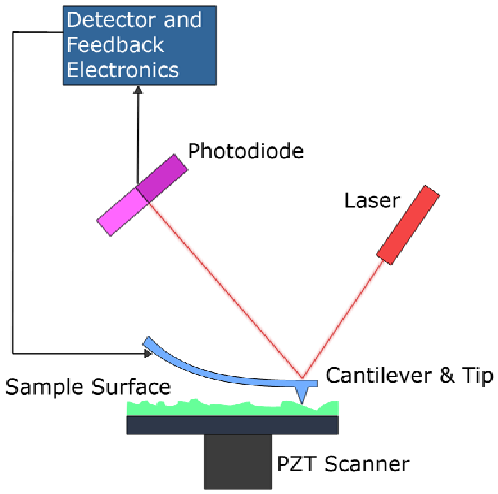


Fig. 3-15: Scheme of an atomic force microscope.
(http://en.wikipedia.org/wiki/Atomic_force_microscope)

There are three different modes of AFM measurements.

Contact mode: In contact mode the tip is brought into contact with the surface and the cantilever deflection is kept constant during scanning by a feedback loop. The measured surfaces of constant force represent the topography. Because the tip is permanently in contact with the surface while scanning, a considerably shear force can be generated, causing damage to the sample, especially on very soft specimens. Atoms or molecules can be pulled out of the surface which leads to a modified surface topography and uncontinuous imaging conditions.

Tapping mode: In tapping mode (also: intermittent contact mode) the tip is not constantly in contact with the sample. The cantilever is stimulated to vibrate near its resonance frequency and scans the surface in a distance of typically 1 to 100 nm. The tip touches the surface only intermittently. Interaction between sample and tip leads to a damping of the tip oscillation and a reduction of the amplitude (fig. 3-16). The oscillation amplitude is maintained constant by a

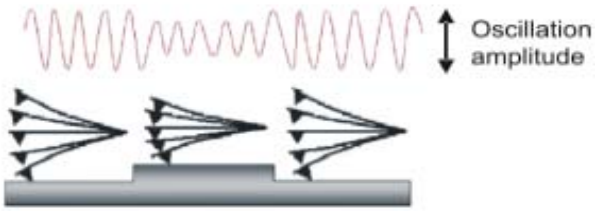


Fig. 3-16: Schematic representation of an AFM tip operating in the tapping mode (Alessandrini *et al.*, 2005).

feedback loop. The short tip – sample contact time prevents inelastic surface modification.

Non-contact mode:

In non-contact mode the cantilever is oscillating near its resonance frequency, like in tapping mode, and brought into proximity of the surface, however without touching it. The van-der-Waals attractive forces are sensed. Again, the oscillation amplitude acts as feedback parameter.

Measurement setup: AFM measurements were performed with a Nanoscope IV Multimode atomic force microscope of Veeco Instruments in tapping mode. Veeco tapping mode cantilevers RTESP5 (1–10 cm n-doped silicon, f_0[7] = 251 − 287 kHz) were used. The AFM-images provide a detailed topography of the measured protein layers.

4. Two-step microcontact printing for directed growth of neurons

Previous experiments performed by A. Vogt (Vogt, 2003a) showed that protein-grids consisting of one protein (ECM, poly-D-lysine or laminin) do not induce directed growth of neurons. A main signal direction within the neuronal network cultured on these substrates was not observed.

Several groups achieved directed growth of neurons due to the effect of micropatterns consisting of two different proteins. Esch *et al.* (1999) cultured rat hippocampal neurons on substrates patterned with stripes of poly-L-lysine and either laminin or neuron-glia cell adhesion molecule (NgCAM). The axons were preferentially formed on contact with laminin and NgCAM although the immature neurons attached on poly-L-lysine and either laminin or NgCAM equally. If the neurons were already polarized into an axonal and a dendritic compartment contact with laminin or NgCAM enhanced axon elongation. Similar results have been observed by Oliva *et al.* (2003). Patterned substrates with poly-L-lysine lines crossing lines of the cell adhesion molecule L1 were produced without denaturing the proteins. In cell culture rat cortical axons preferentially grew on the L1-lines while the dendrites remained unaffected.

Therefore, a protein-grid consisting of axon-guiding biomolecules and “neutral” biomolecules which have no axon-guiding effect is a promising approach for the induction of polarity in a neuronal network. Netrin-1 and laminin were chosen as axon-guiding biomolecule. Although the axon-guiding effect of netrin-1 has not been tested in a stripe-assay, it acts as an axon-guiding cue for cortical neurons in explant cocultures (Metin *et al.*, 1997; Richards *et al.*, 1997). Moreover, ECM-gel was selected as axon-guiding biomolecule due to its high content of laminin (about 60 %). Poly-D-Lysine was printed as neutral biomolecule.

4.1 Manual two-step microcontact printing

Two-step microcontact printing (2-step µCP) allows the printing of a protein-grid consisting of two different proteins (scheme fig. 4-1). For manual two-step microcontact printing first a pattern of lines with nodes was stamped on the substrate as described in materials and methods (3.1). In the second step a pattern of lines was printed on top of the first pattern in a 90° angle. The PDMS-stamps were pierced with a thin copper wire (1 mm diameter) in order to mark the direction of the lines.

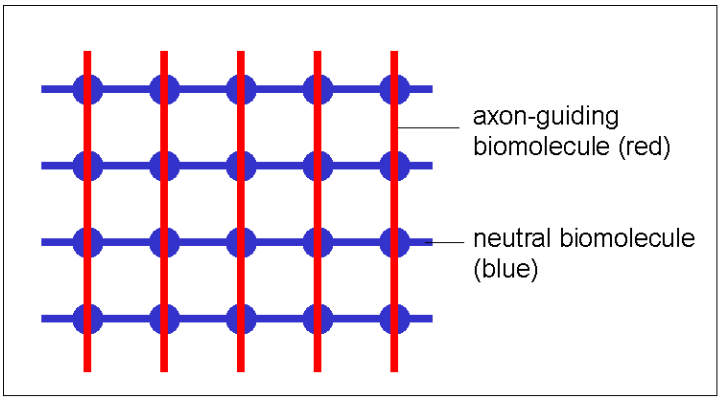


Fig. 4-1: Scheme of manual two-step microcontact printing substrates. A line of an axon-guiding biomolecule (netrin-1, laminin or ECM) is printed in a 90° angle on a preprinted line with nodes of a neutral biomolecule (poly-D-lysine).

The effect of manual two-step microcontact printing on the protein transfer of first and second protein was observed using fluorescence microscopy, atomic force microscopy (AFM) and ellipsometry. This allowed to quantificate protein thickness and the homogeneity of pattern transfer (see 4.1.2 and 4.1.3)

4.1.1 Improved printing of hydrophilic protein “inks” with low viscosity

Compared to the pattern transfer of hydrophilic protein “inks” with a high viscosity (ECM, PECM) onto glass the pattern transfer of hydrophilic protein “inks” with a low viscosity (mixture of poly-D-lysine/laminin, laminin) is inhomogenous during microcontact printing although the hydrophilicity of the stamps was increased by incubation in Milli Q (Vogt, 2003a). Similar observations were made for microcontact printing with the hydrophilic and low-viscosity proteins poly-D-Lysine and netrin-1 (data not shown).

As soon as it is possible to define the polarity within a neuronal network the neural networks should grow on microdevices (FETs and MEAs) with silicon dioxide surface for detailed studies of signal transmissions within a neural network. Thus a good protein transfer on glass (100 % silicon dioxide) is mandatory.

In first experiments the transfer of proteins was tested by printing grids of FITC-coupled poly-L-lysine (FITC-PLL, 50 µg/ml) or TRITC-mixed (50 µg/ml) ECM (80-120 µg/ml), netrin-1 (5 µg/ml) or laminin (25 µg/ml) on glass. For enhanced protein transfer the printing of hydrophilic protein “inks” with low viscosity (e.g. poly-D-lysine) was modified according to Chang *et al.* (2003). This enabled to print these proteins with a similar quality as a mixture of polylysine and ECM. The pattern transfer was homogenous for all tested proteins (fig. 4-2).

The buffers used for the dilution of each protein are listed in materials and methods (see Microcontact printing, 3.1).

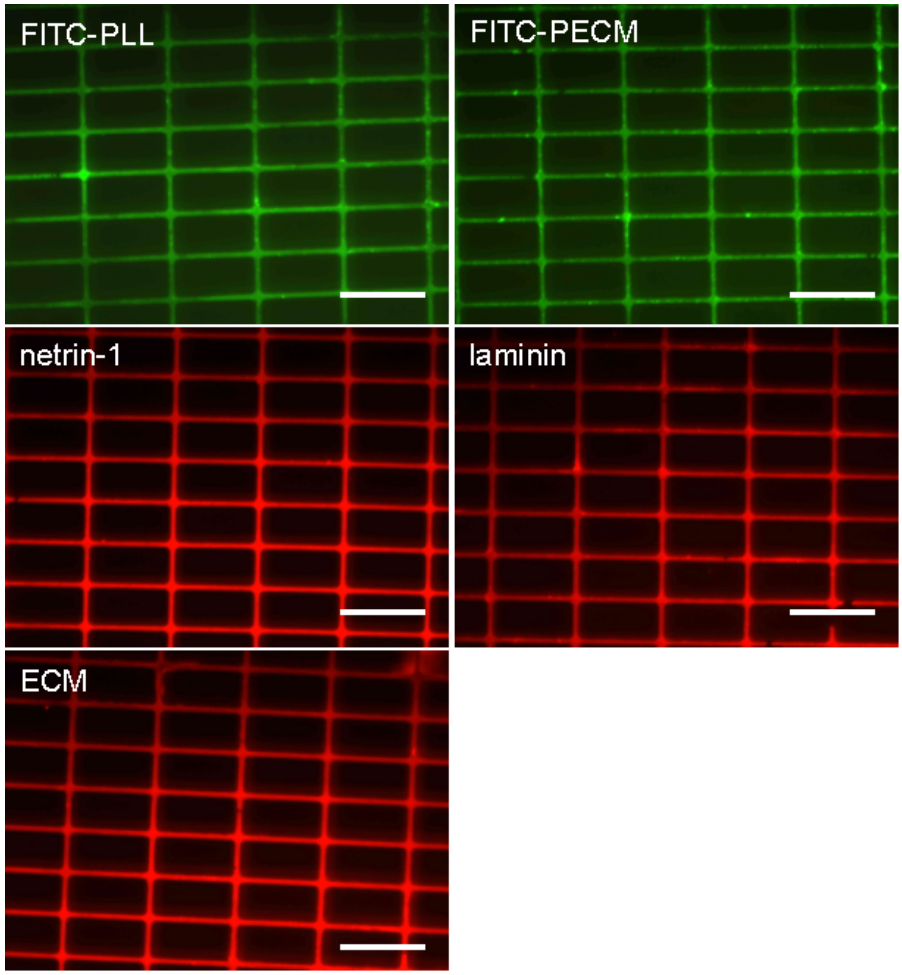


Fig. 4-2: Enhanced transfer of hydrophilic proteins on glass.

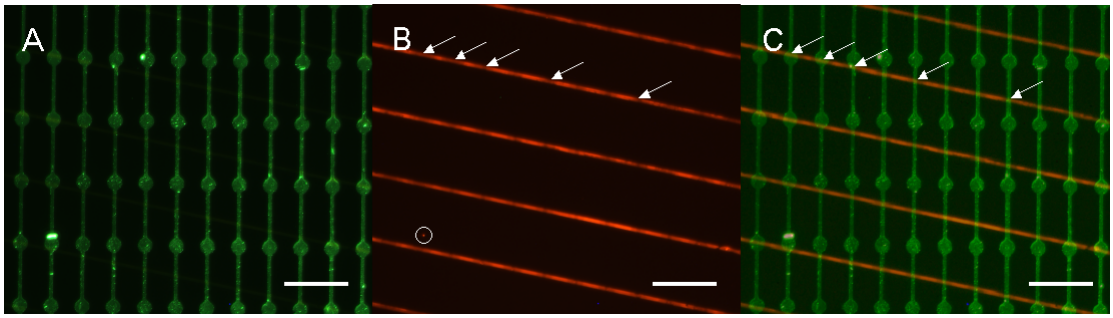
FITC-PLL: FITC-labeled poly-L-lysine (50 µg/ml); FITC-PECM: control, FITC-labeled poly-L-lysine (50 µg/ml) and ECM (80-120 µg/ml); netrin-1: netrin-1 (5 µg/ml) mixed with TRITC; laminin: laminin (25 µg/ml) mixed with TRITC; ECM: control, ECM (80-120 µg/ml) mixed with TRITC. TRITC was added in a concentration of 50 µg/ml. The scale bar is 100 µm.

4.1.2 Analysis of pattern transfer by fluorescence microscopy

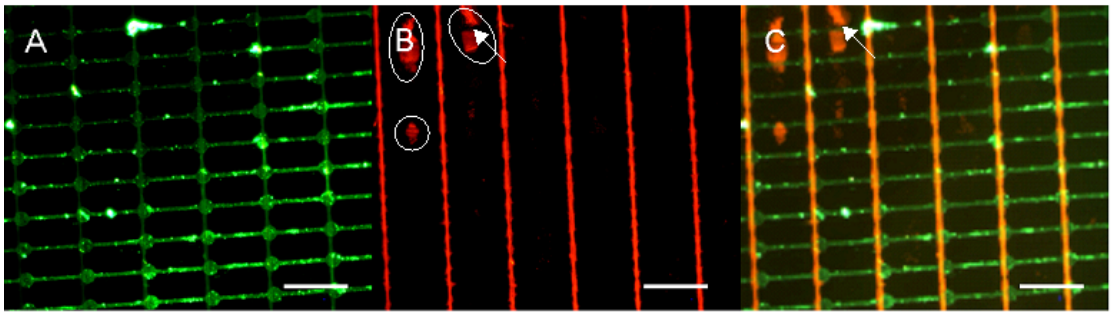
In order to test if manual two-step microcontact printing leads to a blurred pattern or if the preprinted protein is removed during the second printing step lines of TRITC-mixed ECM, netrin-1 or laminin were printed onto lines with nodes of FITC-labeled poly-L-lysine (concentrations see 4.1.1).

The fluorescence images in fig. 4-3 show no blurring of the protein pattern due to the printing method. The transfer of ECM (fig. 4-3; 1B) was inhomogenous in areas with preprinted poly-L-Lysine (arrows mark the most demonstrative areas). This lower protein transfer was also observed for netrin-1(fig. 4-3; 2B) and laminin (fig. 4-3; 3B). The netrin-1 transfer between the printed lines (fig. 4-3; 2B) was probably due to sagging of the stamp (marked by a circle). Sagging occurs when the area between the stamp structures bends too much and touches the substrate (Sharp *et al.*, 2004; Decré *et al.*, 2005). Sagging was also visible in patterns of laminin (fig. 4-3; 3B) and ECM (fig. 4-3; 1B). The poly-L-lysine transfer was mainly homogenous (fig. 4-3, images 1A and 3A) although some of the nodes were transferred inhomogenously onto the glass surface. Nevertheless, the partially transfer of nodes can also be observed in PECM-patterns (Vogt, 2003a).

1. FITC-PLL/TRITC mixed ECM



2. FITC-PLL/TRITC mixed netrin-1



3. FITC-PLL/ TRITC mixed laminin

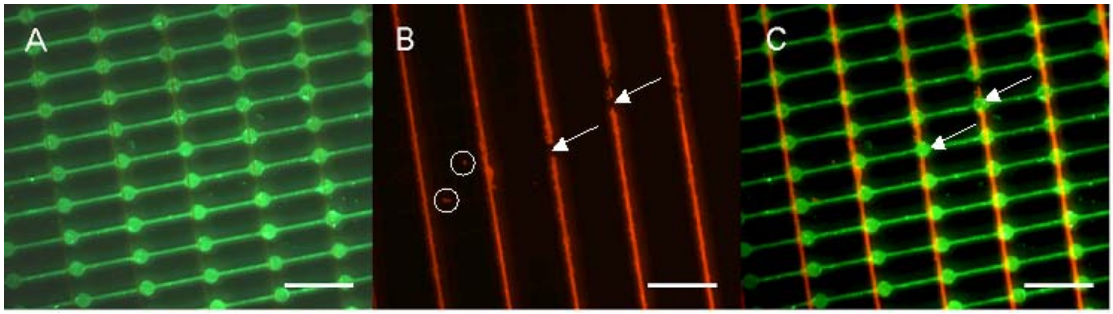


Fig. 4-3: Two-step microcontact printing with lines of axon-guiding biomolecules over polylysine-lines with nodes on glass. Circles mark areas with sagging. The arrows mark areas where a lower amount of axon-guiding protein was printed. 1-3 A: FITC-PLL (50 µg/ml) stamped with structure 4-22-L; 1 B: TRITC-mixed ECM-gel (80-120 µg/ml) stamped with structure 2-100; 2 B: TRITC-mixed netrin-1 (5 µg/ml) stamped with structure 2-100; 3 B: TRITC-mixed laminin (25 µg/ml) stamped with structure 2-100; 1-3 C: Overlays of A and B. TRITC was added in a concentration of 50 µg/ml; scale bar 100 µm.

4.1.3 Characterization of substrates with ellipsometry and with atomic force microscopy

4.1.3.1 Quantification of ECM/PDL; laminin/PDL and netrin-1/PDL protein thickness with the ellipsometer

The average protein thickness across an area can be measured with an ellipsometer. This allows observation of the homogenity and the reproducability of protein thickness. Ellipsometer measurements were made at least at two different areas per substrate (proteins on silicondioxide) with 10x and 50x magnification. Three substrates were measured per protein pair.

ECM printed over PDL

The ECM thickness varied across a substrate (fig. 4-4, A1, A3 and B1 compared to A2, A4 and B2). In some areas more protein was transferred onto the substrate, resulting in a spotted appearance of the printed ECM-lines (fig. 4-4, A3, A2, A4 and B2). Nevertheless, in other areas ECM was printed homogenously (fig. 4-4, A3 and B1). Although the ECM pattern seemed to be intercepted at the crossing points with PDL in 10x magnification (fig. 4-4, A1), this observation was disproved in 50x magnification (fig. 4-4, A3). The average ECM thickness is 26.9 ± 17.4 nm.

The PDL thickness was inhomogenous across the substrate (fig. 4-4, A1, A3 and B1 compared to A2, A4 and B2). As observed for ECM, in some areas more PDL was transferred during printing and the PDL-lines had a spotted appearance (fig. 4-4, A4 and B2). In 50x magnification accumulation of protein can be observed at the outer rim of PDL lines and nodes and at crossing points (fig. 4-4, A3 and B1). The average PDL thickness is 19.5 ± 8.6 nm.

Interestingly, the protein thickness at the crossing points did not always match the calculated value, e.g at crossing point A3_4 the calculated protein thickness is 38.9 nm, while the measured protein thickness is 27 nm. Similar observation could be made at the crossing points A4_7, B1_5, B1_7 and B2_4. The detailed values for protein thickness are listed in tab. 4-1.

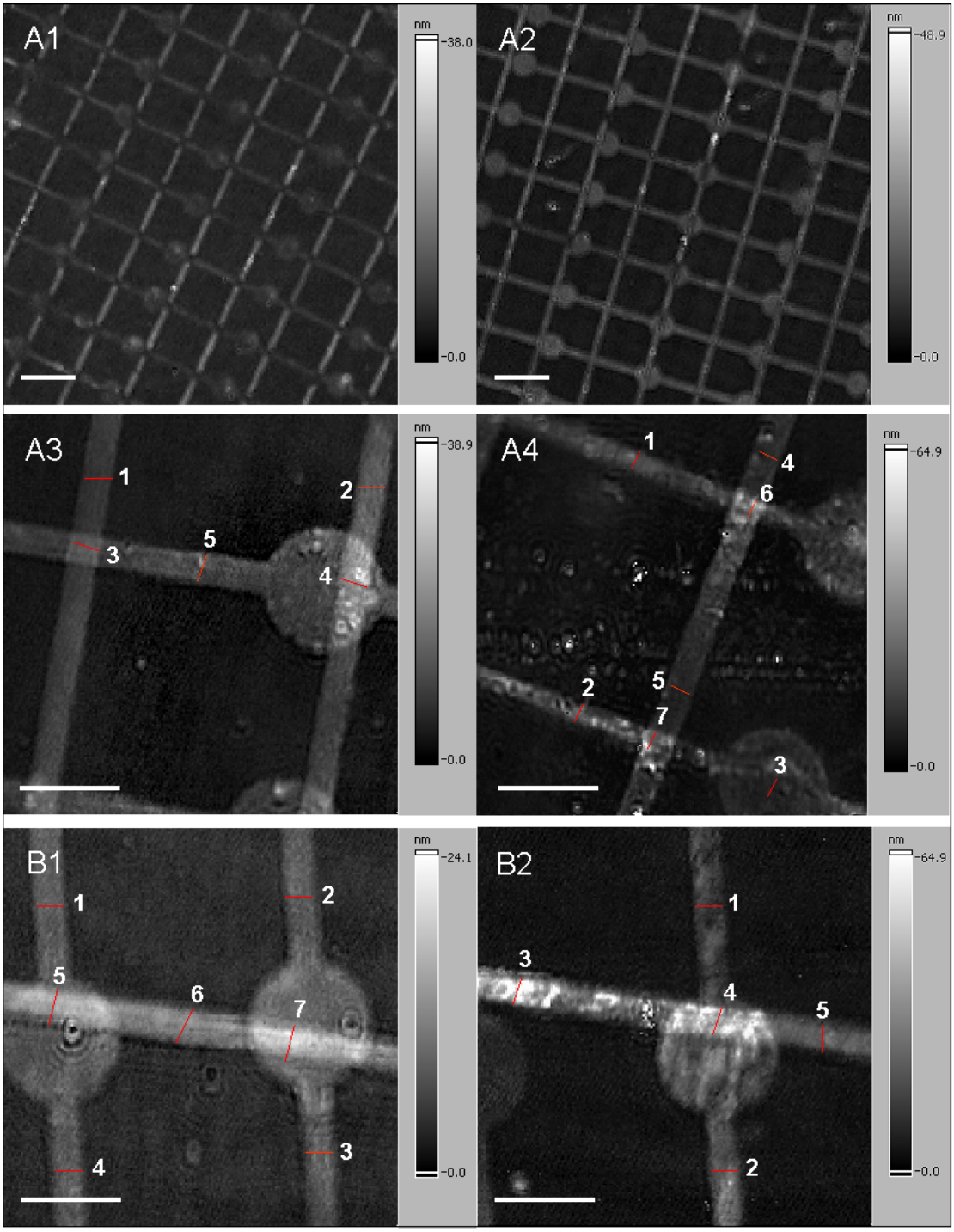


Fig. 4-4 : Protein thickness of the ECM/PDL 2-step µCP substrates.

A1, A2: Overview of two different areas of substrate A (10x magnification, scale bar 50 µm); A3, A4: Details of printed ECM and PDL on substrate A (50x magnification, scale bar 20 µm); B1, B2: Details of printed ECM and PDL on substrate B (50x magnification, scale bar 20 µm). The line with nodes is PDL, the printed line is ECM. The average protein thickness was measured at the red lines (marked by numbers, data see tab. 4-1).

.

Protein	Thickness measured at fig.	Protein thickness [nm]
ECM	4-4, A3_1	7.9
ECM	4-4, A3_2	23.0
ECM on PDL	4-4, A3_3	23.8
ECM on PDL	4-4, A3_4	27.0
PDL	4-4, A3_5	15.9
PDL	4-4, A4_1	27.8
PDL	4-4, A4_2	29.1
PDL	4-4, A4_3	14.6
ECM	4-4, A4_4	17.2
ECM	4-4, A4_5	19.9
ECM on PDL	4-4, A4_6	41.0
ECM on PDL	4-4, A4_7	38.4
PDL	4-4, B1_1	10.8
PDL	4-4, B1_2	12.8
PDL	4-4, B1_3	10.3
PDL	4-4, B1_4	12.3
ECM on PDL	4-4, B1_5	19.2
ECM	4-4, B1_6	17.2
ECM on PDL	4-4, B1_7	22.6
PDL	4-4, B2_1	25.2
PDL	4-4, B2_2	35.7
ECM	4-4, B2_3	63.6
ECM on PDL	4-4, B2_4	51.6
ECM	4-4, B2_5	39.7

Tab. 4-1: Average protein thickness on the ECM/PDL substrates. The average ECM thickness is 26.9 ± 17.4 nm. The average PDL thickness is 19.5 ± 8.6 nm.

Laminin printed over PDL

The laminin thickness varied about 10 nm across substrate A from 10 to 20 nm (fig. 4-5, A1 and A3). In some areas more protein was transferred onto the substrate, resulting in a spotted appearance of the printed laminin-lines (fig. 4-5, A1 and A2), similar to the transfer of ECM onto the silicon dioxide surface. Nevertheless, laminin was printed homogenously on substrate B (fig. 4-5, B1 and B2). The granular, lighter structures in fig. 4-5, B2 are artifacts due to dust on the surface. The average laminin thickness is 15.6 ± 3.6 nm.

The PDL thickness was inhomogenous across substrate A and increased from about 8 nm in fig. 4-5,A3 to 16 nm in fig. 4-5,A4. Compared to substrate A, the PDL thickness on substrate B was more homogenous, although an accumulation of protein can be observed at the outer rim of PDL lines and nodes in 50x magnification (fig. 4-5, B1). The average PDL thickness is 14.3 ± 3.6 nm.

As observed for ECM printed on PDL, the protein thickness at the crossing points did not always match the calculated value, e.g at crossing point A3_6 the calculated protein thickness is 28.2 nm, while the measured protein thickness is 20.4 nm. Similar observation could be made at the crossing points A4_7, B1_5 and B1_6. The detailed values for protein thickness are listed in tab. 4-2.

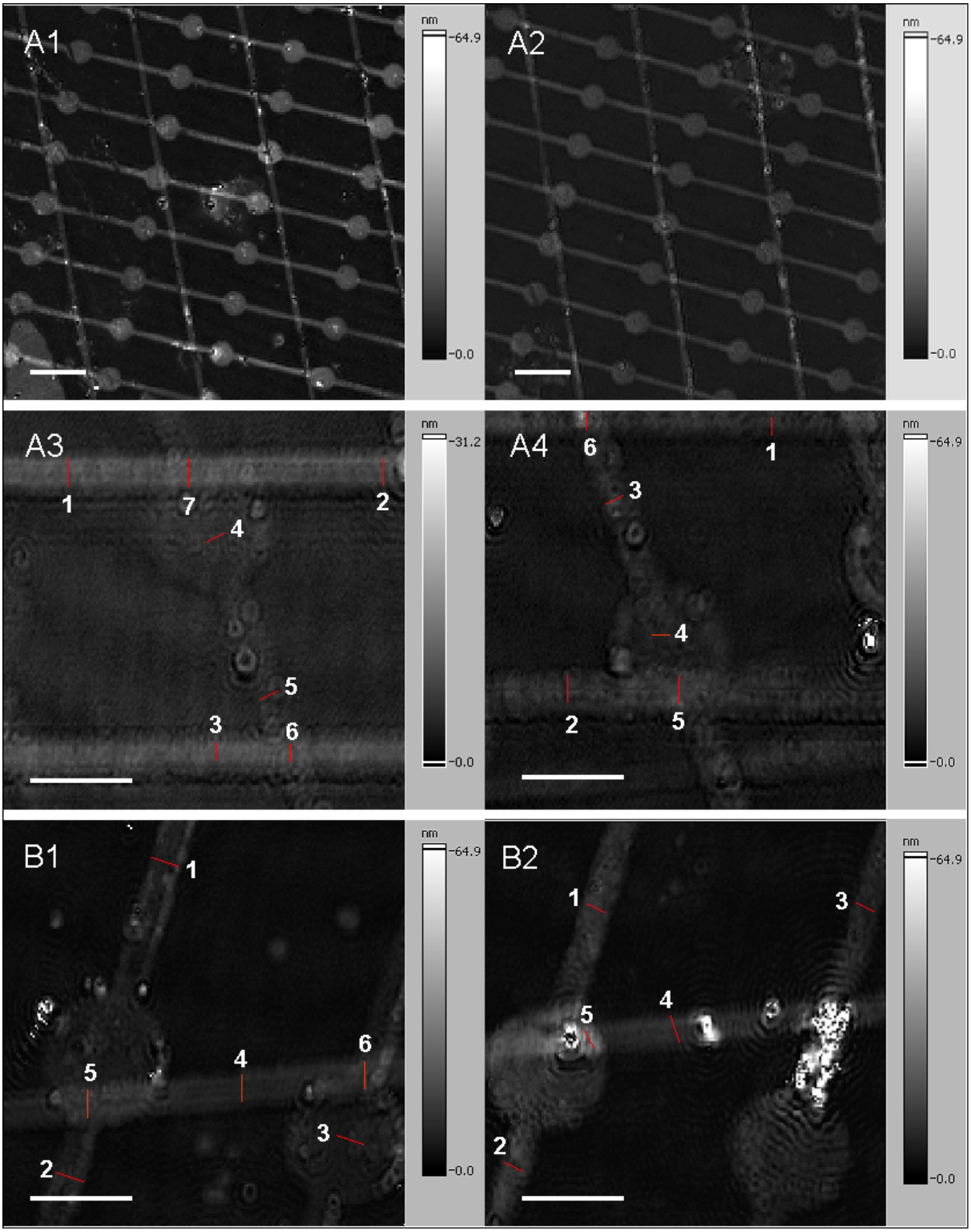


Fig. 4-5 : Protein thickness of the laminin/PDL 2-step µCP substrates. A1, A2: Overview of two different areas of substrate A (10x magnification, scale bar 50 µm); A3, A4: Details of printed laminin and PDL on substrate A (50x magnification, scale bar 20 µm); B1, B2: Details of printed laminin and PDL on substrate B (50x magnification, scale bar 20 µm). The line with nodes is PDL, the printed line is laminin. The average protein thickness was measured at the red lines (marked by numbers, data see tab. 4-2).

Protein	Thickness measured at fig.	Protein thickness [nm]
laminin	4-5, A3_1	19.8
laminin	4-5, A3_2	10.8
laminin	4-5, A3_3	20.4
PDL	4-5, A3_4	8.4
PDL	4-5, A3_5	7.8
laminin over PDL	4-5, A3_6	20.4
laminin over PDL	4-5, A3_7	21.0
laminin	4-5, A4_1	11.3
laminin	4-5, A4_2	13.8
PDL	4-5, A4_3	16.3
PDL	4-5, A4_4	15.0
laminin over PDL	4-5, A4_5	20
laminin over PDL	4-5, A4_6	28.75
PDL	4-5, B1_1	15
PDL	4-5, B1_2	13.8
PDL	4-5, B1_3	12.5
laminin	4-5, B1_4	15
laminin over PDL	4-5, B1_5	17.5
laminin over PDL	4-5, B1_6	18.8
PDL	4-5, B2_1	18.8
PDL	4-5, B2_2	18.8
PDL	4-5, B2_3	16.2
laminin	4-5, B2_4	18.1
laminin over PDL	4-5, B2_5	32.5

Tab. 4-2: Average protein thickness on the laminin/PDL substrates. The average laminin thickness is 15.6 ± 3.6 nm. The average PDL thickness is 14.3 ± 3.6 nm.

Netrin-1 printed over PDL

Although there were areas with increased protein transfer in 10x magnification (fig. 4-6, A1 and A2), similar to the spotted appearance of ECM- and laminin-lines, the netrin-1-thickness observed in the 50x magnification was homogeneous (fig. 4-6, A3 , A4, B1 and B2). The average netrin-1 thickness was 25.5 ± 3.5 nm.

As on the ECM/PDL and laminin/PDL-substrates, the PDL-thickness varied across the substrates. Due to increased protein transfer, the PDL-lines with nodes had a spotted appearance (fig. 4-6, B1 and B2). The average PDL thickness is 17.2 ± 10.6 nm.

As shown for ECM/PDL and laminin/PDL substrates, the protein thickness at the crossing points did not match the calculated value, e.g at crossing point A4_6 the calculated protein thickness is 47.8 nm, while the measured protein thickness is 29.3 nm. Similar observation could be made at the other crossing points (fig.4-6 A3_4, B1_4 and B2_5). The detailed values for protein thickness are listed in tab. 4-3.

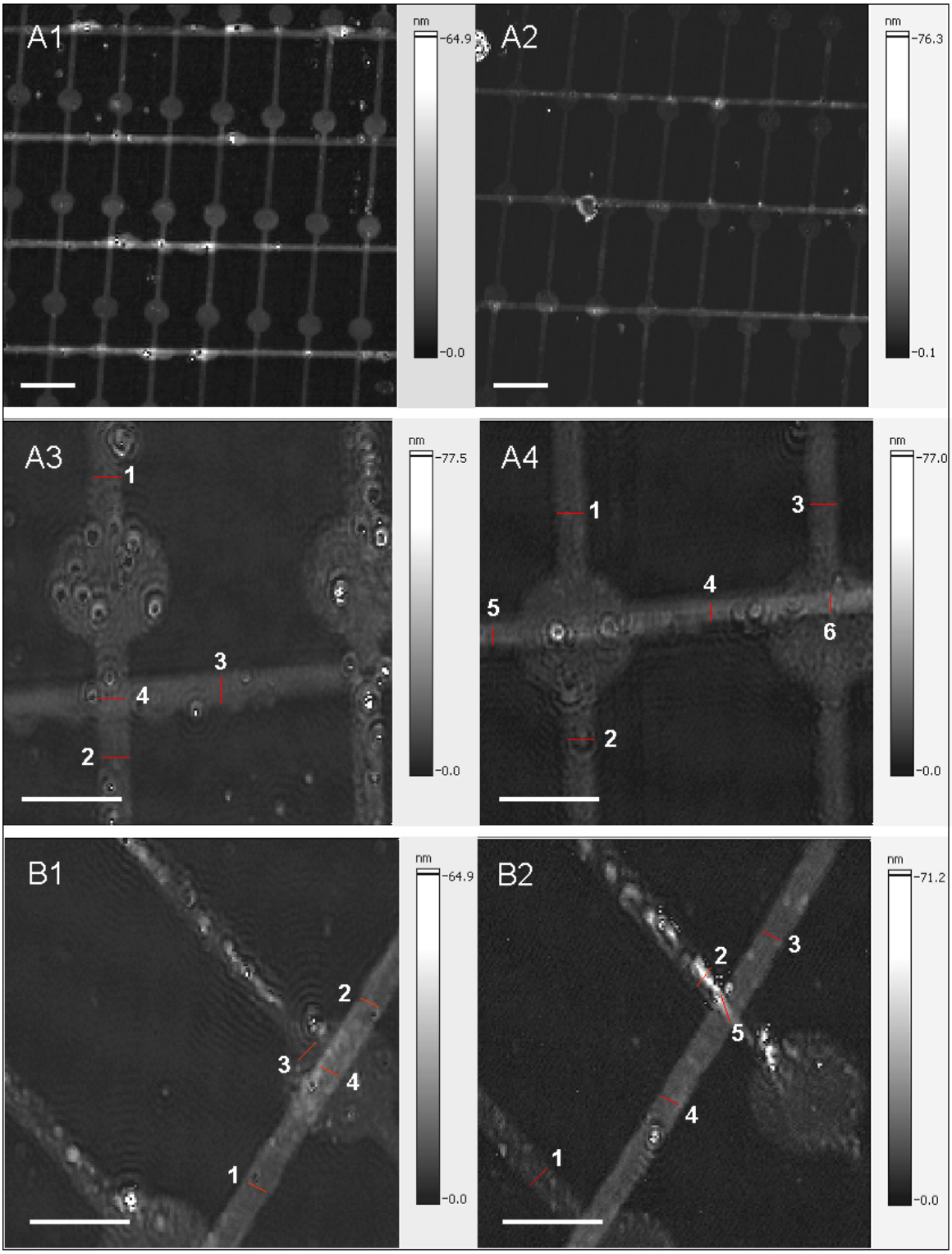


Fig. 4-6 : Protein thickness of the netrin-1/PDL 2-step µCP substrates. A1, A2: Overview of two different areas of substrate A (10x magnification, scale bar 50 µm); A3, A4: Details of printed netrin-1and PDL on substrate A (50x magnification, scale bar 20 µm); B1, B2: Details of printed netrin-1 and PDL on substrate B (50x magnification, scale bar 20 µm). The line with nodes is PDL, the printed line is netrin-1.

Protein	Thickness measured at fig.	Protein thickness [nm]
PDL	4-6, A3_1	12.4
PDL	4-6, A3_2	10.9
netrin-1	4-6, A3_3	24.8
netrin-1 on PDL	4-6, A3_4	27.9
PDL	4-6, A4_1	16.9
PDL	4-6, A4_2	13.9
PDL	4-6, A4_3	18.5
netrin-1	4-6, A4_4	29.3
netrin-1	4-6, A4_5	26.1
netrin-1 on PDL	4-6, A4_6	33.9
netrin-1	4-6, B1_1	19.5
netrin-1	4-6, B1_2	22.1
PDL	4-6, B1_3	9.1
netrin-1 on PDL	4-6, B1_4	28.6
PDL	4-6, B2_1	11.4
PDL	4-6, B2_2	44.1
netrin-1	4-6, B2_3	27.1
netrin-1	4-6, B2_4	29.9
netrin-1 on PDL	4-6, B2_5	38.4

Tab. 4-3: Average protein thickness on the netrin-1/PDL substrates. The average netrin-1 thickness is 25.5 ± 3.5 nm. The average PDL thickness is 17.2 ± 10.6 nm.

4.1.3.2 Quantification of protein homogenity of ECM/PDL, laminin/PDL and netrin-1/PDL patterns by atomic force microscopy

Atomic force microscopy (AFM) gives a detailed image of a surface and is a good method to analyze the homogenity of the microstructured protein pattern. The following images are individual images and cannot be generalized.

The protein thickness varied across the printed protein lines: Although the PDL-lines were printed with the same stamp and the same method on the same day, the protein thickness was very different on the three substrates. It had a range from 3.3 nm to 59.38 nm (fig. 4-7 to fig. 4-9). Even within one printed PDL line the protein thickness was not homogeneous and decreased about 13 nm from one corner of the image to the other (fig. 4-7 A and B). The ECM-line showed an accumulation of protein at the left rim (fig. 4-7 A and C). Similar observations could be made on netrin-1. The netrin-1-thickness varied about 2 nm. In addition, protein had accumulated at the upper rim (fig. 4-8). The laminin-line was the most inhomogeneous protein-line. Deep holes were visible in the overview (fig. 4-9). The section analysis showed an irregular profile with a lot of protein peaks across the protein-lines for PDL, ECM, netrin-1 and laminin (fig. 4-7 to 4-9).

At the crossing points of the printed protein lines the protein thickness increased. It was not always identical to the calculated values. At the ECM/PDL crossing point the protein thickness was calculated to 95.65 nm and 73.58 nm were measured on average. For the laminin/PDL-crossing point the protein thickness was calculated to 62.56 nm and 51.19 nm were measured on average. Only at the netrin-1/PDL crossing point the calculated thickness and the measured value were close; they differed only about 2 nm (fig. 4-7 to 4-9).

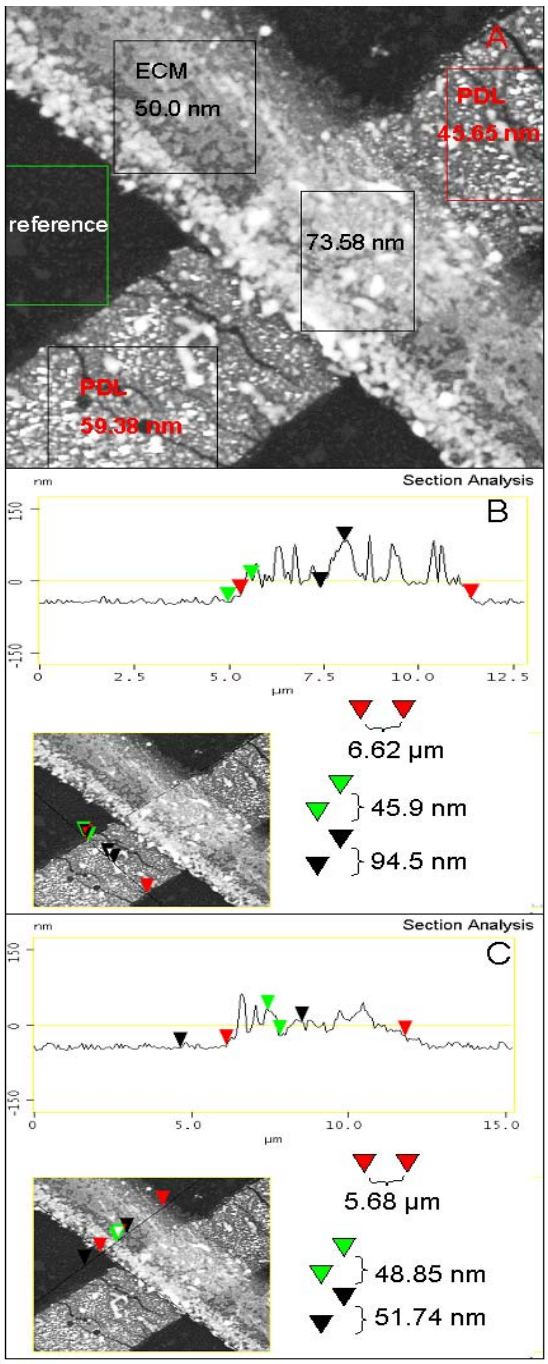


Fig. 4-7: ECM/PDL pattern printed on 7.5 nm SiO_2. A: AFM-image. The numbers in the squares in each AFM-image mark the average protein-thickness in this area. B: section through a PDL-line. C: section through a ECM-line. The red arrows in B and C mark the line-bridth; the black and green arrows mark the height of specific protein peaks.

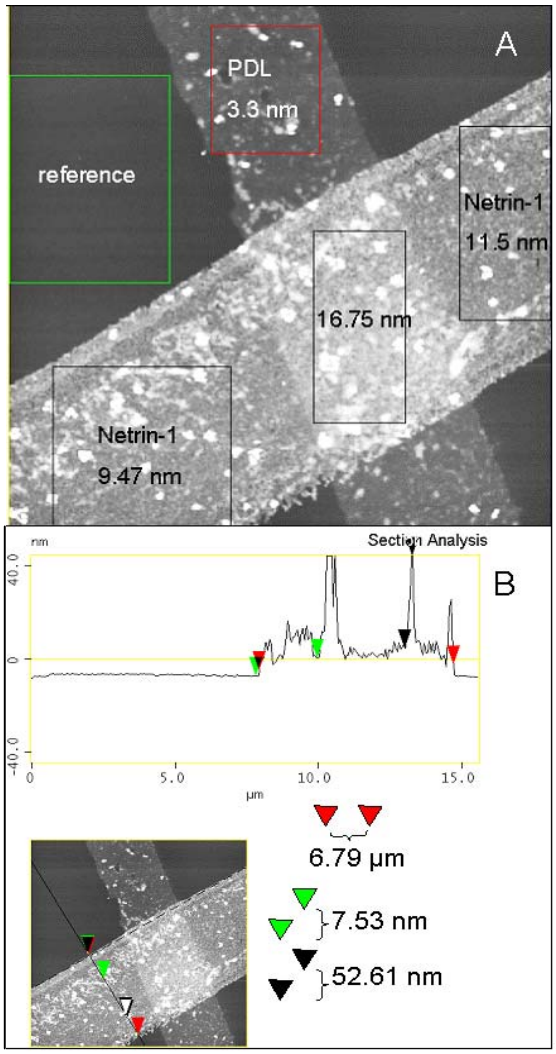


Fig. 4-8: Netrin-1/PDL pattern printed on 7.5 nm SiO_2. A: AFM-image. The numbers in the squares in each AFM-image mark the average protein-thickness in this area. B: section through a netrin-1-line. The red arrows in B mark the line-bridth; the black and green arrows mark the height of specific protein peaks.

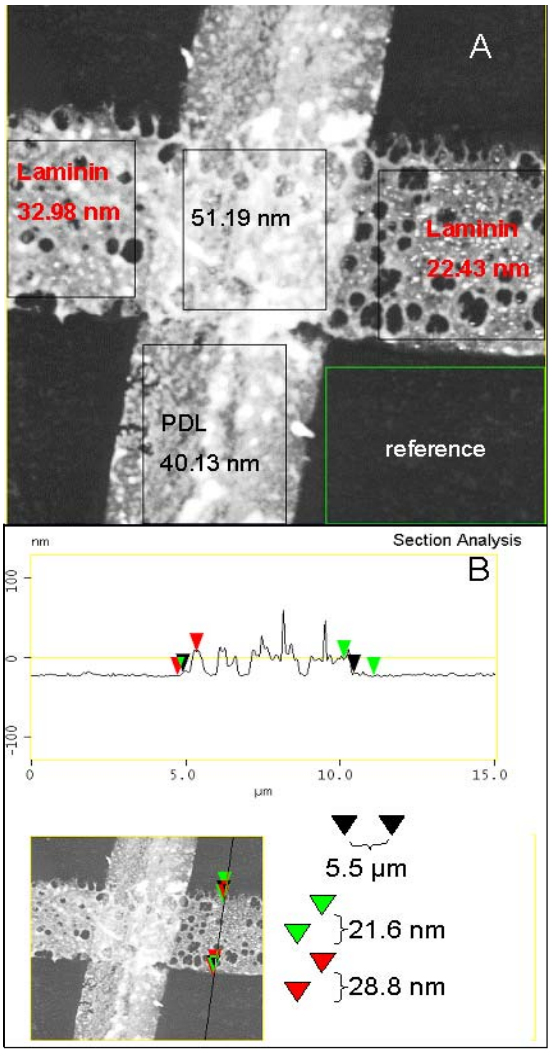


Fig. 4-9: Laminin/PDL pattern printed on 7.5 nm SiO_2. A: AFM-image. The numbers in the squares in each AFM-image mark the average protein-thickness in this area. B: section through a laminin-line. The black arrows in B mark the line-bridth; the red and green arrows mark the height of specific protein peaks.

4.1.4 Comparison of ellipsometer- and AFM-results

The AFM-measurements confirmed the inhomogenous transfer of proteins which lead to a spotted appearance of the printed lines (fig. 4-7 to 4-9, all proteins). Moreover, as observed in the ellipsometer measurements, the AFM-measurements showed that the measured values for protein thickness at crossing points are lower than calculated. The protein thickness measured with the AFM varied for each protein even across an area of 15 µm x 15 µm. The averaged ECM, laminin-, netrin-1, and PDL-thickness determined by AFM-measurements is compared to the protein thickness derived from the ellipsometer-measurements in fig. 4-10. Due to the single-measurements the AFM-derived protein thicknesses differ greatly from the ellipsometer derived values. While the PDL-, ECM- and laminin-thickness was higher than the averaged protein thickness determined by the Ellipsometer, the netrin-1 thickness was lower. Nevertheless, similar values were determined with ellipsometer measurements (see 4.1.3.1).

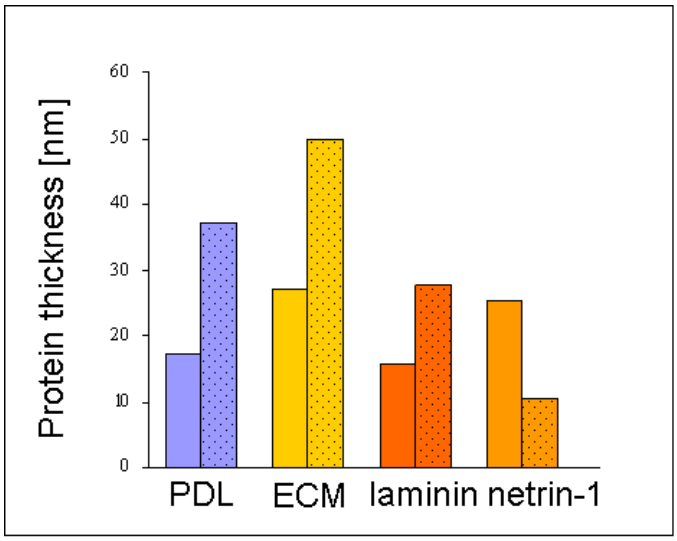


Fig.4-10 : Comparison between the averaged protein thickness determined by AFM and ellipsometer. Unstructured columns: ellipsometer-measurement; dotted columns: AFM-measurement.

4.1.5 Cell culture on manual two-step microcontact printing substrates

Cortical or striatal neurons were cultured on the microstructured 2-step µCP substrates. They were patched between day 10-14.

Striatal neurons cultured on netrin-1/PDL-substrates appeared healthy and grew mostly along the printed pattern, but a higher amount of dead cells as on the PECM grid patterns was observed (fig. 4-11). In some cases the neurites did not grow along the netrin-1 lines but directly towards the next poly-D-lysine-node (fig. 4-11). Neurons cultured on laminin/PDL substrates also appeared healthy and grew mostly along the pattern (fig. 4-11).

Striatal neurons cultured on ECM/PDL substrates had a bright, healthy appeareance. In some cases the neurites did not grow along the printed pattern (fig. 4-11). Neurons cultured on the ECM/PDL- and on laminin/PDL-substrates

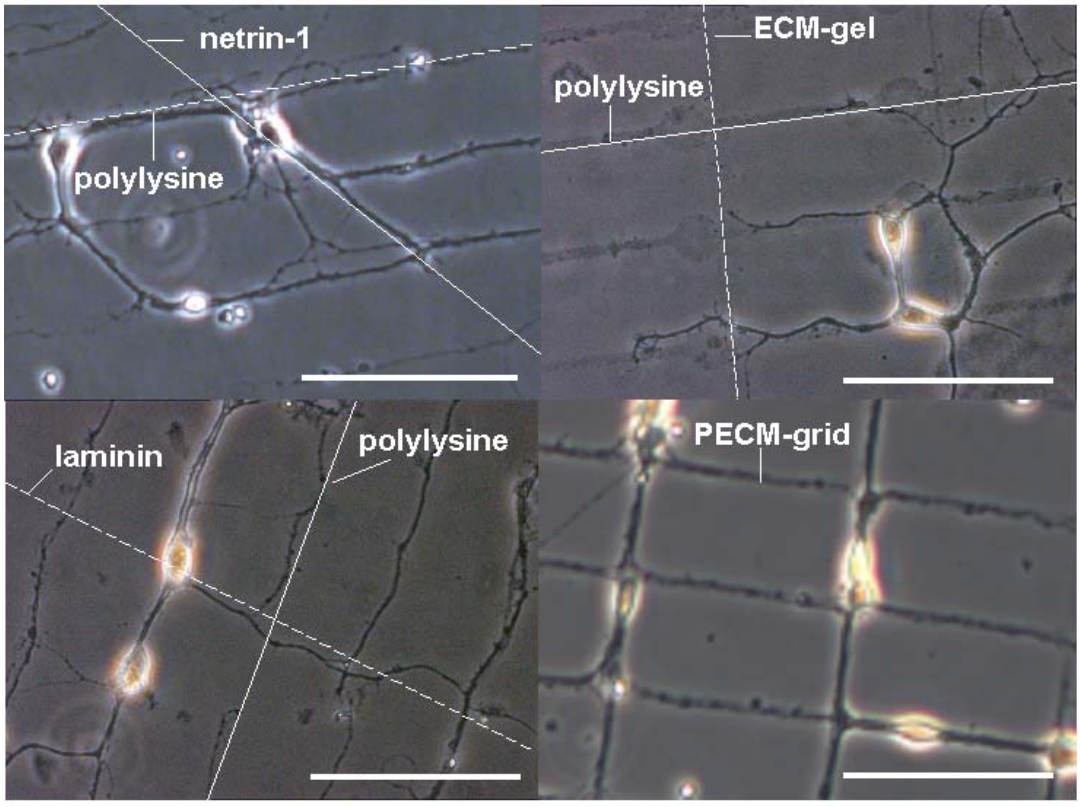


Fig. 4-11: Rat E18 striatal neurons cultured on manual microcontact printing substrates compared to rat E18 striatal neurons cultured on a PECM-grid.
Upper left corner: Netrin-1/poly-D-lysine, DIV 11; upper right corner: ECM/poly-D-lysine, DIV 12; lower left corner: laminin/poly-D-lysine, DIV 12; lower right corner: PECM-grid as control, DIV 10. Scale bar 100 µm.

seemed to be very fit, comparable to the good viability of neurons on PECM grid patterns (fig. 4-11). Due to its high viscosity it is easier to print ECM than laminin. Thus this ECM/PDL substrates were used for further experiments.

4.2 Aligned two-step microcontact printing with the Fineplacer

In order to test the effect of axon-guiding biomolecules combined with the neutral biomolecule poly-D-lysine on the polarity of neurons the basic grid pattern had been redesigned for aligned 2-step µCP: One line with a node made of the axon-guiding biomolecule is the starting point of three lines made of poly-D-lysine (fig. 4-12). Due to this design the aligning of the different patterns in the second printing step could only be done under visual control with the Fineplacer.

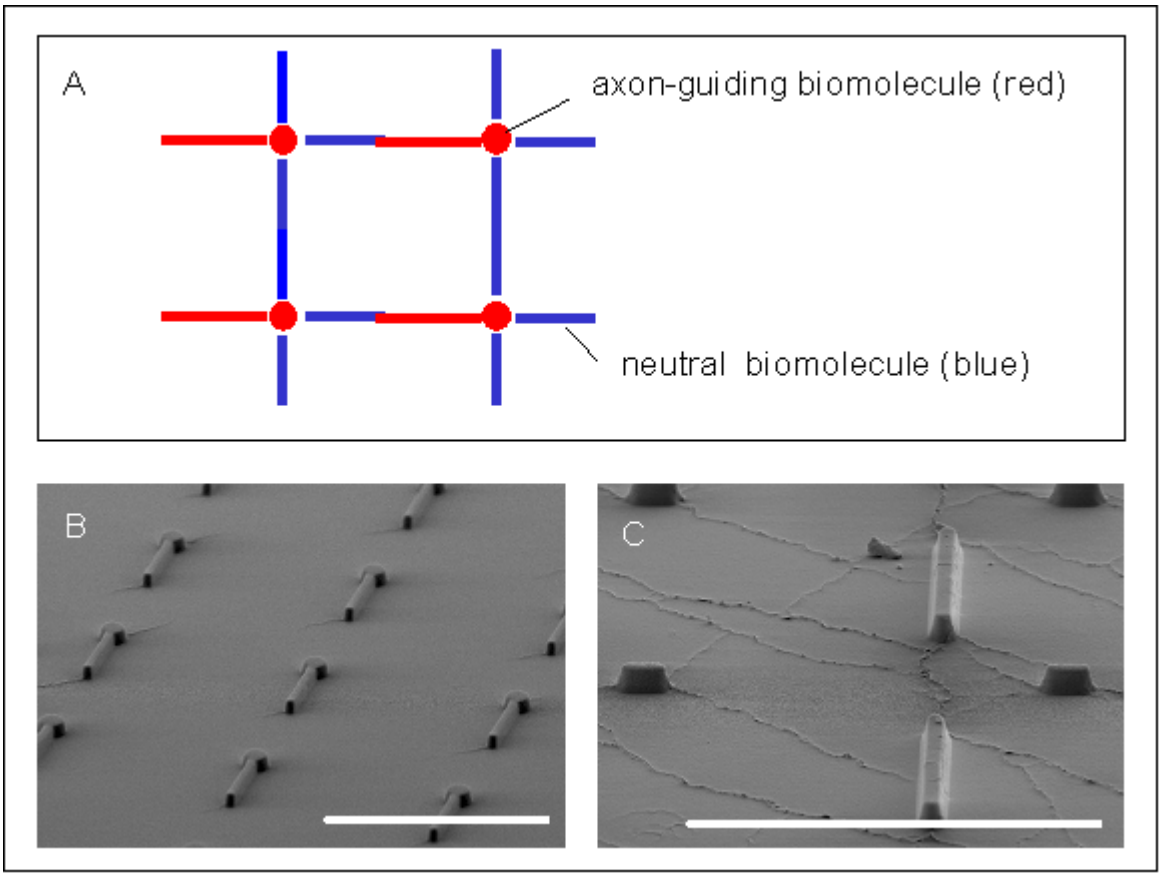


Fig. 4-12: Scheme of the new pattern design and SEM- pictures of new structures. A: New design for testing the effects of different biomolecules on the polarity of neurons. The axon-guiding biomolecules are printed in a node with one line (red); the residue of the grid consists of a neutral biomolecule (blue). B: This structure is used for printing the axon-guiding biomolecules laminin, ECM-gel and netrin-1; scale bar 100 µm. C: One example of a structure used for printing the neutral biomolecule poly-D-lysine; scale bar 100 µm.

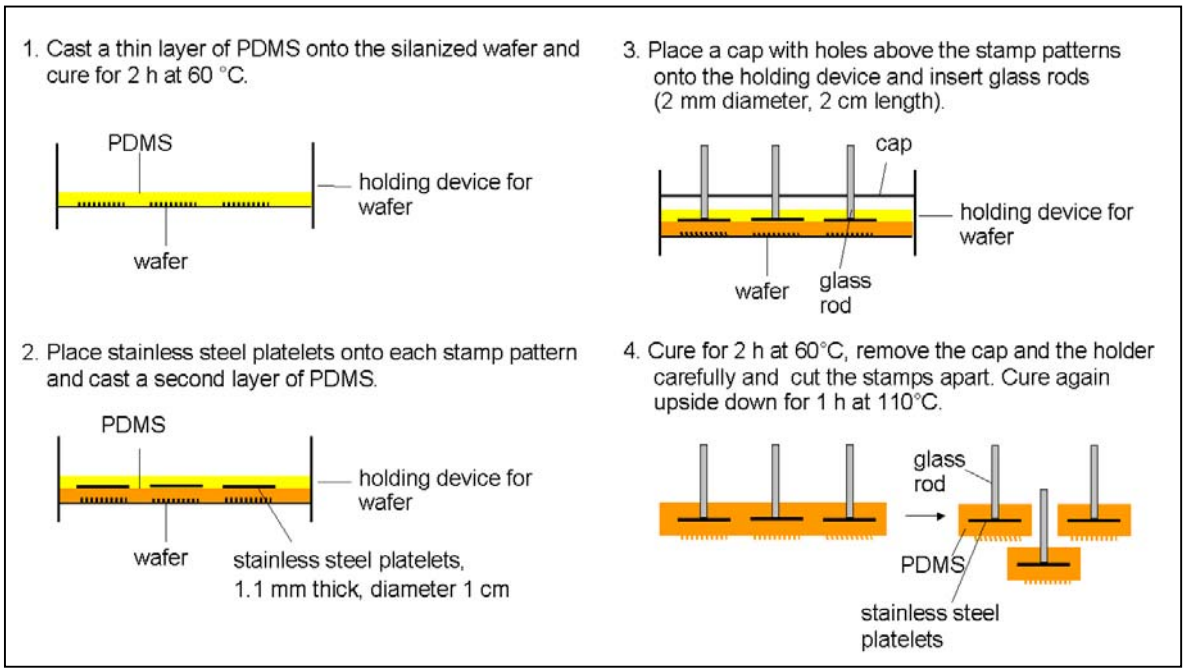


Fig. 4-13 : Casting of the stamps for aligned two-step microcontact printing.

The stamps used for microcontact printing by hand were not appropriate for this application. The convex upside of the stamps did not allow stabilization of the stamps in a 90° angle to the substrate surface. Cutting of the upper part also lead to an irregular surface. Thus specific stamps were designed which allowed the excact printing in a 90° angle to the substrate surface (fig. 4-13). These stamps consist of PDMS, a stainless steel platelet (1cm diameter, 1.1 mm thick) and a glass rod (2 cm long, 2 mm diameter). For casting of the stamps a wafer with the desired structures was clamped into a holding device. A thin layer of PDMs was cast onto the wafer and cured for 2 h at 60 °C. After this steel platelets were put on top of each stamp structure. A second layer of PDMs was cast onto the wafer. A cap with small holes above the stamp structures was placed onto the holding device. This allowed the insertion and stabilization of glass rods in a 90° angle to the stamp surface. After further curing the cap was carefully removed, the PDMS stamps could be peeled of the wafer and were cut apart. The stamps were cured again upside down for 1 h at 110°C.

For printing the stamp was pretreated as described above, it was incubated in the protein solution for 20 minutes. For drying the stamp was placed upside down into a teflon-holder. The protein solution remaining on top of the stamp was air-dried for 15 minutes, after this time the surface was dried with nitrogen for 1 minute. Stamping in the Fineplacer was done with a pressure of 50 g for 15 minutes. The printed substrates were controlled visually using phase contrast.

In first experiments we printed ECM-gel (80-120 µg/ml) as axon-guiding biomolecule and poly-D-lysine (25 µg/ml) as neutral biomolecule (fig. 4-14). First structures 1,2 ,3 or 4 were preprinted on a culture dish with poly-D-lysine by hand. In the second printing step PDMS-stamps with structure 0 were coated with ECM-gel and carefully dried under the clean bench, while the stamping was done under visual control with the Fineplacer.

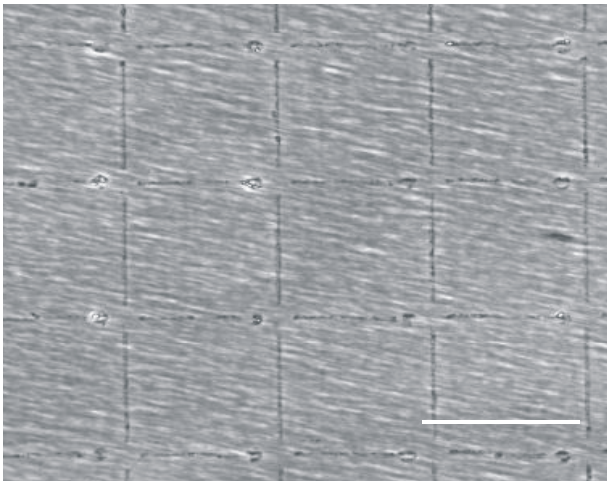


Fig. 4-14: Structure 1 (PDL, 25 µg/ml) stamped with the Fineplacer over preprinted structure 0 (ECM, 80-120 µg/ml). The scale bar is 100 µm.

In order to visualize the transferred protein better, structures 1-4 were prestamped by hand under the bench with FITC-PLL (50 µg/ml for a better fluorescence signal). Structure 0 was stamped with TRITC-mixed netrin-1 (5 µg/ml), ECM-gel (80-120 µg/ml) and laminin (25 µg/ml). The TRITC-concentration in each protein solution was 50 µg/ml. The buffers used for the dilution of each protein are listed in materials and methods (see Microcontact printing, 3.1).

The PLL-patterns preprinted for aligned 2-step µCP differ in the quality of protein transfer from a high to a low protein transfer (fig. 4-15, images A). The PLL-pattern preprinted for the PLL/netrin-1 substrate was printed a twice due to slightly shifting of the stamp during positioning on the substrate (fig. 4-15, PLL/netrin-1 image A). Printing of ECM, laminin or netrin-1 on these patterns did not lead to blurring or removing the PLL. ECM, laminin and netrin-1 were transferred to the substrate homogenously and with similar quality. In a few cases, nodes of the pattern missed or were not complete (fig. 4-15, images B), independent of the printed protein. The alignment of the second pattern onto the first one was only possible

for an area about 300 µm x 300 µm. Thus the second patterns were not completely aligned over the whole stamp, resulting in pattern irregularities (fig. 4-15, images C).

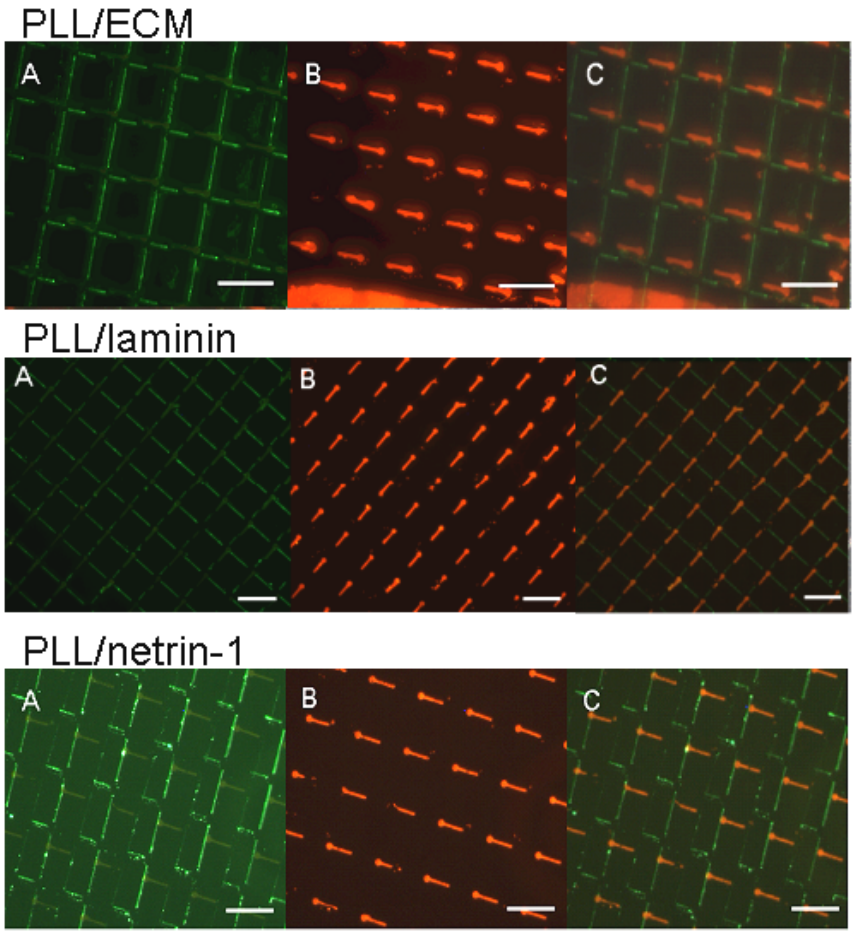


Fig. 4-15 : Fluorescent images of PLL/ECM (structure 2/0); PLL/laminin (structure 1/0) and PLL/netrin-1 (structure 2/0). A: printed FITC-PLL pattern; B: printed TRITC-conjugated ECM-, laminin- or netrin-1 pattern; C: Overlay of A and B; scale bar 100 µm.

4.2.1 Cell culture on aligned two-step microcontact printing substrates

Cortical neurons cultured on the aligned 2-step µCP substrates up to DIV 11 have a healthy morphology and a bright appearance (fig. 4-16, A-C). Although the printed pattern seemed to be homogenous, the neurites did not always grow along the pattern (fig. 4-16 B). The cortical neurons adhered as well on the PDL-nodes, which provided more adherance area, as on the PDL- or ECM-lines (fig. 4-16 C). Compared to cortical neurons cultured on PECM-grids cortical neurons on the aligned ECM/PDL substrates grew more independent from the pattern. In addition, the amount of dead cells in the medium was slighly increased.

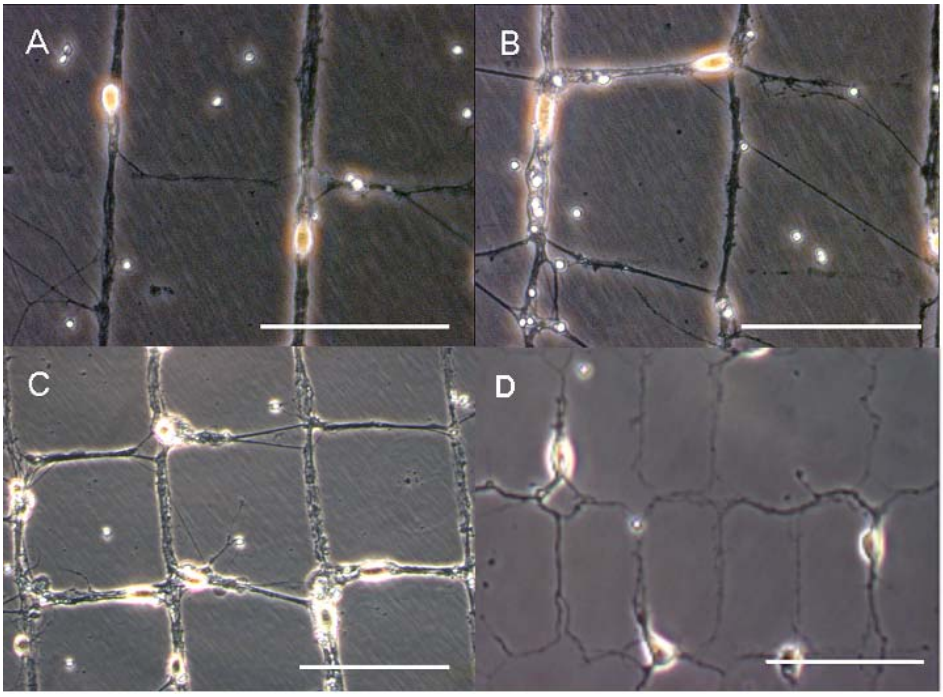


Fig. 4-16: Rat E18 cortical neurons DIV 11 cultured on a pattern made of ECM (structure 0) and PDL (structure 3) compared to cortical neurons DIV 10 cultured on a PECM-grid. A-C show different areas of the ECM/PDL substrate. The neurites sometimes grow independent of the printed pattern. D: control, PECM-grid. Scale bars 100 µm.

Due to the fact, that the axon-specific staining against tau is only specific until DIV 3-5 (diploma thesis K. Adamiak, 2007), no anti-tau staining was performed on cortical neurons grown on ECM/PDL-structures. Moreover, the polarity within a neuron can switch during developement (Mattson *et al.*, 1999; Hayashi *et al.*,

2002), thus a staining at DIV 3-5 cannot be used to estimate a certain polarity within a neural network at DIV 11. Electrophysiological measurements are another method in order to determine the polarity of synapses within a neural network and can be performed at DIV 11.

4.2.2 Electrophysiology on aligned two-step microcontact printing substrates

The electrophysiological characteristics of cortical neurons cultured on ECM/PDL grids showed significant differences compared to cortical neurons cultured on PECM grids. The amount of APs at 150 pA was significant lower ($p<0.05$). Other variations in the electrophysiological properties were not significant (see tab. 4-4).

Substrate	PECM-grids (-70 mV)	PECM-grids (RP)	Two-step µCP grids PDL-ECM (RP)
n of patched neurons	113 (74 with AP at 150 pA)	24 (21 with AP at 150 pA)	8 (8 with APs at 150 pA)
Resting potential [mV]	-62 ± 7	-61 ± 7	-65 ± 5
FLHM at 150 pA [ms]	2.0 ± 0.7	2.4 ± 0.8*	2.0 ± 0.4
APs at 150 pA	1.4 ± 0.6	1.6 ± 0.6	1.1 ± 0.3*
AP-Amplitude at 150 pA [mV]	61 ± 13	63 ± 12	59 ± 2
tau [ms]	18 ± 8	15 ± 7	12 ± 4

Tab. 4-4: Electrophysiological characteristics of cortical neurons (DIV 10-12) cultured on PECM-grid-patterns (clamped to –70 mV and at resting potential) and on two-step µCP grids consisting of PDL-ECM (at resting potential). Significant differences are marked with a* ($p<=0.05$ in a student´s t-test).

The similar electrophysiological properties show that PDL/ECM substrates had a similar effect on neuronal growth as PECM-substrates. The lower amount of APs induced at 150 pA may be due to the low amount of patched neurons. Another reason could be a slower kinetic of the ion channels in the cell membrane, but this would lead to significant slower rising and falling APs, resulting in a significant higher FLHM. This was not observed in the patched neurons.

5. Coculture system

Another strategy for induction of polarity in neuronal networks is the reconstruction of a natural polarity *in vitro*. The corticostriatal pathway (see 2.2.2.1 for details) is well suited for a reconstruction *in vitro*: *In vivo* cortical afferents release glutamate into the striatum (Divac *et al.*, 1977; Perschak *et al.*, 1990) and form synapses to the medium spiny neurons (Somogyi *et al.*, 1981), while the striatal afferents project only to other areas of the basal ganglia (Wickens *et al.*, 2000). This polarity can also be observed in organotypic cocultures of cortical and striatal slices of newborn rats. Moreover, the electrophysiological properties of striatal and cortical neurons *in vitro* are similar to neurons *in vivo* (Plenz *et al.*, 1996a; 1996b).

A low density coculture of dissociated cortical and striatal neonatal rat neurons with a spatial separation resembles the physiological situation and allows to observe the polarity and synaptogenesis of corticostriatal synapses on a single-cell level.

The coculture chamber has to meet certain requirements: The coculture should allow easy access to the neurons in order to allow patch-clamp experiments. It should provide spatial separation for up to 10-12 days *in vitro*. Although the polarization of a neuron is completed after 7 days (Dotti *et al.*, 1988), this time is required for the maturation of synapses (Granger *et al*., 2006).

5.1 Mechanical coculture

5.1.1 Striatal cell culture

In order to test if the natural polarity between cortex and striatum remains *in vitro* a striatal cell culture was established with slight modifications of cortical cell culture (see materials and methods). The quality of the striatal cell culture was compared to the cortical cell culture by immunohistological stainings against neurons and gial cells. A double-staining with anti-MAP2 (neuron-specific) and anti-GFAP (glia-specific) showed that 68 % of the cells in the striatal cell culture on homogeneously coated glass are glial cells (fig. 5-1). This was similar to cortical cell culture on homogenously coated glass (72 % glial cells in culture, fig. 5-1). The amount of glial cells on patterned substrates on glass correnspondes the value on homogenously coated glass: On patterned substrates 68 % of the cultured cells are glial cells (fig. 5-1). These data were obtained from 1 preparation. Immunological double-stainings with anti-tau and anti-MAP2 did not provide axon specific staining at DIV 11 (data not shown). Anti-Tau seems to be axon-specific only up to DIV 3-5 (diploma thesis K. Adamiak, 2007).

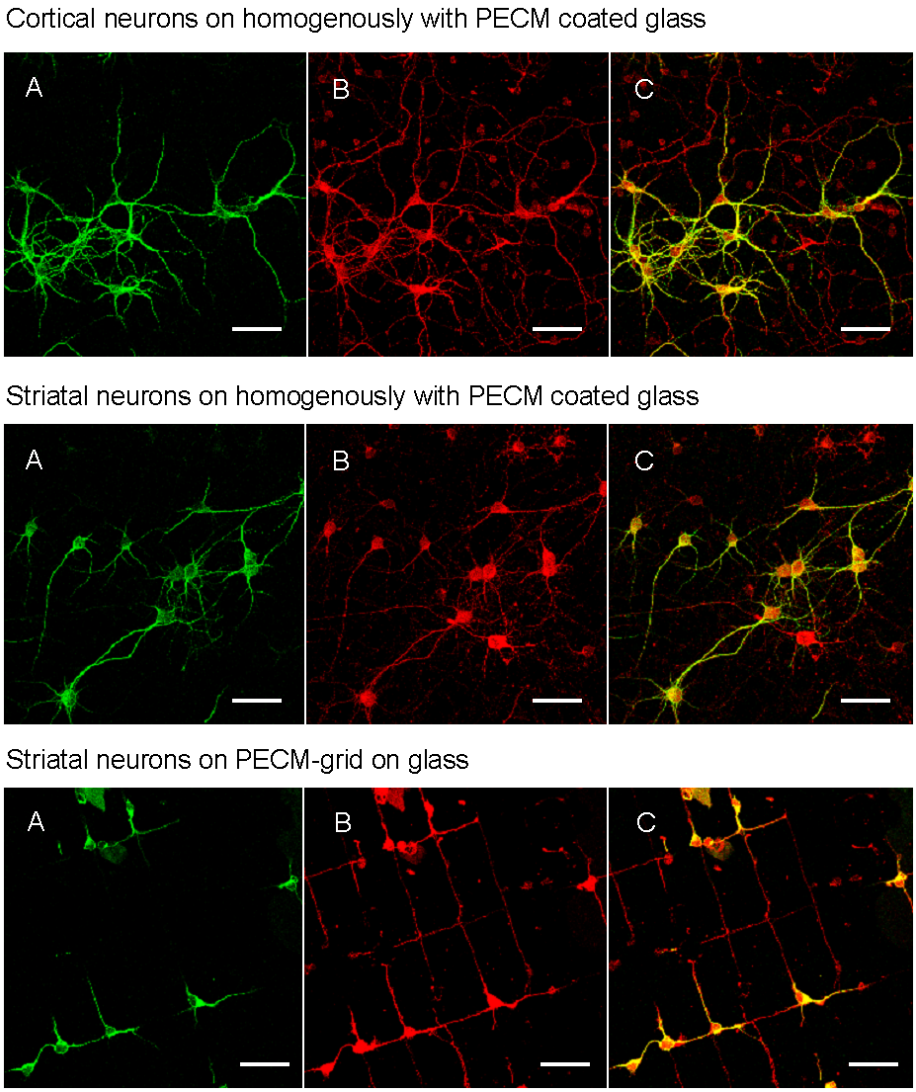


Fig. 5-1 : Double-staining with anti-MAP2 (neuron-specific, green) and anti-GFAP (glia-specific, red) at DIV 11. A: anti-MAP2 staining, secondary antibody Alexa 488 conjugated; B: anti-GFAP-staining, secondary antibody Alexa 586 conjugated; C: Overlay of A and B. Scale bar: 50 µm.

The purity of striatal cell culture was tested by single-cell PCR (RT-PCR). About 70 % of the striatal cell culture were identified as striatal neurons (unpuplished data, R. Helpenstein *et al.*, 2007) by expressing striatum-specific G-protein coupled receptor-RNA-transcripts (Mizushima *et al*., 2000).

Due to the same culture conditions striatal and cortical neurons should possess similar electrophysiological characteristics. For electrophysiological measurements the striatal neurons were cultured on PECM patterns (fig. 5-2).

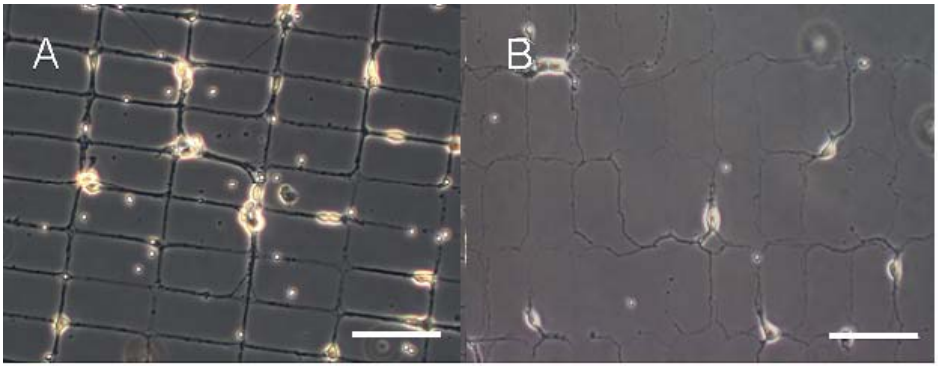


Fig. 5-2 : Comparision of rat E18 striatal and cortical neurons cultured in NB-medium on patterned substrates. A: Striatal neurons DIV 10; B: Cortical neurons DIV 10. Scale bar 100 µm.

A typical CC-measurement of a striatal neuron is shown in fig. 5-3. Compared to the electrophysiological properties of cortical neurons the striatal neurons showed

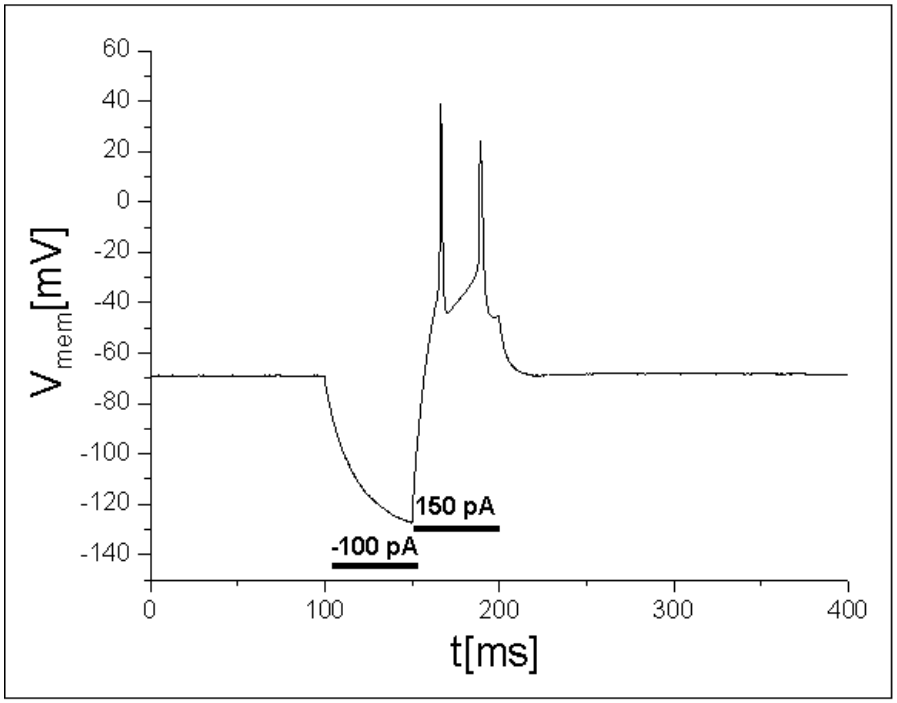


Fig. 5-3 : Current-Clamp measurement of a striatal neuron DIV 10 cultured on a PECM-grid. The resting potential was –66 mV, the leak 1.53 ns. The neuron spiked 2 times during the stimulation with 150 pA.

a significant lower FLHM. The other parameters differed not significantly (tab. 5-1). In literature the striatal resting potential in low density culture is about –60 mV

(Segal *et al.*, 2003). In a organotypic coculture of striatal and cortical slices the average resting membrane potential is –62 ± 3 mV (Plenz *et al.*, 1996a). AP-amplitude and FLHM are also similar to the electrophysiological properties measured in the striatal low density culture (Plenz *et al.*, 1996a).

	Cortical neurons (-70 mV)	Striatal neurons (-70 mV)
n of patched neurons	113 (74 with AP at 150 pA)	10 (10 with AP at 150 pA)
Resting potential [mV]	-62 ± 7	-65 ± 10
FLHM at 150 pA [ms]	2.0 ± 0.7	1.6 ± 0.5*
APs at 150 pA	1.4 ± 0.6	1.35 ± 0.6
AP-Amplitude at 150 pA [mV]	61 ± 13	57 ± 9
tau [ms]	18 ± 8	17 ± 8

Tab. 5-1: Electrophysiological characteristics of striatal neurons compared to cortical neurons (DIV10-12; both clamped to - 70 mV) cultured on PECM-grid-patterns. Significant differences are marked with a* (p<=0.05 in a student´s t-test).

5.1.2 Mechanical coculture system

The coculture chamber should provide spatial separation up to DIV 10-12 in order to provide enough time for synapse maturation. Due to the fact that the coculter chamber has to enable patch-clamp measurements open multicompartment

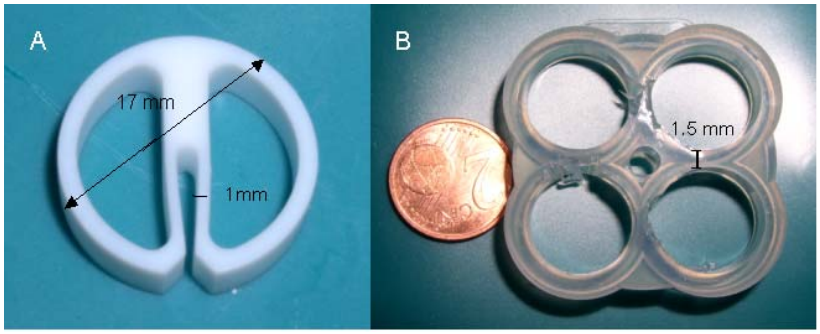


Fig. 5-4: Different commercially available coculture chambers. A: Campenot-divider from Protomatic Inc. made of teflon; B: Flexi-perm disc from Greiner Bio-one upside down with partially cut away walls.

systems with a mechanical separation of different neuron types seem to be more appropriate for the cortex-striatum coculture than closed microfluidic multicompartment systems. A multicompartment device for neuritic isolation of primary cultures of sympathetic neurons was first described by Campenot (Campenot 1977; Campenot 1982). In this method a three-compartment divider made of teflon is sealed to a collagen-coated tissue culture dish with vacuum silicone grease. Before sealing parallel scratches, spaced 200 µm, are made into the surface of the dish. Neurons plated into the small middle compartment send neurites along the scratches. They grow into the outer compartments while the neuronal cell body remains in the middle compartment (Campenot 1977). The teflon barrier is 300 µm thick and it takes about 8 days for the neurites to reach the other side. The removal of the chamber before patch-clamp experiments would destroy the neurites growing through the vacuum grease barrier. In addition, the commercially available Campenot-chamber has walls with a thickness of 1 mm (fig. 5-4). This prevents an early contact of the different neurites; they would reach the other compartment after 25 days (calculated from the results of Campenot, 1977).

Flexiperm discs are silicone chambers which attach themselves to smooth surfaces without vacuum silicone grease (fig. 5-4). Nevertheless, they are not appropriate for the coculture of two different neuron types. The walls have a thickness of 1.5 mm. A neurite is not able to grow over such a distance within 11 DIV (calculated from the results of Campenot, 1977).

For a mechanical separation of two different neuron types the existing multicompartment devices had to be modified. The walls had to be thinner in order to allow the growth of neurites into the other compartment within a few days. Silicon vacuum grease should not be used for sealing because negative effects on the electrophysiological properties of neurons cannot be excluded. Several coculture chamber prototypes with a mechanical barrier were constructed and tested in cell culture. The latest and most promising prototype was constructed as following: The flexiperm disc was combined with a stainless steel separation. The flexiperm disc has 4 subcompartiments which were cut asunder. Each of it was set into a culture dish (8 cm²) and a stainless steel separation (100 µm thick, 1.6 cm long) was inserted. The separation was hold in place by the elastic silicone walls of the flexiperm disc (fig. 5-5). Cortical and striatal cells were cocultured up to 2 weeks.

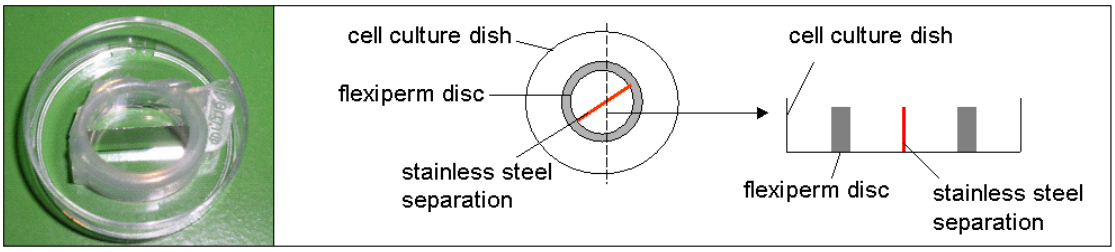


Fig. 5-5: Mechanical coculture chamber made by flexiperm disc with inserted stainless steel separation in a culture dish (8 cm²). Left: image of the mechanical coculture chamber. Right: schematic overview and section.

The chamber and the separation were removed after 3 days in culture. The cleft between the two different neuron types was clearly visible (fig. 5-6). After 11 days in culture the cleft was overgrown by neurites and it was not further possible to distinguish between the different neuron types (fig. 5-7). Nevertheless, the neurites from different sides of the cleft contacted each other and formed functional synapses (data not shown). Also on patterned substrates cocultured neurons could not be distinguished 1 week after removing the separation (fig. 5-8). Thus

the spatial separation of cortical and striatal neurons by a mechanical coculture chamber was discarded.

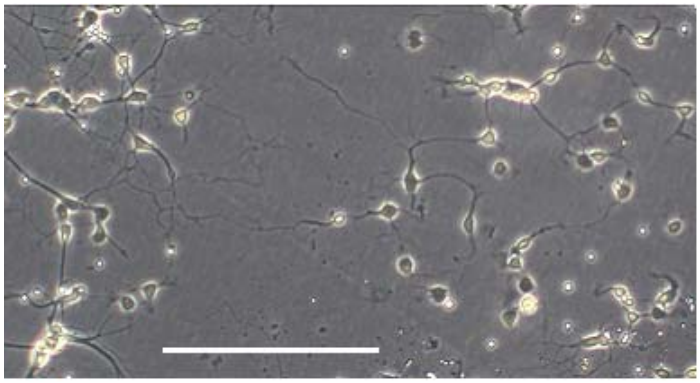


Fig. 5-6 : Striatal (left side of the cleft) and cortical neurons (right side of the cleft) after removal of the barrier at DIV 3. The cleft is clearly visible. Scale bar: 100 µm.

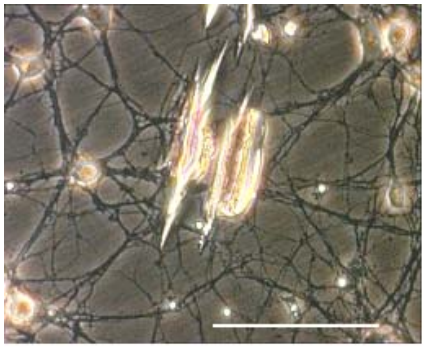


Fig. 5-7: Seven days after removal of the separation, the cleft between cortical (left) and striatal (right) neurons on unstructured PECM is not visible. The scratch marks the position of the barrier; scale bar 100 µm.

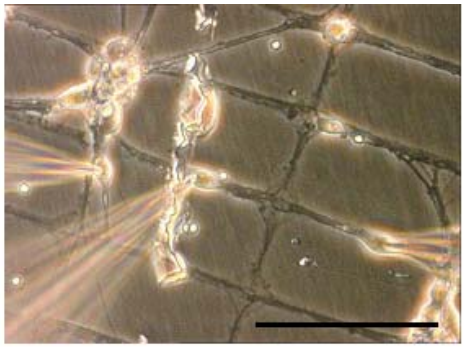


Fig. 5-8: Seven days after removal of the separation, the cleft between cortical (right) and striatal (left) neurons on patterned PECM is not visible. The scratch marks the position of the barrier; scale bar 100 µm.

5.2 Microstructured coculture chamber

Due to the lack of spatial separation in the mechanical coculture chamber it was nescessary to develope a coculture chamber which provides spatial separation for 10-12 days and allows patch-clamp measurements. The microfluidic chamber described by Taylor *et al.* (2003) enabled spatial separation of two different neuron types. Nevertheless, it was irreversible sealed and could not be removed for patch-clamp measurements. Taylor *et al*. (2005) managed to seal a microfluidic chamber reversible on homogenously coated glass. In order to prevent the destruction of neurites and synapses between cortical and striatal neurons at DIV 10-12 the microfluidic chamber has to be removed at DIV 3. The spatial separation between cortical and striatal neurons would be lost and due to migration of neurons cortical and striatal neurons could not be distinguished from each other at DIV 10-12. Based on the microfluidic chamber described by Taylor *et al.* (2003) we designed and produced a microstructured coculture chamber (see materials and methods, 3.2). The coculture chamber has to be coated after sealing to the substrate in order to provide a PECM-micropattern which allows spatial separation after the coculture chamber removal. Striatal and cortical neurons should adhere in front of the microfluidic channels, grow towards each other and form functional synapses. The microstructured coculture chamber has to seal good enough to the substrate for providing spatial separation of cortical and striatal neurons and weak enough to be removed at DIV 3. The strength of a seal between the microstructured coculture chamber (made from PDMS, see materials and methods, 3.2) and glass or polystyrene depends from the strength of surface hydrophilization. Thus we tested different hydrophilization methods on the substrates and the coculture chambers.

5.2.1 Sealing of the microstructured coculture chamber

We tested different hydrophilization methods in order to achieve reversible sealing, beginning with the strongest hydrophilization methods for each surface.
Thus, we tested the seal on uncoated glass coverslips (8 cm²) hydrophilized by a strong acid (one part 30% H_2O_2 and two parts concentrated H_2SO_4) and polystyrene culture dishes (8 cm²) hydrophilized by UV/ozone plasma followed by NaOH treatment. The PDMS-chambers were hydrophilized by O_2-plasma (30 sec., 1.1 mbar, 40 Watt) and carefully pressed onto the hydrophilized substrates. The seal was controlled by filling a mixture of FITC-labeled polylysine (10 µg/ml) and ECM (80-120 µg/ml) into the channels using a vacuum pump. After incubation for 1 h at room temperature the channels were washed with destilled water and checked for leaks. All microstructured coculture chambers sealed well on hydrophilized glass (fig. 5.9), but it was irreversible. The seal between polystyrene was reversible, but only a low amount of coculture chambers sealed on polystyrene (on average 3 coculture chambers out of 10). Thus polystyrene as substrate was discarded.

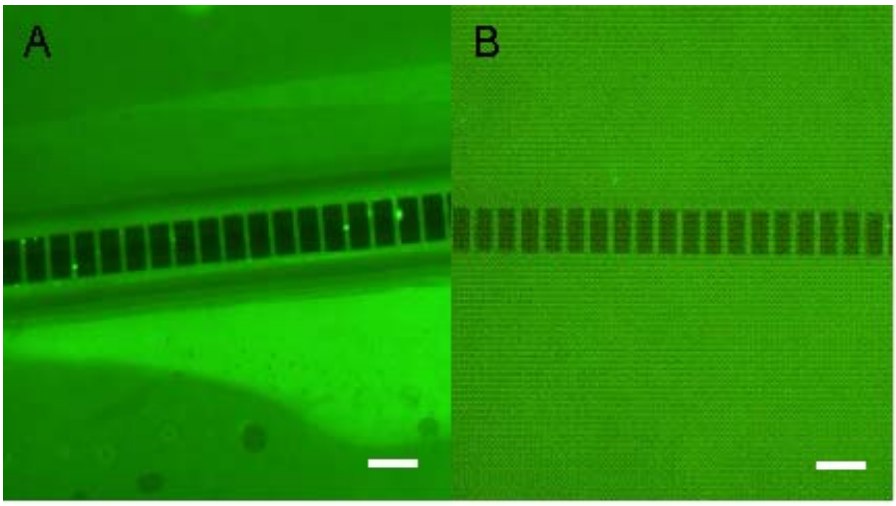


Fig. 5-9: Fluorescence images of the microstructured micropattern (FITC-conjugated polylysine (10 µg/ml) mixed with ECM (80-120µg/ml)) after washing the chamber once with destilled water. A: on hydrophilized glass ; B: on hydrophilized polystyrene; scale bars 50 µm.

In the next experiments a weaker acid (20 % H_2SO_4) was used for the hydrophilization of glass coverslips. The coculture chambers were O_2-plasma-activated and directly sealed to the glass coverslips. The hydrophilization was still too strong, the seal was irreversible.

For a weaker hydrophilization the coculture chambers were hydrophilized using UV/ozone plasma and incubation in 0.1 M NaOH while the glass coverslips were hydrophilized by 20 % H_2SO_4 (for details see 3.2). The chambers were washed thoroughly before sealing and carefully dried before sealing them to the hydrophilized glass coverslips. These hydrophilizations lead to a good seal which was reversible at DIV 3. On average 10 microstructured coculture chambers were prepared in parallel. 81 % of the chambers sealed to the glass coverslips (n=281). Coating was done as described in 3.3.1.

The irreversible sealed coculture chambers could be used for applications which do not require the removal of the coculture chambers, e.g. immunofluorescence and optical analysis of cell growth. Thus they were also tested in cell culture.

5.2.2 Cell culture in the microstructured coculture chamber

Cortical and striatal neurons were prepared in parallel from rat embryos (E18). In first experiments different cell densities ($1.6x10^5$ cells/ml, $3.6x10^5$ cells/ml, $7.5x10^5$ cells/ml and $1x10^6$ cells/ml; n=3 per cell density) were tested (see tab.5-2 for cell density/cm²).

cells/ml	cells/cm²
$1x10^6$	$3.8x10^4$
$7.5\ x10^5$	$1.8\ x10^4$
$3.6\ x10^5$	$8.5\ x10^3$
$1.6\ x10^5$	$3.8\ x10^3$
$*1.6\ x10^5$	$*1.6\ x10^4$

Tab. 5-2.: Calculation of the cell densities/cm² used for the coculture. The values for the optimized cell culture are marked with a *. The coculture chamber has an area of 0.79 cm² and is filled with 180 µl medium.

30 µl of cortical or striatal cell suspension respectively were placed into one filling hole and pulled carefully to the second filling hole using a vacuum pump. After 1h 30 µl medium were added to each filling hole. Neurons plated in a density of $3.8x10^4$ cells/cm² were viable at DIV 3 (fig. 5-10 and 5-11). All other tested cell densities were not appropriate for microstructured coculture; no viable neurons could be observed at DIV 3 (data not shown). In later experiments the growth channels and the microfluidic channels were filled with medium 2 h before plating. Directly before plating the medium was removed. This allowed the flow of cell suspension to the second filling hole without using a vacuum pump due to the previously wetting of the surface and reduced the shearing forces during plating.

In the irreversible sealed coculture chamber the neurons could be cultured up to DIV 3 (fig. 5-10). Although medium was changed half at DIV 3 the neurons degraded afterwards in culture. Even daily change of half of the medium did not prevent neuronal degradation. Therefore, the irreversible sealed coculture chambers were discarded.

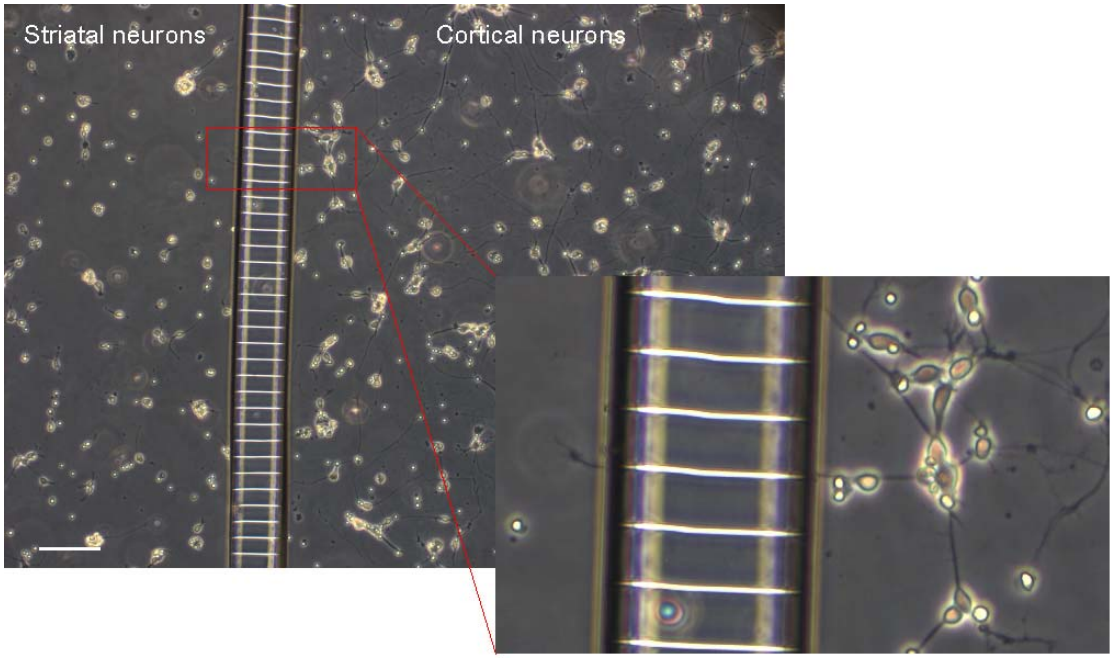


Fig. 5-10: Rat striatal (left) and cortical (right) E18 neurons at DIV 3 cultivated in the irreversible sealed microstructured coculture chamber. A neurite from a cortical neuron grows through a 100 µm long and 3 µm wide microfluidic channel; scale bar 100 µm.

Neurons cultured in the microstructured coculture chambers which were sealed reversible onto glass coverslips appeared healthy at DIV 3 in 25% of microstructured chambers (n = 147, fig. 5-11). The coculture chambers were covered with 1.6 ml medium. In comparison to normal cortical cell culture the cell density of cocultured striatal and cortical neurons is lower. In order to provide enough neurotrophic factors during further cultivation conditioned NB medium was taken from cortical neurons DIV 3 and used for the coculture. The coculture chambers were carefully removed and medium was changed half every 3-4 days. The neurons cultured in conditioned NB-medium degraded after the removal of the coculture chamber (data not shown).

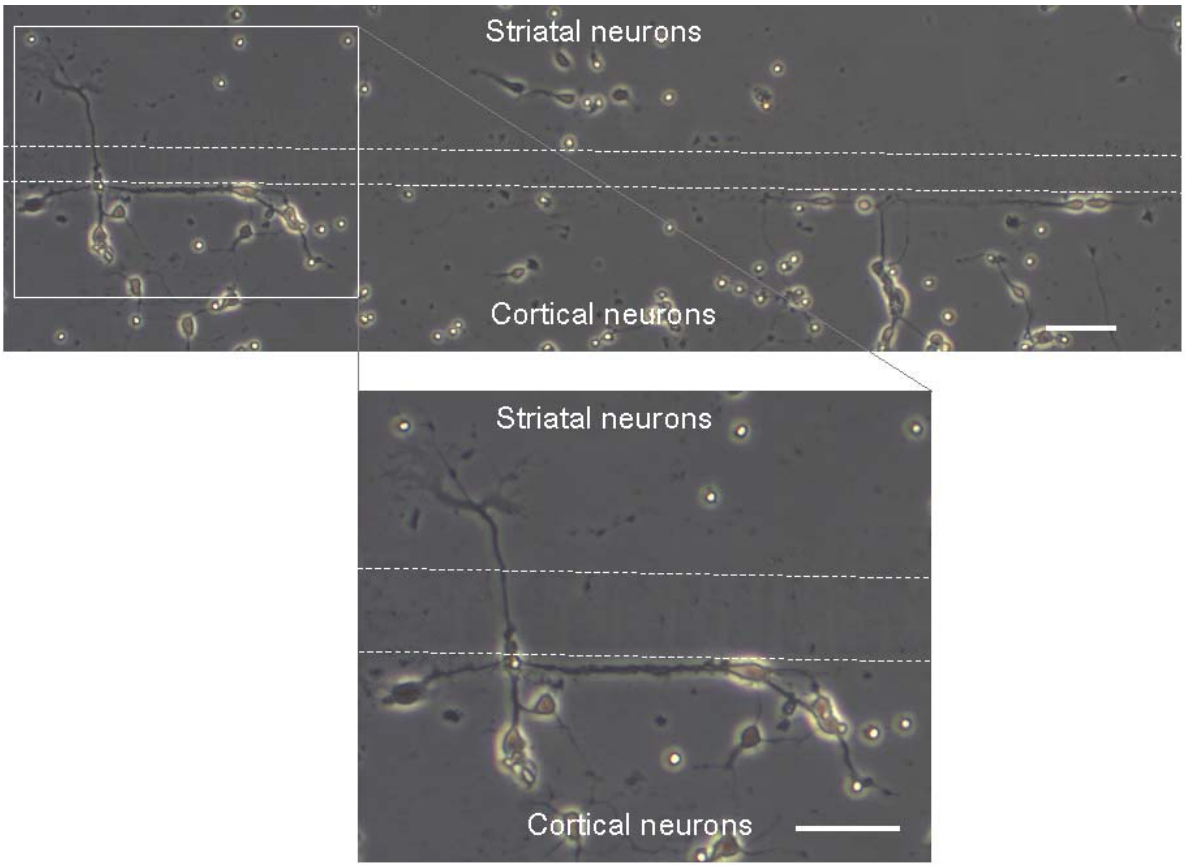


Fig. 5-11: Rat striatal (above the microfluidic channels) and cortical (below the microfluidic channels) E18 neurons at DIV 3 cultivated in the reversible sealed microstructured coculture chamber. The chamber was removed; the PDMS residues and the microfluidic channels are visible in the middle of the picture. A neurite from a cortical neuron grows through a 50 µm long and 5 µm wide microfluidic channel. Several neurites grow parallel to the PDMS-residues but not through the microfluidic channels. The former position of the wall with microfluidic channels is marked by dashed lines; scale bar 50 µm.

For further optimization of the cell density half of a coverslip with 3 days old cortical neurons in a density of 1.6 x10^4 cells/cm² was added to the striatal and cortical neurons at DIV 3. As a result 38 % (n = 37) of the striatal and cortical neurons which could be cultured until DIV 3 survived up to DIV 7 (fig. 5-12 and 5-13).

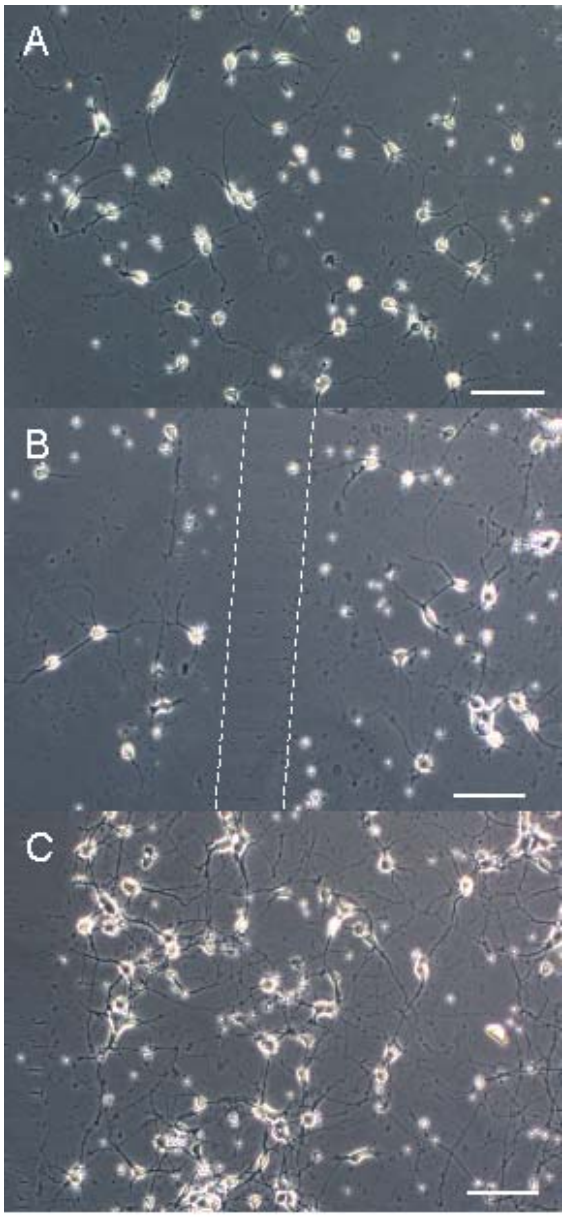


Fig. 5-12: Rat cortical and striatal E18 neurons at DIV 7 cultivated in the reversible sealed microstructured coculture chamber.

A: Overview of striatal neurons in a growth channel; B: Striatal neurons grow on the left side of the microfluidic channels (marked by dashed lines), cortical neurons on the right side; C: Overview of cortical neurons in a growth channel. Scale bar: 100 µm.

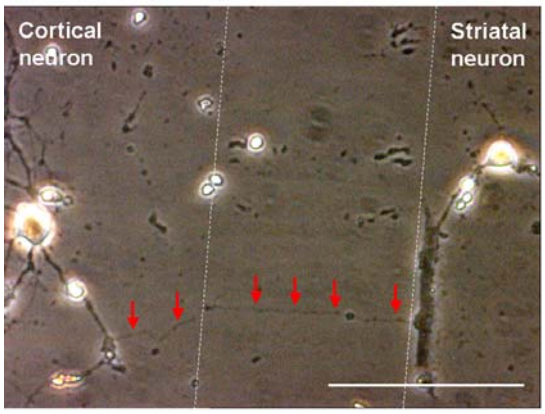


Fig. 5-13: Rat striatal (right) and cortical (left) E18 neurons at DIV 7 cultivated in the reversible sealed microstructured coculture chamber. The chamber was removed at DIV 3, at DIV 7 the neurites of a cortical and striatal neuron formed a physical contact (marked by red arrows). The former position of the wall with microfluidic channels is marked by dashed lines. Scale bar: 100 µm.

In some cases (14 %, n=37) it was possible to culture the striatal and cortical neurons up to DIV 11 (fig. 5-14 and 5-15).

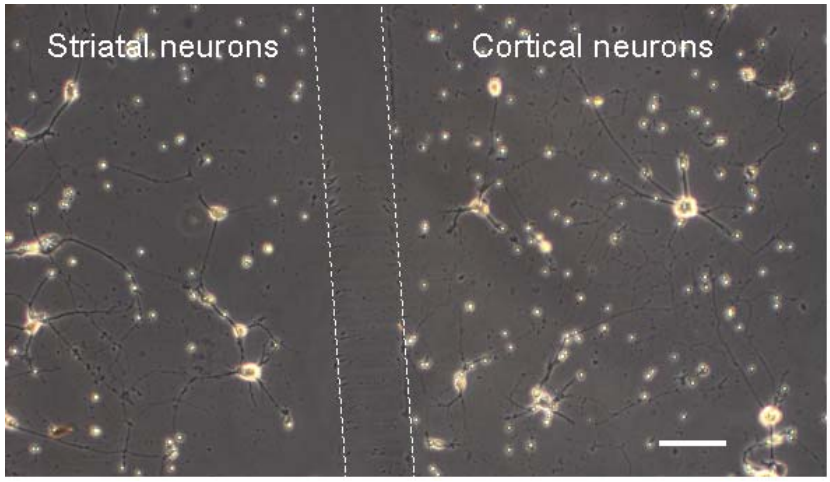


Fig. 5-14: Rat striatal and cortical E18 neurons at DIV 10 in the microstructured coculture chamber. Although a lot of cell debris is in the cell culture, the remaining neurons have a healthy morphology. The former position of the wall with microfluidic channels is marked by dashed lines. Scale bar: 100 µm.

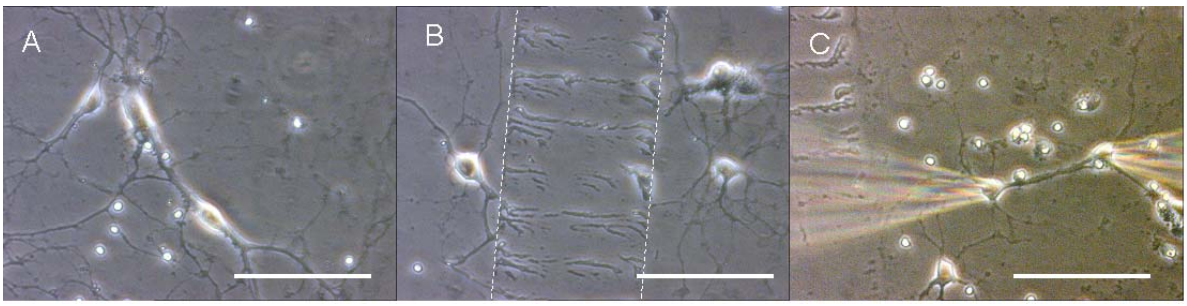


Fig. 5-15: Rat striatal and cortical E18 neurons at DIV 11 in the microstructured coculture. A: Striatal neurons; B: Striatal neuron on the left side of the PDMS-residues, cortical neurons on the right side. The former position of the wall with microfluidic channels is marked by dashed lines.; C: Cortical neurons during patch clamp measurement. Scale bar: 50 µm.

5.2.3 Electrophysiology of cocultured neurons

At DIV 11 cortical and striatal neurons cultured in a microstructured coculture chamber could be used for electrophysiological measurements. Although a lot of neurons degenerated from DIV 3 to DIV 11, the remaining neurons had a healthy morphology which could be confirmed by electrophysiological measurements: The analyzed cocultured neurons showed similar electrophysiological characteristics to cortical and striatal neurons respectively grown on PECM grid patterns (fig. 5-16, tab. 5-3 and 5-4). The cocultured cortical neurons had a significant lower FLHM compared to cortical neurons cultured on PECM grids. A synapse was measured between two striatal neurons cultured in the microfluidic coculture chamber up to DIV 11 *in vitro* (fig. 5-17).

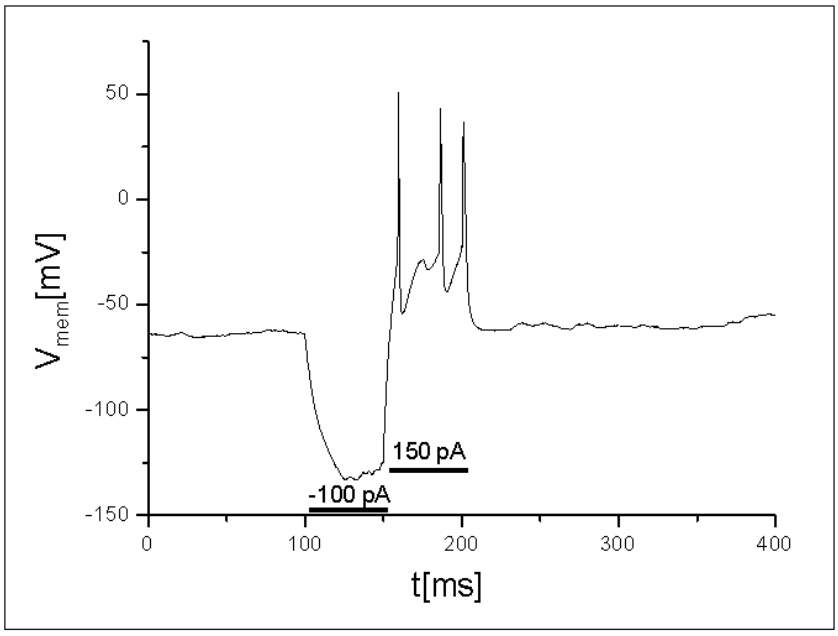


Fig. 5-16: Current-clamp measurement of a cortical neuron cultured in a microstructured coculture chamber up to DIV 11. The neuron was measured in the current clamp mode; the resting potential was –60 mV; the leak was 1.12 ns. The neuron spiked 3 times during the stimulation.

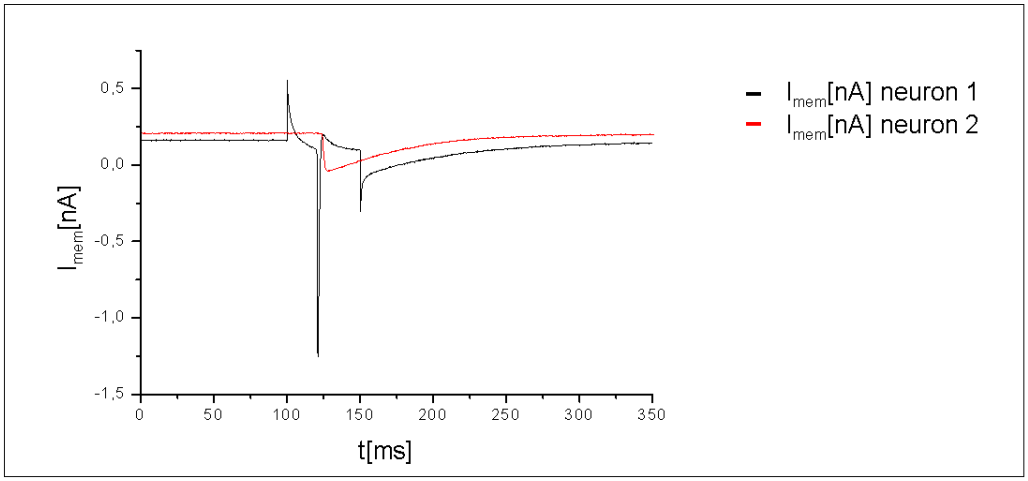


Fig. 5-17 : Synapse between two striatal neurons cultured in the microstructured coculture up to DIV 11. Both neurons were held in the VC-mode at –70 mV. Neuron 1 was stimulated with 30 mV for 50 ms. The resting potential was –59 mV. Neuron 2 had a resting potential of –65 mV.

	Cortical neurons (-70 mV)	Cocultured cortical neurons (-70 mV)
n of patched neurons	113 (74 with AP at 150 pA)	6 (6 with AP at 150 pA)
Resting potential [mV]	-62 ± 7	-64 ± 8
FLHM at 150 pA [ms]	2.0 ± 0.7	1.3 ± 0.6*
APs at 150 pA	1.4 ± 0.6	1.9 ± 0.6
AP-Amplitude at 150 pA [mV]	61 ± 13	72 ± 13
tau [ms]	18 ± 8	10 ± 4

Tab. 5-3: Electrophysiological characteristics of cortical neurons DIV 10-12 cocultured with striatal neurons compared to cortical neurons DIV 10-12 cultured on PECM-grid-patterns. Significant differences are marked with a* (p<=0.05 in a student´s t-test).

	Striatal neurons (-70 mV)	Cocultured striatal neurons (-70 mV)
n of patched neurons	10 (10 with AP at 150 pA)	3 (3 with AP at 150 pA)
Resting potential [mV]	-65 ± 10	-63 ± 9
FLHM at 150 pA [ms]	1.6 ± 0.6	2.2 ± 1.0
APs at 150 pA	1.4 ± 0.6	1 ± 0
AP-Amplitude at 150 pA [mV]	57 ± 9	65 ± 9
tau [ms]	17 ± 8	16 ± 9

Tab. 5-4: Electrophysiological characteristics of striatal neurons DIV 10-12 cocultured with cortical neurons compared to striatal neurons DIV 10-12 cultured on PECM-grid-patterns. In a student´s t-test no significant differences were observed (p<=0.05 in a student´s t-test).

6. Discussion

6.1 Two-step microcontact printing

Manual two-step microcontact printing

Two-step microcontact printing (2-step µCP) was established in order to create a grid pattern consisting of axon-guiding and neutral proteins. These complementary protein patterns should induce directed polarity in neuronal networks of rat cortical neurons grown on these substrates. In future works these patterns should also be printed on the surface of field effect transistors and multielectrode arrays, which is mainly composed of SiO_2 (Pine, 1980; Offenhäusser *et al*., 1997). The 2-step µCP experiments were therefore done on SiO_2 or silica glass which contains 100% SiO_2 and has similar chemical properties.

For substrate characterization lines of axon-guiding proteins were printed onto lines of neutral proteins using manual 2-step µCP. The characterization of protein transfer was done by fluorescence microscopy, ellipsometry and atomic force microscopy (AFM). Moreover, the effect of the second printing step on the preprinted protein pattern was tested.

In first experiments the printing of hydrophilic proteins with low viscosity (poly-D-lysine, laminin, netrin-1) on glass substrates was established. The elastomeric PDMS-stamps used for microcontact printing are hydrophobic due to the nonpolar methyl sidegroups along the siloxane backbone of the polymer chain (James *et al*., 1998). Wetting of the stamp surface with hydrophilic proteins requires hydrophilization of the stamp surface. Although in previous reports (Lauer *et al*., 2001, Yeung *et al*., 2001) microcontact printing of proteins was done without SDS-pretreatment of the stamps, in this study the microcontact printing method was modified according to Chang *et al.* (2003) by using 10 % SDS for pretreatment of the stamp surface. This method affords to print grid-patterns of ECM, laminin, netrin-1 and FITC-PLL on glass with similar good protein transfer. As Chang *et al.* (2003) already hypothesized, the SDS used for release of the stamp from the master may also act as release agent during printing. SDS is an amphiphile consisting of a hydrophilic head and a hydrophobic carbon tail and could therefore

mediate an adequate transfer of protein onto the glass substrate (Chang *et al*., 2003).

The fluorescence images of the 2-step µCP substrates showed a mainly homogeneous transfer of FITC-PLL except at the nodes, where the FITC-PLL-transfer was incomplete. A similar incomplete transfer of protein at the nodes was also observed for PECM, laminin and PLL by A. Vogt (2003a) who suggested that this effect was caused by the hydrophobicity of the PDMS-stamp. Therefore, in this study an incomplete SDS-layer at the nodes may lead to a partially hydrophobic stamp surface, resulting in incomplete protein transfer at the nodes.

The transfer of ECM, laminin and netrin-1 onto the substrates was inhomogeneous, marked by a lower protein transfer in areas with preprinted FITC-PLL. This may be explained by the different surface properties of polylysine and silica glass. Polylysine adsorbed to substrates has a rough surface with protein peaks and deep valleys (see AFM-measurements; James *et al*., 1998; Lin *et al*., 2007). In contrast, silica glass has a smooth surface (see AFM-measurements), which could result in a higher protein transfer. Moreover, the chemically properties of the silica glass surface and the surface of the printed FITC-PLL are different. The surface of silica glass coverslips is cleaned from all organic contaminations by flaming. After cooling a capillary film of water forms on the surface, resulting in a hydrophilization of the silicon-oxygen groups (Si-O) to silanole groups (Si-OH). Printing of polylysine masks the silanole groups with amino groups and changes the surface charge, resulting in a lower protein transfer.

An additional protein transfer was observed for netrin-1, laminin and ECM in the interspace of the printed line patterns. It occurs when the roof of the stamp structure collapses (so-called sagging) and touches the substrate, either due to too much pressure or a low aspect ratio of structure height and width (Sharp *et al*., 2004; Decré *et al.*, 2005). In contrast to the 2-step µCP line patterns no sagging of stamps was observed in the 2-step µCP grid patterns, although these patterns were printed using stamps with the same aspect ratio as the stamps with line structure. This can be explained by the missing perpendicular structures and the missing nodes of the stamps with lines, resulting in a lower stability of the roof of the stamp.

Mapping of protein thickness using ellipsometry showed an inhomogeneous protein transfer for all printed proteins. ECM, laminin and netrin-1 lines had a spotted appearance characterized by increased protein transfer in some spots of the printed lines, while PDL accumulated at the outer rim of lines and nodes. The protein thickness of ECM and PDL varied strongly across a substrate, while both netrin-1 and laminin showed less variation. The thickness variation of the transferred protein could be generated by the drying process which leads to unregular drying of the protein drop on the stamp surface. Therefore, a randomly distributed protein-multilayer could be formed. The proteins in this multilayer could self-assembly, resulting in the local transfer of huge amounts of protein .

For detailed surface analysis AFM-measurements were made with one substrate per protein pair. All proteins had a highly irregular surface, which correlates with the data of ellipsometry and is also consistent to previous AFM-studies of James *et al*. (1998) and Lin *et al*. (2007). Moreover, the thickness of ECM and PDL varied strongly within one line of the pattern, confirming the data gathered by ellipsometry. AFM-measurements of the laminin surface showed a mesh-like structure in some areas of the transferred protein pattern. Similar structures were shown by Freire *et al.* (2002). Laminin is able to self-assemble and forms a network of polygonal structures representing a physiological organization (Yurchenco *et al.*, 1985; 1993; Freire *et al.*, 2002). This self-assembly is mediated by Ca^{2+}-ions (Yurchenco *et al.*, 1985). In this work a laminin network intersected by areas of unorganized laminin was observed, which could be generated by a lack of Ca^{2+}-ions in the solvent ($HBSS^{-}$) as described in the study of Freire *et al. (*2002). Another possible reason is the concentration of laminin used in this work (25 µg/ml). Sgarbi *et al*. (2004) showed that laminin printed in a concentration of 10 µg/ml was able to self-assemble to a network of polygonal structures, while a concentration of 30 µg/ml lead to transfer of a multilayer of overlapping molecules. The authors hypothesized that laminin could form a dense cross-linked three-dimensional protein matrix in solution at a concentration of 30 µg/ml. This matrix could collapse during drying, resulting in a printed multiplayer of overlapping proteins (Sgarbi *et al*., 2004). The ability to print completely self-assembled laminin layers could be reduced gradually with concentrations > 10 µg/ml. Nevertheless, the printed laminin was still able to bind specifically to a polyclonal laminin-

antibody (Sgarbi *et al*., 2004). Successful outgrowth of neurons on printed laminin was also demonstrated by other groups (Kam *et al*., 2001; Schmalenberg *et al*., 2004). Comparable observations were made by Shi *et al*. (2007) for printed N-cadherin: The neuron outgrowth on N-cadherin patterns printed with hydrophobic PDMS-stamps directly on glass was similar to neuron outgrowth on recombinant N-cadherin which was covalently bound to preprinted patterns of protein A**.** This protein, which binds specifically to the Fc-part of immunoglobins (Lindmark *et al.,* 1983), reacts also with recombinant proteins including an IgG-domain (e.g. N-cadherin) and allows to bind these proteins in their native conformation. In contrast, Hodginson *et al.* (2006) showed that a monoclonal IgG1 antibody against a growth-promoting epitope at the carboxy terminal globular domain of the A chain of laminin did not bind on laminin patterned directly without protein A (standard microcontact printing). The authors assumed that the growth-promoting epitopes were masked by other domains of the protein during the printing process. Nevertheless, also some growth-promoting epitopes of proteins are masked by standard microcontact printing, it could be proved that enough epitopes remain intact to allow a comparable neuronal outgrowth as on native protein (Kam *et al*., 2001; Schmalenberg *et al*., 2004; Shi *et al*. ; 2007).

The protein thicknesses determined by AFM measurements were comparable to the values received with ellipsometry for all proteins. Ellipsometer and AFM measurements, respectively, showed that the protein thickness at the crossing points were lower than expected by adding the values derived from measurements of the adjacent protein lines. Independent of the protein pair, it seems that the second protein was not completely transferred at the crossing points onto the first printed protein line. As explained previously, this may be caused by the different surface properties of silica glass and printed polylysine.

Cell culture experiments on the manual 2-step µCP substrates showed that neurons cultured on ECM/PDL substrates and on laminin/PDL had a similar good morphology and viability as neurons cultured on PECM-grids, while on netrin-1/PDL substrates the amount of dead cells was higher.

Aligned two-step microcontact printing

In order to produce a protein-grid pattern with axon-guiding properties in only one direction two complementary patterns were needed. The pattern specifically for printing the axon-guiding protein consists of a node with a line, while the pattern for the neutral protein consists of three lines outgoing from the node. This required the alignment of the second pattern under visual control with the fineplacer (see 4.2). Fluorescence images showed a homogeneous protein transfer for ECM, laminin and netrin-1, while the transfer of FITC-PLL was inhomogeneous. This could be due the different printing methods: FITC-PLL was preprinted manually with a not identical pressure in each printing process, while the other proteins were printed with the fineplacer enabling the control of the pressure. Sagging did not occur, probably due to the stabilizing effect of the stainless steel platelet in the stamp or the precise control of pressure by use of the fineplacer. Although the fineplacer allowed alignment with an accuracy of 1 µm only a part of the stamped area (about 300 µm x 300 µm) could be aligned exactly by optical control. Minor, nearly invisible misalignments in this area can lead to complete misalignment of the contemplary pattern surrounding the part of the pattern which could be visually controlled. It was also a very time-consuming procedure; about 30 minutes were needed for the production of one aligned 2-step µCP substrate (see materials and methods). ECM was easier to print than laminin, PDL and netrin-1, probably due to its higher adsorbtion rate on glass substrates. Thus ECM and PDL were used for aligned 2-step µCP to create grid patterns which were tested on compatibility for neurons in cell culture and on electrophysiologal activity of neurons by patch-clamp experiments.

Neurons plated on the aligned ECM/PDL substrates could be cultured up to DIV 11. The neurons did not always grow exclusively along the printed pattern, but also across uncoated areas of the substrate towards PDL-nodes or protein-lines. This could be caused by locally distinct protein concentrations within the pattern demonstrated by ellipsometer and AFM measurements. It is commonly known that growth cones of neurites orient themselves along gradients of secreted guiding cues *in vivo* and *in vitro* (Song *et al.*, 2001; Dickson, 2002). Further it could be demonstrated by *in vitro* studies that surface-bound gradients of the laminin IKVAV-peptide induced turning of axons extending from a chicken dorsal root

explant towards the highest concentration of the peptide (Adams *et al*., 2005). In this study, neurites would also grow towards higher concentrations of an attractive protein. This chemical gradient could be developed due to protein accumulation at the nodes or the outer rim of protein lines.

Cortical neurons cultured on the aligned ECM/PDL substrates showed similar electrophysiological properties as neurons cultured on PECM grid patterns except for the AP-frequency, which was significantly lower in comparison to the neurons on the PECM substrates. It was shown, that a higher amount of neurons adheres on PECM than on ECM and PDL alone (A. Vogt, 2003a). Thus, ECM or PDL may be a less optimal substrate for cell growth than PECM. By future double patch-clamp experiments it could be analyzed, if neuronal growth on aligned 2-step µCP substrates is guided by the complementary patterns of axon-guiding and neutral proteins, thus enabling the control of neuronal polarity.

6.2 Coculture system

Striatal cell culture

The striatal cell culture protocol was adapted from the cortical cell culture. Immunocytological stainings against MAP2 and GFAP showed that about 68 % of the cultured cells on patterned and unpatterned substrates were glial cells at 11 DIV, similar to the amount observed in cortical cell culture. This is probably due to the same conditions in cultivation. Laser scanning microscopy images proved that nearly each neuron grew upon a glial cell. Moreover, all cells tested in patch-clamp experiments showed APs and membrane currents, which evidenced the electrophysiological activity of the striatal cells.

The purity of striatal cell culture was tested by single-cell PCR (RT-PCR). About 70 % of the cells could be identified as striatal neurons (unpublished data, R. Helpenstein *et al.*) by expressing striatum-specific G-protein coupled receptor-RNA-transcripts (Mizushima *et al*., 2000). The remaining 30 % should be neurons obtained from the surrounding basal ganglia and the thalamus.

In vivo the resting membrane potential of striatal neurons switches from a hyperpolarized “down”-state to a depolarized “up”-state (Reynolds *et al.*, 2000). This could not be observed in the striatal cell culture. The striatal neurons had

stable resting potentials of - 65 mV, probably due to missing input from cortical afferents, which corresponds to the literature. In low density cultures (Segal *et al.*, 2003) as well as in organtypic cocultures of striatal and cortical slices obtained from newborn rats (Plenz *et al.* 1996a) a resting potential of about – 60 mV was measured in striatal neurons. AP-amplitude and FLHM of the striatal neurons in monoculture were also similar to the electrophysiological properties measured in an organotypic coculture (Plenz *et al*., 1996a), but the measured membrane time constant τ of 17 ± 8 was significant different to the value found in literature (6 ± 3 ms). The membrane time constant τ is defined as response-time of the neuron due to interferences in the membrane potential (Nicholls *et al.*, 1995). This response-time can be adjusted by several factors. Cortical pyramidal neurons in a neocortical slice without spontaneous activity, which were activated by synaptical inputs due to external stimulation of adjacent neurons, exhibited a significant lower τ than cortical neurons without this input (Koch *et al.,* 1996). The decrease of τ in neurons with synaptical input was induced by depolarization of the cell membrane which lead to the opening of voltage–gated Na^+ and K^+ channels and therefore to an increased flow of leak currents (Koch *et al.,* 1996). Moreover, τ is influenced by the membrane conductance, which can be modulated by changes in membrane voltage and ligand-binding (Koch *et al.,* 1996). The significantly increased τ in striatal low density culture could therefore be explained by the different type of culture: In a low density culture derived from dissociated embryonic tissue striatal neurons receive a reduced synaptic input in comparison to an organotypic slice coculture with high cell density and increased amount of synaptic connections. In addition, the striatal neurons in monoculture did not receive synaptical inputs from cortical afferents. Thus the membrane time constant τ in the striatal low density culture is lower than in the organotypic coculture.

Compared to cortical neurons striatal neurons possess a significantly lower FLHM, the other electrophysiological parameters are not significantly different. This was also observed in organotypic cocultures of striatum and cortex (Plenz *et al*., 1996a). The lower FLHM could be caused either by a higher amount of Na^+- and K^+ -channel proteins or the expression of Na^+- and K^+ -channels with a faster kinetic.

Microstructured coculture chamber

As shown in the cell culture experiments striatal and cortical neurons could be cultured under the same conditions. The main problem was not the coculture of the different neuron types, but the spatial separation of striatal and cortical neurons for at least 10 DIV. Although the spatial separation with mechanical removable barriers which were clamped into a flexiperm disc provided a clear separation it was not possible to maintain this separation for more than 3 DIV. The steel barriers had to be removed latest at DIV 3, otherwise the neurites would not have been able to grow towards each other and form synaptical contacts. Due to the completely coated substrate the cortical and striatal neurons grew randomly over the cleft and therefore the neuronal cultures could not be distinguished from each other at DIV 11. The same result was observed for a mechanical separation on PECM-grids.

A more sophisticated technique for the spatial separation of neurons was the microstructured coculture chamber. Taylor *et al.* (2003) described a microstructured chamber for fluidic isolation of neurites and soma in neuronal cell culture which irreversible sealed onto glass substrates. This irreversible seal was induced by oxygen-plasma activation of glass substrate and the PDMS coculture-chamber. Oxygen-plasma induces the formation of oxygen radicals on the glass surface and the formation of a thin SiO_2-film on PDMS (Glasmästar *et al*., 2002). At air a capillary film of water forms on both surfaces, resulting in a hydrophilization due to silanole groups. At contact of the surfaces oxygen-plasma activated glass and PDMS bound covalently to each other. Since following removal of the coculture chamber was not possible, this sealing method probably leads to a high amount of covalent bonds. Patch-clamp experiments require removing of the microstructured chamber, thus in this work a sealing method was established for reversible sealing of the coculture chamber to glass substrates. By gradually reducing the strength of hydrophilization due to testing of different hydrophilization methods the optimal grade of hydrophilization for reversible sealing could be achieved using UV/ozone plasma. It was assumed that UV/ozone plasma treatment of PDMS produces a similar surface chemistry as oxygen plasma treatment (Glasmästar *et al*., 2002). UV/ozone plasma also oxidizes the PDMS–surface and leads to the formation of a thin SiO_2-film. In contrast to Taylor

et al. (2003) the coculture chamber was not immediately sealed onto sulfuric acid-activated glass. Before sealing the coculture chambers were incubated for 2 h in sodium hydroxide. The incubation in polar solvents caused a surface hydrophilization due to silanole groups, but over time this effect diminished (Murakami *et al.*, 1998). In comparison to the oxygen-plasma activation a lower amount of covalent bonds could be formed by UV/ozone plasma treatment and subsequent chemical hydrophilization by sodium hydroxide, which enabled removal of the coculture chamber at DIV 3.

The next challenge was the culturing of cells in the microstructured coculture chamber. The plating method was important for neuronal viability. Without preincubation of the microfluidic channels with medium the cell suspension had to be drawn into the channels by vacuum. This resulted in cell harming and reduced cell viability by high shearing forces. By prewetting the growth channels and the microfluidic channels with medium, application of vacuum was not further required. The cells were drawn through the growth channel to the second filling hole by hydrostatic pressure. This method allowed adhesion and growth of neurons in all compartments of the microstructured chamber. The amount of viable neurons could also be increased. Due to the low amount of medium (180 µl) evaporation of medium could lead to increased osmolarity. Thereby the coculture chamber was removed at DIV 3 and filled up with 1.6 ml medium in order to prevent too much evaporation of medium. Different cell densities were tested in order to further increase the number of surviving neurons at DIV 3. A density of $3.8x10^4$ cells/cm² per growth channel allowed a good growth of cortical and striatal neurons up to DIV 3 in 25 % of the coculture chambers. Moreover, due to the high amount of neurons in a low amount of medium ($3.8x10^4$ cells/cm² in 180 µl medium) the concentration of metabolic end products in the cell culture could increase and become cytotoxic until DIV 3, leading to death of neurons.

The removal of the coculture chamber allowed outgrowth of neurites and the forming of synaptical contacts between cocultured striatal and cortical neurons. A later removal at DIV 11 would destroy the neurites grown along the microfluidic channels, as shown by experiments with monocultures of cortical neurons (data not shown). The cell density of estimated 10-50 % of the originally plated cells at DIV 3 was too low for optimized cell culture, therefore cocultured neurons cultured

in 1.6 ml fresh or conditioned culture medium could only survive up to DIV 6. Increasing the total cell density by adding half of a coverslip with 3 days old cortical neurons in a density of 1.6 $x10^4$ cells/cm² improved the viability of neurons up to DIV 11. This could be explained by the increase of neurotrophic factors in the coculture system.

Electrophysiological analysis of the cocultured striatal and cortical cells confirmed their neuronal identity and functionality. No significant differences could be observed between the electrophysiological properties of striatal monocultures in comparison to striatal neurons cocultured with cortical neurons (n=3). In contrast, the cocultured cortical neurons (n=8) showed a significant lower FLHM (10 ± 4) compared to cortical monocultures on PECM-grids (18 ± 8). The lower FLHM could be caused either by a higher amount of Na^+- and K^+ -channel proteins or the expression of Na^+- and K^+ -channels with a faster kinetic (McCormick *et al*., 1987). This supports the conclusion that a selection of a subgroup of cortical neurons occurs in the microstructured coculture. By double patch-clamp measurements a synapse between two cocultured striatal neurons could be measured, confirming the ability of the cocultured neurons to form synaptic contacts. Due to the dissection of the whole striatum, medium spiny neurons and striatal interneurons were cultured together. Synapses could be formed either between an interneuron and a medium spiny neuron or between two medium spiny neurons: Fast spiking striatal interneurons provide inhibition to medium spiny neurons, as shown in several studies (Plenz *et al.*, 1998; Koos *et al.,* 1999). Moreover, in organotypic cortex-striatum-substantia nigra cocultures a fast GABAergic connection optimized for burst transmission was observed between 30 % of medium spiny neurons (Czubayko *et al*., 2002).

The established microstructured coculture system enables a spatially separated coculture of striatal and cortical neurons up to DIV 11. Due to the reversible seal of the coculture chamber it can be tested by further double patch-clamp measurements, if the functional polarity between cortical and striatal neurons in the central nervous system remains in cell culture.

7. Summary

This work focused on the control of neuronal polarity in patterned neuronal networks. Two different approaches were taken in order to direct polarity within a neuronal network. The first strategy was to chemically pattern two proteins with distinct effects on neurite growth. As second strategy, the reconstruction of the natural polarity between cortex and striatum in cell culture was chosen. The results of this work are summarized as follows:

Two-step Microcontact printing:

1) In this work the contrast between axon-guiding and neutral regions was increased not simply by interrupting a grid pattern of PECM but by printing complementary patterns of proteins with different effects on axon outgrowth. Netrin-1, laminin and ECM were chosen as axon-guiding proteins, while polylysine was printed as neutral protein.
2) In this work aligned two-step microcontact printing was developed, a printing technique which allows accurate aligned printing of two complementary protein patterns under visual control.
3) The protein transfer of low-viscosity hydrophilic proteins like poly-D-lysine with microcontact printing was shown not to be as satisfactory as the transfer of high-viscosity proteins like ECM (Vogt, 2003a). A pretreatment of the stamps with 10 % SDS resulted in a similar good protein transfer of ECM, laminin, netrin-1 and FITC-PLL on glass substrates.
4) The protein transfer during two-step microcontact printing and the effect of the second printed pattern on the primary ones was characterized by fluorescence microscopy, ellipsometry and atomic force microscopy (AFM) using manual two-step microcontact printing (2-step μCP) substrates. Each method showed, that the first printed pattern consisting of polylysine was not blurred or removed by printing of the second pattern. Moreover, the transfer of ECM, laminin and netrin-1 onto the substrates was inhomogeneous, characterized by a lower protein transfer at areas with preprinted polylysine. A highly irregular protein surface was observed for all proteins by ellipsometry and AFM measurements. Additionally, AFM measurements showed a mesh-like structure in some areas of the

transferred laminin pattern, representing a physiological organization of the printed laminin.

5) Cell culture experiments on the manual 2-step µCP substrates showed that neurons cultured on ECM/PDL substrates and on laminin/PDL had a similar good morphology and viability as neurons cultured on PECM-grids, while on netrin 1/PDL substrates the amount of dead cells was increased.
6) Electrophysiological measurements showed that cortical neurons cultured on the aligned ECM/PDL substrates possessed similar electrophysiological properties as neurons cultured on PECM grid patterns except for the AP-frequency, which was significantly lower in comparison to the neurons on the PECM substrates.

Coculture system:

1) For reconstruction of a natural polarity between cortical and striatal neurons in cell culture, striatal cell culture was established based on the already existing cortical cell culture. About 70 % of the cells could be identified as striatal neurons by expressing striatum-specific G-protein coupled receptor-RNA-transcripts. The striatal neurons in monoculture had similar electrophysiological properties as described in literature, except for a significantly higher membrane time constant τ.
2) By gradually reducing the strength of hydrophilization the optimal grade of hydrophilization for reversible sealing could be achieved using activation by UV/ozone plasma and subsequent chemical hydrophilization by sodium hydroxide. This enabled removal of the coculture chambers and therefore patch-clamp measurements.
3) Cell culture experiments in the coculture chambers showed, that 25 % of the chambers contained viable cortical and striatal neurons at DIV 3. By removing the coculture chamber at DIV 3 and increasing the cell density, neurons in 14 % of these chambers could survive up to DIV 11. This allowed patch-clamp experiments on matured synapses.
4) Electrophysiological analysis of the cocultured striatal and cortical cells by patch-clamp measurements at DIV 10-12 confirmed their neuronal identity and functionality. No significant differences could be observed between the electrophysiological properties of striatal monocultures in comparison to

striatal neurons cocultured with cortical neurons. In contrast, the cocultured cortical neurons showed a significant lower FLHM compared to cortical monocultures on PECM-grids. By double patch-clamp measurements a synapse between two cocultured striatal neurons could be measured, confirming the ability of the cocultured neurons to form synaptic contacts.

8. Outlook

Two-step microcontact printing

Due to the low amount of analyzed neurons it is still open, if neuronal growth on aligned 2-step µCP substrates is guided by the complementary patterns of axon-guiding and neutral proteins. For the evaluation of polarity in this system the aligned printing method has to be technically improved. If the printing of the aligned second pattern with the fine placer could be done in parallel for several substrates instead of consecutively, more substrates could be cultured and electrophysiologically analyzed. For this a stamp holder has to be designed which allows the removal of the substrate with positioned stamp during the second printing step without moving the stamp.

By future double patch-clamp experiments it could be analyzed, if neuronal growth on aligned 2-step µCP substrates is guided by the complementary patterns of axon-guiding and neutral proteins, thus enabling control of directed neuronal polarity in patterned neuronal networks.

Coculture system

Further patch-clamp experiments are required in order to test if the natural polarity between cortex and striatum could be reconstructed in cell culture.

One remaining challenge is the positioning of cocultured neurons in front of the microfluidic channels. A controlled adherance of striatal and cortical neurons in front of these channels could be achieved by sealing the coculture chamber onto a preprinted PECM grid pattern, thereby increasing the amount of synaptical contacts. The spatial separation between the two different neuron types remains visible after removal of the chamber due to the PDMS-residues which stick to the glass surface.

An alternative method to enable the easy differentiation of cocultured cortical and striatal neurons is the transfection of striatal neurons with green fluorescence-protein (GFP) after preparation. Neurons transfected with GFP fluorescate green under a wavelength of 488 nm. The electrophysiological properties of GFP-transfected striatal neurons do not differ significantly from untransfected neurons (Sandler *et al.*, 2002).

A very interesting phenomenon for further studies is the induction of long term potentiation on single synapse level. Vogt *et al.* (2005a) showed that repetitive low frequency stimulation in cortical cell culture lead to short term depression instead of long term potentiation. Another method to induce long term potentiation is high frequency stimulation (Grover *et al*, 1990; Huang *et al*.; 1997; Hernandez *et al*., 2005) or several trains of tetanic burst stimulation (Hernandez *et al*., 2005; Raymond *et al.*, 2006). The corticostriatal pathway is very important for memory formation (Wickens *et al.*, 2003). If an LTP is induced at corticostriatal synapses with one of these protocols, the neurons could be removed by a glass pipette afterwards. This allows RT-PCR screening for genes which are up- or downregulated during LTP.

If the polarity between cortex and striatum can be confirmed *in vitro* and the signal direction within the network can be fixed onto mainly one direction within the network the next step is to build these networks on MEAs. This allows extracellular stimulation and recording of neurons without damaging or destroying them for long time measurements. This would finally allow to observe LTP and further network plasticity within a neuronal network on single-cell level over several days in cell culture.

9. Literature

A

Abraham WC, Otani S (1991). Macromolecules and the maintenance of long-term potentiation. Kindling and Synaptic Plasticity. The Legacy of Graham Goddard, *Morrell F (Editor), Birkhauser,* :92–109.

Abraham WC, Huggett A (1997). Induction and reversal of long-term potentiation by repeated high-frequency stimulation in rat hippocampal slices. *Hippocampus* 7: 137–145.

Abraham WC, Logan B, Greenwood JM, Dragunow M (2002). Induction and experience-dependent consolidation of stable long-term potentiation lasting months in the hippocampus. *J. Neurosci.* 22: 9626–9634.

Abraham WC, Williams JM (2003). Properties and mechanisms of LTP maintenance. *Neuroscientist* 9: 463–474.

Abdullaev YG, Posner MI (1998). Event-related brain potential imaging of semantic encoding during processing single words. *Neuroimage* 7(1): 1-13.

Adamiak K (2007). Diploma thesis at the university of cologne:High impact of in-situ printed cell adhesion peptides on neuronal network functionality.

Adams DN, Kao EY, Hypolite CL, Distefano MD, Hu WS, Letourneau PC (2005). Growth cones turn and migrate up an immobilized gradient of the laminin IKVAV peptide. *J Neurobiol.* 62(1): 134-47.

Alessandrini A, Facci P (2005). AFM: aversatile tool in biophysics. *Measurement Science and Technology* 16: R65.

Altman, Bayer, Shirley (1994). Atlas Of Prenatal Rat Brain Development. *CRC Press* 418-419.

B

Baas PW (1997). Microtubules and axonal growth. *Curr Opin Cell Biol* 9: 29–36.

Baas PW, Buster DW (2004). Slow axonal transport and the genesis of neuronal morphology. *J Neurobiol* 58: 3–17.

Banker G, Goslin K (1991). Culturing nerve cells. *MIT Press:* Cambridge Ma.

Bhalla US, Bower JM (1997). Multiday recordings from olfactory bulb neurons in awake freely moving rats: spatially and temporally organized variability in odorant response properties. *J Comput Neurosci.* 4(3): 221-56.

Bi GQ, Poo MM (1998). Synaptic modifications in cultured hippocampal neurons: dependence on spike timing, synaptic strength, and postsynaptic cell type. *J. Neurosci.* 18: 10464–10472.

Binder LI, Frankfurter A, Rebhun LI (1985). The distribution of tau in the mammalian central nervous system. *J Cell Biol.* 101(4): 1371-8.

Blackwell KT, Czubayko U, Plenz D (2003). Quantitative estimate of synaptic inputs to striatal neurons during up and down states in vitro. *J Neurosci.* 23(27): 9123-32.

Bliss TVP, Lømo T (1973). Long-lasting potentiation of synaptic transmission in the dentate area of the anaesthetized rabbit following stimulation of the perforant path. *J Physiol.* 232(2): 331-56.

Bliss TVP, Collingridge GL (1993). A synaptic model of memory: long-term potentiation in the hippocampus. *Nature* 361: 31–39.

Boehm J, Malinow R (2005). AMPA receptor phosphorylation during synaptic plasticity. *Biochem Soc Trans.* 33 (Pt 6):1354-6.

Bouyer JJ, Park DH, Joh TH, Pickel VM (1984). Chemical and structural analysis of the relation between cortical inputs and tyrosine hydroxylase-containing terminals in rat neostriatum. *Brain Research* 302: 267–275.
Bradke F, Dotti CG (2000). Establishment of neuronal polarity: lessons from cultured hippocampal neurons. *Curr Opin Neurobiol* 10: 574–581.
Brown A, Li Y, Slaughter T, Black MM (1993). Composite microtubules of the axon: quantitative analysis of tyrosinated and acetylated tubulin along individual axonal microtubules. *J Cell Sci* 104: 339–352.
Brown A, Slaughter T, Black MM (1992). Newly assembled microtubules are concentrated in the proximal and distal regions of growing axons. *J Cell Biol* 119:.867–882.
Bruch M, Landwehr R, Engel J (1989). Dissection of laminin by cathepsin G into its long-arm and short-arm structures and localization of regions involved in calcium dependent stabilization and self-association. *Eur J Biochem.* 185(2): 271-279.
C
Caceres A, Banker GA, Binder L (1986). Immunocytochemical localization of tubulin and microtubule-associated protein 2 during the development of hippocampal neurons in culture. *J Neurosci* 6: 714–722.
Calabresi P, Saulle E, Marfia GA, Centonze D, Mulloy R, Picconi B, Hipskind RA, Conquet F, Bernardi G (2001). Activation of metabotropic glutamate receptor subtype 1/protein kinase C/mitogen-activated protein kinase pathway is required for postischemic long-term potentiation in the striatum. *Mol Pharmacol*. 60(4): 808-15.
Campbell DS, Holt CE (2001). Chemotropic responses of retinal growth cones mediated by rapid local protein synthesis and degradation. *Neuron* 32: 1013–1026.
Campbell DS, Holt CE (2003). Apoptotic pathway and MAPKs differentially regulate chemotropic responses of retinal growth cones. *Neuron* 37: 939–952.
Campenot RB (1977). Local control of neurite development by nerve growth factor. *Proc. Natl. Acad. Sci. USA 74* (10): 4516-4519.
Campenot RB (1982). Development of sympathetic neurons in compartmentalized cultures. I. Local control of neurite growth by nerve growth factor. *Dev. Biol. 93* (1) : 1-12.
Chang JY, Janak PH, Woodward DJ. (1998). Comparison of mesocorticolimbic neuronal responses during cocaine and heroin self-administration in freely moving rats. *J Neurosci.* 18(8): 3098-115.
Chang JC, Brewer GJ, Wheeler BC (2003). A modified microstamping technique enhances polylysine transfer and neuronal cell patterning. *Biomaterials* 24(17): 2863-70.
Chen CH, Clegg DO, Hansma HG (1998). Structures and dynamic motion of laminin-1 as observed by atomic force microscopy. *Biochemistry.* 37(22): 8262-7.
Cohen A, Spira ME, Yitshaik S, Borghs G, Shwartzglass O, Shappir J (2004). Depletion type floating gate p-channel MOS transistor for recording action potentials generated by cultured neurons. *Biosens Bioelectron*. 19(12):1703-9.
Cohen-Cory S, Lom B. (2004). Neurotrophic regulation of retinal ganglion cell synaptic connectivity: from axons and dendrites to synapses. *Int J Dev Biol.* 48(8-9): 947-56.

Craig AM, Blackstone CD, Huganir RL, Banker G (1993). The distribution of glutamate receptors in cultured rat hippocampal neurons: postsynaptic clustering of AMPA-selective subunits. *Neuron* 10: 1055–1068.
Craig AM, Banker G (1994). Neuronal polarity. *Annu Rev Neurosci* 17: 267–310.
Czubayko U, Plenz D (2002). Fast synaptic transmission between striatal spiny projection neurons. *Proc Natl Acad Sci U S A.* 99(24): 15764-9.
D
Debanne D, Gahwiler BH, Thompson SM (1998). Long-term synaptic plasticity between pairs of individual CA3 pyramidal cells in rat hippocampal slice cultures. *J. Physiol.* 507: 237–247.
Decré MM, Timmermans PH, van der Sluis O, Schroeders R (2005). Numerical and experimental study of critical roof collapse conditions in soft lithography. *Langmuir*. 21(17): 7971-8.
Dent EW, Barnes AM, Tang F, Kalil K (2004). Netrin-1 and semaphorin 3A promote or inhibit cortical axon branching, respectively, by reorganization of the cytoskeleton. *J Neurosci.* 24(12): 3002-12.
Dertinger SK, Chiu D, Jeon NL, Whitesides GM (2001). Generation of Gradients Having Complex Shapes Using Microfluidic Networks. *Anal. Chem*. 73: 1240-1246.
Dertinger SK, Jiang X, Li Z, Murthy VN, Whitesides GM. (2002). Gradients of substrate-bound laminin orient axonal specification of neurons. *Proc Natl Acad Sci U S A.* 99(20):12542-7.
Dichter MA (1978). Rat cortical neurons in cell culture: culture methods, cell morphology, electrophysiology, and synapse formation. *Brain Res*. 149(2): 279-93.
Dichter MA, Lisak J, Biales B (1983). Action potential mechanism of mammalian cortical neurons in cell culture. *Brain Res.* 289(1-2): 99-107.
Dickson BJ (2002). Molecular mechanisms of axon guidance. *Science* 298(5600): 1959-64.
Divac I, Fonnum F, Storm-Mathisen J (1977). High affinity uptake of glutamate in terminals of corticostriatal axons. *Nature* 266: 377–378.
Dotti CG, Sullivan CA, Banker GA (1988). The establishment of polarity by hippocampal neurons in culture. *J. Neurosci.* 8:1454–1468.
E
Egger V, Feldmeyer D, Sakmann B (1999). Coincidence detection and changes of synaptic efficacy in spiny stellate neurons in rat barrel cortex. *Nat. Neurosci.* 2: 1098–1105.
Esch T, Lemmon V, Banker G (1999). Local presentation of substrate molecules directs axon specification by cultured hippocampal neurons. *J Neurosci* 19(15): 6417-6426.
F
Feldman DE (2000). Timing-based LTP and LTD at vertical inputs to layer II/III pyramidal cells in rat barrel cortex. *Neuron* 27: 45–56.
Fitzsimonds RM, Song HJ, Poo MM (1997). Propagation of activity-dependent synaptic depression in simple neural networks. *Nature* 388(6641): 439-48.
Flanagan JG, Vanderhaeghen P. (1998). The ephrins and Eph receptors in neural development. *Annu Rev Neurosci.* 21: 309-45.
Forcet C, Stein E, Pays L, Corset V, Llambi F, Tessier-Lavigne M, Mehlen P (2002). Netrin-1-mediated axon outgrowth requires deleted in colorectal cancer-dependent MAPK activation. *Nature* 417: 443–447.

Forscher P, Smith SJ (1988). Actions of cytochalasins on the organization of actin filaments and microtubules in a neuronal growth cone. *J Cell Biol* 107: 1505–1516.
Freire E, Gomes FC, Linden R, Neto VM, Coelho-Sampaio T (2002). Structure of laminin substrate modulates cellular signaling for neuritogenesis.
J Cell Sci. 115(Pt 24): 4867-76.
Freund TF, Powell JF, Smith AD (1984). Tyrosine hydroxylase-immunoreactive boutons in synaptic contact with identified striatonigral neurons, with particular reference to dendritic spines. *Neuroscience* 13:1189–1215.
Fukata Y, Kimura T, Kaibuchi K (2002). Axon specification in hippocampal neurons. Neurosci Res 43:305–315.
G
Garner CC, Waites CL, Ziv NE (2006). Synapse development: still looking for the forest, still lost in the trees. *Cell Tissue Res.* 326(2): 249-62.
Glasmästar K, Gold J, Andersson AF, Sutherland DS, Kasemo B (2003). Silicone Transfer during Microcontact Printing. *Langmuir 19:* 5475-5483.
Goslin K, Schreyer DJ, Skene JH, Banker G (1988). Development of neuronal polarity: GAP-43 distinguishes axonal from dendritic growth cones. *Nature* 336: 672–674.
Goslin K, Schreyer DJ, Skene JH, Banker G (1990). Changes in the distribution of GAP-43 during the development of neuronal polarity. *J Neurosci* 10: 588–602.
Graef IA,Wang F, Charron F, Chen L, Neilson J, Tessier-Lavigne M, Crabtree GR (2003). Neurotrophins and netrins require calcineurin/NFAT signaling to stimulate outgrowth of embryonic axons. *Cell* 113: 657–670.
Graybiel AM, Aosaki T, Flaherty AW, Kimura M (1994). The basal ganglia and adaptive motor control. *Science* 265: 1826–1831.
Grover LM, Teyler TJ (1990).Two components of long-term potentiation induced by different patterns of afferent activation, *Nature* 347: 477–479.
H
Hayashi K, Kawai-Hirai R, Ishikawa K, Takata K (2002). Reversal of neuronal polarity characterized by conversion of dendrites into axons in neonatal rat cortical neurons in vitro. *Neuroscience.* 110(1): 7-17.
Hernandez RV, Navarro MM, Rodriguez WA, Martinez JL Jr, LeBaron RG (2005). Differences in the magnitude of long-term potentiation produced by theta burst and high frequency stimulation protocols matched in stimulus number. *Brain Res Brain Res Protoc.* 15: 6-13.
Hodgkinson GN, Tresco PA, Hlady V (2007). The differential influence of colocalized and segregated dual protein signals on neurite outgrowth on surfaces. *Biomaterials* 28(16): 2590-602.
Hong K, Hinck L, Nishiyama M, Poo MM, Tessier-Lavigne T, Stein E (1999). A ligand-gated association between cytoplasmic domains of UNC5 and DCC family receptors converts netrin-induced growth cone attraction to repulsion. *Cell* 97: 927–941.
Hong K, Nishiyama M, Henley J, Tessier-Lavigne M, Poo MM (2000). Calcium signalling in the guidance of nerve growth by netrin-1. *Nature* 403: 93–98.
Huang LQ, Rowan MJ, Anwyl R (1997). mGluR II agonist inhibition of LTP induction, and mGluR II antagonist inhibition of LTD induction, in the dentate gyrus in vitro. *Neuroreport.* 8: 687-93.
Huber AB, Kolodkin AL, Ginty DD, Cloutier JF (2003). Signaling at the growth cone: ligand–receptor complexes and the control of axon growth and guidance. *Annu Rev Neurosci* 26: 509–563.

I

Ichikawa M, Muramoto K, Kobayashi K, Kawahara M, Kuroda Y (1993). Formation and maturation of synapses in primary cultures of rat cerebral cortical cells: an electron microscopic study. *Neurosci Res.* 16(2): 95-103.

Ishibashi T, Dakin K, Stevens B, Lee P, Kozlov S, Stewart C, Fields R (2006). Astrocytes promote myelination in response to electrical impulses. *Neuron* 49 (6): 823-32.

J

Jacobson BS, Branton D (1977). Plasma membrane: rapid isolation and exposure of the cytoplasmic surface by use of positively charged beads. *Science* 195: 302-4.

James CD**,** Davis RC, Kam L, Craighead HG, Isaacson M, Turner JN, Shain W (1998). Patterned protein layers on solid substrates by thin stamp microcontact printing. *Langmuir* 14: 741-744.

James CD, Spence AJ, Dowell-Mesfin NM, Hussain RJ, Smith KL, Craighead HG, Isaacson MS, Shain W, Turner JN (2004). Extracellular recordings from patterned neuronal networks using planar microelectrode arrays. *IEEE Trans Biomed Eng.* 51(9): 1640-8.

Jiang X, Xu Q, Dertinger SK, Stroock AD, Fu TM, Whitesides GM (2005). A general method for patterning gradients of biomolecules on surfaces using microfluidic networks. *Anal Chem.* 77(8): 2338-47.

K

Kandel ER, Schwartz JH, Jessel TM (2000). Principles of Neural Science. *McGraw-Hill Medical.* 4th edition.

Kam L, Shain W, Turner JN, Bizios R (2001). Axonal outgrowth of hippocampal neurons on micro-scale networks of polylysine-conjugated laminin. *Biomaterials* 22(10): 1049-54.

Kappler J, Franken S, Junghans U, Hoffmann R, Linke T, Müller HW, Koch KW (2000). Glycosaminoglycan-binding properties and secondary structure of the C-terminus of netrin-1. *Biochem Biophys Res Commun*. 271(2): 287-91.

Kawaguchi Y, Wilson CJ, Augood SJ, Emson PC (1995). Striatal interneurones: chemical, physiological and morphological characterization. *Trends Neurosci.* 18: 527–535.

Kirkwood A, Bear MF (1994). Homosynaptic long-term depression in the visual cortex. *J. Neurosci.* 14: 3404–3412.

Koch C, Rapp M, Segev I (1996). A Brief History of Time (Constants). *Cerebral Cortex* 6: 93–101.

Koos T, Tepper JM (1999). Inhibitory control of neostriatal projection neurons by GABAergic interneurons. *Nat Neurosci* 2: 467-472.

Kumar A, Whitesides GM (1993). Features of Gold Having Micrometer to Centimeter Dimensions Can Be Formed through a Combination of Stamping with an Elastomeric Stamp and an Alkanethiol Ink Followed by Chemical Etching. *Applied Physics Letters* 63: 2002-2003.

L

Lauer L, Ingebrandt S, Scholl M, Offenhausser A. (2001). Aligned microcontact printing of biomolecules on microelectronic device surfaces. *IEEE Trans Biomed Eng.* 48(7): 838-42.

Lauer L, Vogt AK, Kauff C, Nelles G, Yasuda A, Knoll W, Offenhausser A. (2004). Analysis of electrotonic coupling in patterned neuronal networks. *IEE Proc Nanobiotechnol.* 151(3): 122-7.

Laiwand R, Brown DA (1992). Synapse formation between dissociated basal forebrain neurones and hippocampal cells in culture. *Neurosci Lett.* 138(2): 221-4.
Levy LM, Henkin RI, Hutter A, Lin CS, Martins D, Schellinger D. (1997). Functional MRI of human olfaction. *J Comput Assist Tomogr.* 21(6): 849-56.
Li W, Lee J, Vikis HG, Lee SH, Liu G,Aurandt J, Shen TL, Fearon ER, Guan JL, Han M (2004). Activation of FAK and Src are receptor-proximal events required for netrin signaling. *Nat Neurosci* 7: 1213–1221.
Lin SP, Chen JJ, Liao JD, Tzeng SF (2007). Characterization of surface modification on microelectrode arrays for in vitro cell culture. *Biomed Microdevices.* 2007 Aug 3 (E-pub ehead of print).
Lindmark R, Thorén-Tolling K, Sjöquist J (1983). Binding of immunoglobulins to protein A and immunoglobulin levels in mammalian sera. *J Immunol Methods.* 62(1): 1-13.
Lisman J, Schulman H, Cline H (2002). The molecular basis of CaMKII function in synaptic and behavioural memory. *Nat. Rev. Neurosci.* 3:175–190.
Liu G, Beggs H, Jurgensen C, Park HT, Tang H, Gorski J,Jones KR, Reichardt LF, Wu J,Rao Y (2004). Netrin requires focal adhesion kinase and Src family kinases for axon outgrowth and attraction. *Nat Neurosci* 7: 1222–1232.
Lynch MA (2004). Long-term potentiation and memory. *Physiol. Rev.* 84: 87–136.
M
Magee JC, Johnston D (1997). A synaptically controlled, associative signal for Hebbian plasticity in hippocampal neurons. *Science* 275: 209–213.
Mahon S, Deniau JM, Charpier S (2004). Corticostriatal plasticity: life after the depression. *Trends Neurosci.* 27: 460–467.
Malenka RC, Bear MF (2004). LTP and LTD: an embarrassment of riches. *Neuron* 44: 5–21.
Markram H, Lubke J, Frotscher M, Sakmann B (1997). Regulation of synaptic efficacy by coincidence of postsynaptic APs and EPSPs. *Science* 275: 213–215.
Mattacotta FC, Ottaviani G (editors) (1995). Science and Technology of Thin Films. *World scientific.*
Matsuzaki M, Honkura N, Ellis-Davies GC, Kasai H (2004). Structural basis of long-term potentiation in single dendritic spines. *Nature* 429:761–766.
Matthews GG Neurobiology (2001). Molecules, Cells and System 2nd edition. *Blackwell publishing, USA.*
Mattson MP (1999). Establishment and plasticity of neuronal polarity. *J Neurosci Res*.1; 57(5): 577-89.
McCormick DA, Prince DA (1987). Post-natal development of electrophysiological properties of rat cerebral cortical pyramidal neurones. *J Physiol*. 393: 743-62.
McDonald RJ, White NM (1993). A triple dissociation of memory system: hippocampus, amygdala, and dorsal striatum. *Behav Neurosci* 107: 3–22.
McGeorge AJ, Faull RL (1989). The organization of the projection from the cerebral cortex to the striatum in the rat. *Neuroscience* 29: 503–537.
McKenna MP, Raper JA (1988). Growth cone behavior on gradients of substratum bound laminin. *Dev Biol.* 130: 232-6.
Menager C, Arimura N, Fukata Y, Kaibuchi K (2004). PIP_3 is involved in neuronal polarization and axon formation. *J Neurochem* 89: 109–118.
Meriane M, Tcherkezian J, Webber CA, Danek EI, Triki I, McFarlane S, Bloch-Gallego E, Lamarche-Vane N (2004). Phosphorylation of DCC by Fyn mediates Netrin-1 signaling in growth cone guidance. *J Cell Biol* 167: 687–698.

Metin C, Deleglise D, Serafini T, Kennedy TE, Tessier-Lavigne M (1997). A role for netrin-1 in the guidance of cortical efferents. *Development* 124: 5063–5074.
Mirenowicz J, Schultz W (1994). Importance of unpredictability for reward responses in primate dopamine neurons. *Journal of Neurophysiology* 72: 1024–1027.
Mirenowicz J, Schultz W (1996).Preferential activation of midbrain dopamine neurons by appetitive rather than aversive stimuli. *Nature* 379: 449–451.
Mizushima K, Miyamoto Y, Tsukahara F, Hirai M, Sakaki Y, Ito T (2000). A novel G-protein-coupled receptor gene expressed in striatum. *Genomics* 69: 314-321.
Morgan SL, Teyler TJ (2001). Electrical stimuli patterned after the theta-rhythm induce multiple forms of LTP. *J. Neurophysiol.* 86: 1289–1296.
Mulkey RM, Malenka RC (1992). Mechanisms underlying induction of homosynaptic long-term depression in area CA1 of the hippocampus. *Neuron* 9: 967–975.
Murakami T, Kuroda S, Osawa Z (1998). Dynamics of Polymeric Solid Surfaces Treated with Oxygen Plasma: Effect of Aging Media after Plasma Treatment. *J. of Colloid and Interface Sci.* 202: 37-44.
N
Nakamura T , Lasser-Ross N, Nakamura K, Ross WN (2002). Spatial segregation and interaction of calcium signalling mechanisms in rat hippocampal CA1 pyramidal neurons. *J. Physiol.* 543: 465–480.
Neher E, Sakmann B (1976). Single-channel currents recorded from membrane of denervated frog muscle fibres. *Nature* 260: 799-802.
Nguyen PV, Woo NH (2003). Regulation of hippocampal synaptic plasticity by cyclic AMP-dependent protein kinases. *Prog. Neurobiol.* 71: 401–437.
Nicholls JG, Martin AR, Wallace BG (1995): Vom Neuron Zum Gehirn. Gustav Fischer Verlag, Stuttgart, Jena, New York.
Nimchinsky EA, Sabatini BL, Svoboda K (2002). Structure and function of dendritic spines. *Annu. Rev. Physiol.* 64: 313–353.
O
Offenhäusser A, Sprössler C, Matsuzawa M, Knoll W (1997). Field-effect transistor array for monitoring electrical activity from mammalian neurons in culture. *Biosens. Bioelectr.* 12:819–826.
O'Leary DD, Wilkinson DG. (1999). Eph receptors and ephrins in neural development. *Curr Opin Neurobiol*. 9(1): 65-73.
Oliva AA, James CD, Kingman CE, Craighead HG, Banker GA (2003). Patterning axonal guidance molecules using a novel strategy for microcontact printing. *Neurochem Res.* 28(11): 1639-48.
P
Packard MG, Knowlton BJ (2002). Learning and memory functions of the basal ganglia. *Annu Rev Neurosci* 25: 563–593.
Parpura V, Haydon P (2000). Physiological astrocytic calcium levels stimulate glutamate release to modulate adjacent neurons. *Proc Natl Acad Sci USA* 97 (15): 8629-34.
Parri R, Crunelli V (2003). An astrocyte bridge from synapse to blood flow. *Nat Neurosci* 6 (1): 5-6.
Perschak H, Cuenod M (1990). In vivo release of endogenous glutamate and aspartate in the rat striatum during stimulation of the cortex. *Neuroscience* 35:283–287.

Piet R, Vargová L, Syková E, Poulain D, Oliet S (2004). Physiological contribution of the astrocytic environment of neurons to intersynaptic crosstalk. *Proc Natl Acad Sci USA* 101 (7): 2151-5.
Pine J (1980). Recording action potentials from cultured neurons with extracellular microcircuit electrodes. *J. Neurosci. Methods* 2:19–31.
Plenz D, Aertsen A (1996a). Neural dynamics in cortex-striatum co-cultures. I. Anatomy and electrophysiology of neuronal cell types. *Neuroscience* 70: 861-891.
Plenz D, Aertsen A (1996b). Neuronal dynamics in cortex-striatum co-cultures. II. Spatio-temporal characteristics of neuronal activity. *Neuroscience* 70: 893-924.
Plenz D, Kitai ST (1998). `Up' and `down' states in striatal medium spiny neurons simultaneously recorded with spontaneous activity in fast-spiking interneurons studied in cortex-striatum-substantia nigra organotypic cultures. *J Neurosci* 18: 266-283.
Purves D, Augustine GJ, Fitzpatrick D, Katz LC, Lamantia AS, McNamara JO, Mark Williams S (2001) "Neuroscience, second edition" *Sinauer Associates, Inc*. www.ncbi.nlm.nih.gov/books/bv.fcgi?rid=neurosci.box.229
Püschel AW (1996). The semaphorins: a family of axonal guidance molecules? *Eur J Neurosci.* 8(7): 1317-21.
R
Rae MG, Martin DJ, Collingridge GL, Irving AJ (2000). Role of Ca^{2+} stores in metabotropic L-glutamate receptor-mediated supralinear Ca^{2+} signaling in rat hippocampal neurons. *J. Neurosci.* 20: 8628–8636.
Raymond CR, Thompson VL, Tate WP, Abraham WC (2000). Metabotropic glutamate receptors trigger homosynaptic protein synthesis to prolong long-term potentiation. *J. Neurosci.* 20: 969–976.
Raymond CR, Redman SJ (2006). Spatial segregation of neuronal calcium signals encodes different forms of LTP in rat hippocampus. *J. Physiol.* 570: 97–111.
Raymond CR (2007). LTP forms 1, 2 and 3: different mechanisms for the "long" in long-term potentiation. *Trends Neurosci.* 4: 167-75.
Rehder V, Kater SB (1996). Filopodia on neuronal growth cones: Multifuncional structures with sensory and motor capabilities. *The Neurosciences* 8: 81-88.
Ren XR, Ming GL, Xie Y, Hong Y, Sun DM, Zhao ZQ, Feng Z, Wang Q, Shim S, Chen ZF (2004). Focal adhesion kinase in netrin-1 signaling. *Nat Neurosci* 7: 1204–1212.
Reynolds JN, Wickens JR (2000). Substantia nigra dopamine regulates synaptic plasticity and membrane potential fluctuations in the rat neostriatum in vivo. *Neuroscience* 99: 199-203.
Reynolds JN, Hyland BI, Wickens JR (2001). A cellular mechanism of reward-related learning. *Nature* 413: 67–70.
Rhee SW, Taylor AM, Tu CH, Cribbs DH, Cotman CW, Jeon NL (2005). Patterned cell culture inside microfluidic devices. *Lab Chip.* 5(1): 102-7.
Richards LJ, Koester SE, Tuttle R, O'Leary DD (1997). Directed growth of early cortical axons is influenced by a chemoattractant released from an intermediate target. *J Neurosci* 17: 2445–2458.
S
Sandler VM, Wang S, Angelo K, Lo HG, Breakefield XO, Clapham DE. (2002) Modified herpes simplex virus delivery of enhanced GFP into the central nervous system. *J Neurosci Methods*. 121(2):211-9.

Schmalenberg KE, Buettner HM, Uhrich KE (2004). Microcontact printing of proteins on oxygen plasma-activated poly(methyl methacrylate). *Biomaterials.* 25(10): 1851-7.
Scholl M, Sprossler C, Denyer M, Krause M, Nakajima K, Maelicke A, Knoll W, Offenhausser A (2000). Ordered networks of rat hippocampal neurons attached to silicon oxide surfaces. *J Neurosci Methods.* 104(1): 65-75.
Schultz W (2002). Getting formal with dopamine and reward. *Neuron* 36: 241–263.
Schwaab, D (2007). Dissertation at the RWTH Aachen: Surface patterning by means of Soft Lithography for Molecular and Bio-Electronics.
Segal M, Greenberger V, Korkotian E (2003). Formation of dendritic spines in cultured striatal neurons depends on excitatory afferent activity. *Eur J Neurosci.* 17(12): 2573-85.
Serafini T, Kennedy T, Galko M, Mirzayan C, Jessell T, Tessier-Lavigne M (1994). The netrins define a family of axonoutgrowth-promoting proteins homologous to *C. elegans* UNC-6. *Cell* 78: 409–424.
Sgarbi N, Pisignano D, Di Benedetto F, Gigli G, Cingolani R, Rinaldi R (2004). Self-assembled extracellular matrix protein networks by microcontact printing. *Biomaterials* 25(7-8): 1349-53.
Sharp KG, Blackman GS, Glassmaker NJ, Jagota A, Hui CY (2004). Effect of stamp deformation on the quality of microcontact printing: theory and experiment. *Langmuir* (15): 6430-8.
Shi SH, Jan LY, Jan YN (2003). Hippocampal neuronal polarity specified by spatially localized mPar3/mPar6 and PI 3-kinase activity. *Cell* 112: 63–75.
Shi P, Shen K, Kam LC (2007). Local presentation of L1 and N-cadherin in multicomponent, microscale patterns differentially direct neuron function in vitro. *Dev Neurobiol.* 67(13): 1765-76.
Sjostrom PJ, Turrigiano GG, Nelson SB (2001). Rate, timing, and cooperativity jointly determine cortical synaptic plasticity. *Neuron* 32: 1149–1164.
Small DM, Jones-Gotman M, Dagher A (2003). Feeding-induced dopamine release in dorsal striatum correlates with meal pleasantness ratings in healthy human volunteers. *Neuroimage* 19(4): 1709-15.
Smith AD, Bolam JP (1990). The neural network of the basal ganglia as revealed by the study of synaptic connections of identified neurones. *Trends in Neurosciences* 13: 259–265.
Smith R, Musleh W, Akopian G, Buckwalter G, Walsh JP (2001). Regional differences in the expression of corticostriatal synaptic plasticity. *Neuroscience* 106: 95–101.
Snyder-Keller, A (2004). Pattern of corticostriatal innervation in organotypic cocultures is dependent on the age of the cortical tissue. *Exp Neurol.* 185(2): 262-71.
Somogyi P, Bolam JP, Smith AD (1981). Monosynaptic cortical input and local axon collaterals of identified striatonigral neurons. A light and electron microscopic study using the Golgi-peroxidase transport-degeneration procedure. *Journal of Comparative Neurology* 195:567–584.
Song H, Poo M (2001). The cell biology of neuronal navigation. *Nat Cell Biol.* 3(3): E81-8.
Staubli U, Lynch G (1987). Stable hippocampal long-term potentiation elicited by 'theta' pattern stimulation. *Brain Res.* 435: 227–234.

Stein E, Zou Y, Poo M, Tessier-Lavigne M (2001). Binding of DCC by netrin-1 to mediate axon guidance independent of adenosine A2B receptor activation. *Science* 291: 1976–1982.
Stern EA, Jaeger D, Wilson CJ (1998). Membrane potential synchrony of simultaneously recorded striatal spiny neurons *in vivo. Nature* 394: 475–478.
Stern EA, Kincaid AE, Wilson CJ (1997). Spontaneous subthreshold membrane potential fluctuations and action potential variability of rat corticostriatal and striatal neurons *in vivo. J. Neurophysiol.* 77: 1697–1715.
Streit WJ , Mrak RE, Griffin WST (2004*).* Microglia and neuroinflam-mation: a pathological perspective. *Journal of Neuroinflammation* 1(1):14.
T
Tao H, Zhang LI, Bi G, Poo M (2000). Selective presynaptic propagation of long-term potentiation in defined neural networks. *J Neurosci.* 20(9): 3233-43.
Taylor AM, Rhee SW, Jeon NL (2006). Microfluidic chambers for cell migration and neuroscience research. *Methods Mol Biol.* 321: 167-77.
Taylor AM, Rhee SW, Tu CH, Cribbs DH, Cotman CW, Jeon NL (2003). Microfluidic Multicompartment Device for Neuroscience Research. *Langmuir* 19 (5): 1551 –1556.
Tepper JM, Bolam JP (2004). Functional diversity and specificity of neostriatal interneurons. *Curr. Opin. Neurobiol.* 14: 685–692.
Tessier-Lavigne M, Goodman CS (1996). The molecular biology of axon guidance. *Science* 274: 1123–1133.
Tessier-Lavigne M, Placzek M, Lumsden AGS, Dodd J, Jessell TM (1988). Chemotropic guidance of developing axons in the mammalian central nervous system. *Nature* 336: 775–778.
V
Vogt AK (2003a). Dissertation at the Johannes-Gutenberg university, Mainz: Synaptic Connectivity in Micropatterned Networks of Neuronal Cells.
Vogt AK, Lauer L, Knoll W, Offenhausser A. (2003b). Micropatterned substrates for the growth of functional neuronal networks of defined geometry. *Biotechnol Prog*. 19(5): 1562-8.
Vogt AK, Stefani FD, Best A, Nelles G, Yasuda A, Knoll W, Offenhäusser A (2004). Impact of micropatterned surfaces on neuronal polarity. *J Neurosci Methods.* 134(2): 191-8.
Vogt AK, Brewer GJ, Decker T, Boecker-Meffert S, Jacobsen V, Kreiter M, Knoll W, Offenhausser A. (2005a). Independence of synaptic specificity from neuritic guidance. *Neuroscience* 134(3): 783-90.
Vogt AK, Wrobel G, Meyer W, Knoll W, Offenhausser A. (2005b). Synaptic plasticity in micropatterned neuronal networks. *Biomaterials* 26(15): 2549-57.
Vogt AK, Brewer GJ, Offenhausser A. (2005c). Connectivity patterns in neuronal networks of experimentally defined geometry. *Tissue Eng.* 11(11-12): 1757-67.
W
Wheeler BC, Corey JM, Brewer GJ, Branch DW (1999). Microcontact printing for precise control of nerve cell growth in culture. *J Biomech Eng.* 121(1): 73-8.
Wickens JR, Wilson CJ (1998). Regulation of action-potential firing in spiny neurons of the rat neostriatum in vivo. *J Neurophysiol.* 79(5): 2358-64.
Wickens JR *et al*.(2003). Neural mechanisms of reward-related motor learning. *Curr. Opin. Neurobiol.* 13: 685–690.
Wilson CJ, Kawaguchi Y (1996). The origins of two-state spontaneous membrane potential fluctuations of neostriatal spiny neurons. *J. Neurosci.* 16: 2397–2410.

Y

Yeung CK, Lauer L, Offenhausser A, Knoll W (2001). Modulation of the growth and guidance of rat brain stem neurons using extracellular matrix proteins. *Neurosci Lett* 301: 147–150.

Yoo SS, Jolesz FA (2002). Functional MRI for neurofeedback: feasibility study on a hand motor task. *Neuroreport* 13(11): 1377-81.

Yurchenco PD, Tsilibary EC, Charonis AS, Furthmayr H (1985). Laminin polymerization in vitro. Evidence for a two-step assembly with domain specificity. *J Biol Chem.* 260(12):7636-44.

Yurchenco PD, Cheng YS (1993). Self-assembly and calcium-binding sites in laminin. A three-arm interaction model. *J Biol Chem.* 268(23): 17286-99.

Yuste R, Bonhoeffer T (2001). Morphological changes in dendritic spines associated with long-term synaptic plasticity. *Annu. Rev. Neurosci.* 24:1071–1089.

10. Appendix

10.1 List of materials and devices

Chemicals and materials:

Material	Catalogue-number	Distributor
B 27 supplement	17504-044	GibCo
BSA	A9418	Sigma-Aldrich
Borosilicate Glass pipettes (o.d. 1.5mm, i.d. 0.86mm)	BF150-86-7.5	Sutter instrument Co.
Calciumchloride	A119.1	Roth
Cascade blue	C-687	MoBiTec
CELLSTAR tissue culture dishes, PS, 35 mm	627161	Greiner
CELLSTAR tissue culture dishes, PS, 94x16 mm	633171	Greiner
D-gluconic acid potassium salt	G-4500	Sigma-Aldrich
Disodiumhydrogenphosphate	T876.2	Roth
ECM-gel	E1270	Sigma-Aldrich
EGTA	E-3889	Sigma-Aldrich
Ethanole, p.A.	60011.110	KMF
FITC	F3951	Sigma-Aldrich
FITC-conjugated poly-L-Lysine	P3069	Sigma-Aldrich
Fluorescence Mount medium	S3023	DAKO
Glass coverslips, 12mm diameter	CB00120RA1	Menzel
Glass coverslips, 25mm diameter	CB00250RA1	Menzel
Glass coverslips, 32mm diameter	CB00320RA1	Menzel
Glucose	G5400	Sigma-Aldrich
Goat serum	69023	Sigma-Aldrich
HBSS with Ca^{2+} and Mg^{2+} (10 x)	24020-091	GibCo

Material	Catalogue-number	Distributor
HBSS without Ca^{2+} and Mg^{2+} (10x)	14170-088	GibCo
Hepes	9105.4	Roth
Hydrogen peroxide, 30% per weight	40287	Riedel de Haen
Laminin	L2020	Sigma-Aldrich
L-glutamine	(35050-038	GibCo
Magnesiumdichloride-6-hydrate	A537.1	Roth
Mg-ATP	A9187	Sigma-Aldrich
Na-ATP	A6419	Sigma-Aldrich
Netrin-1, recombinant protein	1109-N1	R&D Systems
Neurobasal medium	21103-049	GibCo
Neurobasalmedium A	10888-022	GibCo
Nuclon™ Polystyrene 24-well-multidish	142485	Nunc
Paraformaldehyde	P-6148	Sigma-Aldrich
1H,1H,2H,2H-Perfluorooctyltrichlorosilane	SI T8175.0	ABCR
Poly-D-Lysine	P6407	Sigma-Aldrich
Potassium hydroxide	1.05012.1000	Merck
Potassiumchloride	P017.1	Roth
Potassiumdihydrogenphosphate	P018.1	Roth
Silver wire, 0.25 mm	AG005130	Goodfellow
Sodium hydroxide	1.06495.0250	Merck
Sodiumbicarbonate	S-8875	Sigma-Aldrich
Sodiumchloride	08-434	KMF
Sodiumdodecyl sulfate	L5750	Sigma-Aldrich
Sodiumhydrogencarbonate	S5761	Sigma-Aldrich
Sodiumpyruvate	P5280	Sigma-Aldrich
Sulphorhodamine 101	S-359	MoBiTec
Sulphuric acid, 95-97%	08-743	KMF
Superfrost glass slides	AA00008032E	Menzel

Material	Catalogue-number	Distributor
Sylgard 184 silikon elastomer kit	-	Down-Corning
TRITC	T2629	Sigma-Aldrich
Triton-X-100	93418	Fluka
Trypan blue	T-8154	Sigma-Aldrich

Buffer solutions :

$HBSS^-$(100 ml)

Chemical	Concentration	Endconcentration	In 100 ml
HBSS without Ca^{2+} and Mg^{2+}	10x	1x	10 ml
Glucose	2000 mM	20 mM	1 ml
Sodiumhydrogencarbonate	1000 mM	1 mM	0.1 ml
Sodiumpyruvate	250 mM	1 mM	0.4 ml
Hepes	1000 mM	10 mM	1 ml

The pH was adjusted to 7.3 with 1 M NaOH and 1 M HCl.

$HBSS^+$(100 ml)

Chemical	Concentration	Endconcentration	In 100 ml
HBSS with Ca^{2+} and Mg^{2+}	10x	1x	10 ml
Glucose	2000 mM	20 mM	1 ml
Sodiumhydrogencarbonate	1000 mM	1 mM	0.1 ml
Sodiumpyruvate	250 mM	1 mM	0.4 ml
Hepes	1000 mM	10 mM	1 ml

The pH was adjusted to 7.3 with 1 M NaOH and 1 M HCl.

PBS (1l)

Chemical	Endconcentration [mM]	In 1 l [g]
NaCl	137	8,006
KCl	2.7	0,201
Na_2HPO	8	1,135
KH_2PO_4	1.8	0,245

The pH was adjusted to 7.3 with 1 M NaOH and 1 M HCl.

Devices:

AFM	Nanoscope IV Multimode atomic force microscope,Veeco Instruments, with Veeco tapping mode cantilevers RTESP5 (1–10cm n-doped silicon, $f_{0\ 7}$ = 251 − 287 kHz)
Centrifuge	Megafuge 1.0R, Heraeus
Cleanbench	Herasafe, Heraeus
Electron beam evaporator	ESV4, Leibold
Ellipsometer	Nanofilm EP3 ellipsometer with Nd:YAG Laser (y= 532 nm) and EP3 View 2.05 software
Fluorescence microscope	IX 50 microscope, Olympus, equipped with a mercury vapour lamp, IX-FLA, Olympus
Incubators	Heracell 240, Heraeus
Laser Scanning Microscope	LSM-FCS, Version 2.8SP, Zeiss
Microscope	Axiovert 25, Zeiss
Osmometer	Osmomat 030, Gonotec
Patch-clamp set-up	See 3.6
Plasma oven	100-E Plasmasystem, Technics Plasma GmbH, Germany
Pipette puller	Model P-97 and P-2000, Sutter Instrument Co.
SEM	Field emission raster electron microscope, Gemini 1550, Leitz Electronic Optic
UVO-cleaner	Model 42-220, Jelight Company Inc., California, USA

Software:

Axiovision	Carl Zeiss, Germany
Corel Photo-Paint 12	Corel Corporation, USA
Coreldraw 12	Corel Corporation, USA
EP3 View 2.05	Nanofilm GmbH
Excel 2000	Microsoft Corporation, USA
Irfanview	Freeware by Irfan Skiljan, http://www.irfanview.com
Junction Potential Calculator	Prof. P.H. Barry, UNSW Sydney, Australia
Leica Confocal Software TCS SP2	Leica Microsystems Heidelberg GmbH, Germany
Origin 7	OriginLab Corporation, USA
Paint Shop Pro 7	Jasc Software Inc., USA
TIDA 5.x	HEKA Elektronik, Lambrecht, Germany
Word 2000	Microsoft Corporation, USA

10.2 List of figures

Fig. 1-1: Fluorescence image of a partially interrupted grid pattern consisting of PECM (mixture of polylysine (10 µg/ml) and ECM (8-12 µg/ml). 10
Fig. 2-1: Types of glial cells in the mammalian nervous system. 15
Fig. 2-2: Examples (A—F) of the rich variety of nerve cell morphologies found in the human nervous system. 16
Fig. 2-3 : Processes of neuronal polarization in cultured hippocampal neurons. 18
Fig. 2-4 : Mechanisms for axon guiding. A growth cone is guided by different guiding cues to the target region. 20
Fig. 2-5. A diagram showing the connections of the striatum and basal ganglia output nuclei with the cerebral cortex and substantia nigra pars compacta. 24
Fig. 2-6: Scheme of an action potential. 28
Fig. 2-7: Saltatory action potential conduction along a myelinated axon. 29
Fig. 2-8: Electrical synapse. 31
Fig. 2-9 : Chemical Synapse. 32
Fig. 2-10 : Common electrical stimulation protocols used to induce LTP. 34
Fig. 3-1: Principle of Microcontact printing. 36
Fig. 3-2: Production of microfluidic coculture chambers (scheme). 42
Fig. 3-3: Production of coverslips with glass feet. 45
Fig. 3-4 : Scheme of neuronal tissue preparation and cell culture. 46
Fig. 3-5: Localization of striatum and cortex in rat E19 brains. 47
Fig. 3-6: The four possible configurations of a patch clamp measurement: Cell attached mode; whole cell mode; inside out mode and outside out mode. 51
Fig. 3-7: Typical voltage-clamp measurement. 52
Fig. 3-8: Typical current clamp experiment. 53
Fig. 3-9: Patch-clamp-setup for double-patches (scheme). 54
Fig. 3-10: Illustration of τ determination. 57
Fig. 3-11: Exemplary illustration of the analysis for current-voltage relations. 58
Fig. 3-12 : Double patch-clamp measurement of two cortical neurons at 11 DIV. 59
Fig. 3-13: Schematic process of ellipsometry. 61
Fig. 3-14: Schematic setup of ellipsometry. 62
Fig. 3-15: Scheme of an atomic force microscope. 64
Fig. 3-16: Schematic representation of an AFM tip operating in the tapping mode. 64
Fig. 4-1: Scheme of manual two-step microcontact printing substrates. 67
Fig. 4-2: Enhanced transfer of hydrophilic proteins on glass. 69
Fig. 4-3: Two-step microcontact printing with lines of axon-guiding biomolecules over polylysine-lines with nodes. 71
Fig. 4-4 : Protein thickness of the ECM/PDL 2-step µCP substrates. 73

Fig. 4-5 : Protein thickness of the laminin/PDL 2-step µCP substrates. 76
Fig. 4-6 : Protein thickness of the netrin-1/PDL 2-step µCP substrates. 79
Fig. 4-7: ECM/PDL pattern printed on 7.5 nm SiO_2. 82
Fig. 4-8: Netrin-1/PDL pattern printed on 7.5 nm SiO_2. 83
Fig. 4-9: Laminin/PDL pattern printed on 7.5 nm SiO_2. 83
Fig. 4-10 : Comparison between the averaged protein thickness determined by AFM and ellipsometer. 84
Fig. 4-11: Rat E18 striatal neurons cultured on manual microcontact printing substrates compared to rat E18 striatal neurons cultured on a PECM-grid. 85
Fig. 4-12: Scheme of the new pattern design and SEM- pictures of new structures. 87
Fig. 4-13 : Casting of the stamps for aligned two-step microcontact printing. 88
Fig. 4-14: Structure 1 (PDL, 25 µg/ml) stamped with the Fineplacer over preprinted structure 0 (ECM, 80-120 µg/ml). 89
Fig. 4-15 : Fluorescent images of PLL/ECM (structure 2/0); PLL/laminin (structure 1/0) and PLL/netrin-1 (structure 2/0). 90
Fig. 4-16: Rat E18 cortical neurons DIV 11 cultured on a pattern made of ECM (structure 0) and PDL (structure 3) compared to cortical neurons DIV 10 cultured on a PECM-grid. 91
Fig. 5-1 : Double-staining with anti-MAP2 (neuron-specific, green) and anti-GFAP (glia-specific, red) at DIV 11. 95
Fig. 5-2 : Comparision of striatal and cortical neurons cultured in NB-medium on patterned substrates. 96
Fig. 5-3 : Current-Clamp measurement of a striatal neuron DIV 12 cultured on a PECM-grid. 96
Fig. 5-4: Different commercially available coculture chambers. 98
Fig. 5-5: Coculture chamber made by Flexiperm disc with inserted stainless steel separation in a culture dish (8 cm^2). 99
Fig. 5-6 : Striatal (left side of the cleft) and cortical neurons (right side of the cleft) after removal of the barrier at DIV 3. 100
Fig. 5-7: Seven days after removal of the separation, the cleft between cortical (left) and striatal (right) neurons on unstructured PECM is not visible. 100
Fig. 5-8: Seven days after removal of the separation, the cleft between cortical (right) and striatal (left) neurons on patterned PECM is not visible. 100
Fig. 5-9: Fluorescence images of the microfluidic micropattern (FITC-PECM) after washing the chamber once with destilled water. 102
Fig. 5-10: Rat cortical striatal (left) and cortical (right) E18 neurons at DIV 3 cultivated in the irreversible sealed microfluidic coculture chamber. 105
Fig. 5-11: Rat cortical striatal and cortical E18 neurons at DIV 3 cultivated in the reversible sealed microfluidic coculture chamber. 106
Fig. 5-12: Rat cortical and striatal E18 neurons at DIV 7 cultivated in the reversible sealed microfluidic coculture chamber. 107

Fig. 5-13: Rat striatal (right) and cortical (left) E18 neurons at DIV 7 cultivated in the reversible sealed microfluidic coculture chamber. 107
Fig. 5-14: Striatal and cortical neurons at DIV 10 in the microfluidic coculture chamber. 108
Fig. 5-15: Striatal and cortical neurons at DIV 11 in the microfluidic coculture. 108
Fig. 5-16: Current-clamp measurement of a cortical neuron cultured in a microfluidic coculture chamber for 11 DIV. 109
Fig. 5-17: Synapse between two striatal neurons cultured in the microfluidic coculture for 11 DIV. 110

10.3 List of tables

Tab. 3-1: Concentrations of proteins used for microcontact printing. 38
Tab. 3-2: Primary antibodies. 49
Tab. 3-3: Secondary antibodies. 49
Tab. 3-4: Composition of extra- and intracellular patch solution. 60
Tab. 4-1: Average protein thickness on the ECM/PDL substrates. 74
Tab. 4-2: Average protein thickness on the laminin/PDL substrates. 77
Tab. 4-3: Average protein thickness on the netrin-1/PDL substrates. 80
Tab. 4-4: Electrophysiological characteristics of cortical neurons (DIV 10-12) cultured on PECM-grid-patterns (clamped to –70 mV and at resting potential) and on two-step µCP grids consisting of PDL-ECM (at resting potential). 92
Tab. 5-1: Electrophysiological characteristics of striatal neurons compared to cortical neurons (DIV10-12; both clamped to -70 mV) cultured on PECM-grid-patterns. 97
Tab. 5-2: Calculation of the cell densities/cm² used for the coculture. 104
Tab. 5-3: Electrophysiological characteristics of cortical neurons DIV 10-12 cocultured with striatal neurons compared to cortical neurons DIV 10-12 cultured on PECM-grid-patterns. 110
Tab. 5-4: Electrophysiological characteristics of striatal neurons DIV 10-12 cocultured with cortical neurons compared to striatal neurons DIV 10-12 cultured on PECM-grid-patterns. 110

10.4 List of abbreviations

Ag / AgCl	silver-silverchloride
AMPA	α -amino-3-hydroxy-5-methyl-4-isoxalone proprionic acid
AP	Action potential
APV	2-amino-5-phosphonovaleric acid
ATP	Adenosine triphosphate
CC	current clamp
Ca^{2+}	calcium
C_{fast}	capacitance of the pipette
Cl^-	chloride
C_{slow}	capacitance of the cell
CNQX	6-Cyano-7-nitroquinoxaline-2,3-dione
DIV	days *in vitro*
ECM	extracellular matrix
EGTA	ethylene glycol bis(2-aminoethyl ether)-N,N,N'N'-tetraacetic acid
E_{ion}	Equilibrium potential for an ion species E_i
E_{Na}, E_K, E_{Cl}	Nernst potential for sodium, potassium or chloride
EPSC	excitatory postsynaptic current
EPSP	excitatory postsynaptic potential
F	Faraday constant (96485 C mol−1)
FITC	fluorescein isothiocyanat
GABA	γ-amino butyric acid
g_{Na}, g_K, g_{Cl}	conductance of the membrane for sodium, potassium or chloride
h	inactivation probability for sodium channels
H_2O_2	hydrogen peroxide
H_2SO_4	sulfuric acid
$HBSS^-$	Hanks Balanced Salt Solution without magnesium and calcium
$HBSS^+$	Hanks Balanced Salt Solution with magnesium and calcium
HCl	hydrochloride acid
Hepes	4-(2-hydroxyethyl)-1-piperazineethanesulfonic acid
HH	Hodgkin-Huxley
Hz	Herz
I_{Ca}^{2+}	calcium current
$I_{in(max)}$	maximal inward current
$[Ion]_{in}$	Concentration of ions inside the cell
$[Ion]_{out}$	Concentration of ions outside the cell
I_K^+	potassium current
I_{mem}	current across the membrane
I_{Na}^+	sodium current
$I_{out(sus)}$	sustained outward current
I_{stim}	stimulation current
IPSC	inhibitory postsynaptic current
IPSP	inhibitory postsynaptic potential
k	Boltzmann constant (1.38 × 10−23JK−1)
K^+	potassium
KCl	potassium chloride
KH_2PO_4	potassium di-hydrogene phosphate
KOH	potassium hydroxide
L	length
LTD	long term depression
LTP	long term potentiation
m	activation probability for sodium channels
mA	milliampere
M	molar
µCP	microcontact printing
µm	micrometer
µl	microliter

2-step µCP	Two-step microcontact printing
Mg^{2+}	magnesium
Mg-ATP	magnesium ATP
ms	millisecond
mV	millivolt
n	activation probability of potassium channels
Na^{+}	sodium
Na_2HPO_4	di-sodium hydrogen phosphate
Na-ATP	sodium ATP
NaH_2HPO_4	sodium di-hydrogen phosphate
NaOH	sodium hydroxide
NMDA	N-methyl-D-aspartate
p.a.	pro analysi
PBS	phosphate buffered saline
PDL	poly-D-lysine
PDMS	polydimethylsiloxane
PECM	mixture of poly-D-lysine (10 µg/ml) and ECM-gel (80-120 µg/ml)
PLL	poly-L-lysine
P_K, P_{Na}, P_{Cl}	permeability for potassium, sodium, chloride
R	gas constant (8.31JK−1 mol−1)
R_{ser}	series resistance
SEM	scanning electron microscopy
s	second
T	temperature
t	time
τ	membrane time constant Tau
TRITC	rhodamine isothiocyanat
UV	ultraviolet
V	voltage
VC	voltage clamp
v/v	volume per volume
V_{mem}	membrane potential
V_{rest}	resting membrane potential
V_{stim}	stimulation voltage
W	width
w/v	weight per volume

10.5 Publications

Paper:

Vogt AK, Brewer GJ, Decker T, Böcker-Meffert S, Jacobsen V, Kreiter M, Knoll W, Offenhäusser A (2005). Independence of synaptic specificity from neuritic guidance. *Neuroscience* 134(3): 783-90.

Offenhäusser A, Böcker-Meffert S, Decker T, Helpenstein R, Gasteier P, Groll J, Möller M, Reska A, Schäfer S, Schulte P, Vogt-Eisele A (2007). Microcontact printing of proteins for neuronal cell guidance. *Soft Matter* 3(3): 290-298.

Poster:

Aligned Two-step Microcontact Printing for the Construction of Defined Neuronal Networks
T. Decker, S. Schäfer, S. Schaal, S. Böcker-Meffert and A. Offenhäusser
30th Göttingen Neurobiology Conference; 6th Meeting of the German Neuroscience Society, 16.-18. February 2005 in Göttingen

Aligned Two-step Microcontact Printing for Patterning of Neuronal Guiding Cues on Field Effector Transistor Arrays
T. Decker, S. Schäfer, S. Schaal, S. Böcker-Meffert and A. Offenhäusser
Nanoelectronic Days 2005, 9-11 February 2005 Research Center Juelich (RWTH Aachen in cooperation with research center Jülich)

Microconstruction of Neuronal Networks on Field Effector Transistor Arrays by Aligned Two-step Microcontact Printing
T. Decker, S. Schäfer, S. Schaal, S. Böcker-Meffert and A. Offenhäusser
3rd International Symposium on Sensor Sciences (I3S 2005)
Juelich, Germany, 18-21 July 2005.

Rebuilding natural polarity between cortical and striatal rat neurons in a microfluidic coculture chamber
T. Decker; R. Helpenstein; M. Banzet; S. Böcker-Meffert; A. Offenhäusser
Nanoelectronic Days 2006, 11-13 Oktober 2006 in Aachen (RWTH Aachen in cooperation with research center Jülich).

10.6 Curriculum vitae

PERSÖNLICHE DATEN

TANJA DECKER
geboren am 22.02.1978
in 48291 Telgte, ledig

Kölnstr. 22
52428 Jülich



BERUFLICHE LAUFBAHN

25.11.03 -25.03.08	**PROMOTION** am Forschungszentrum Jülich, Institut für Bio-und Nanosysteme (IBN-2), Leiter und Betreuer der Arbeit: Prof. A. Offenhäusser Thema: Methods to induce polarity in constructed neuronal networks
01.11.03 -25.11.03	Suche nach einer Promotionsstelle
01.11.02-31.10.03	**WISSENSCHAFTLICHE MITARBEITERIN** am Max-Planck-Institut für Vaskuläre Biologie in Münster, Leiter: Prof. Vestweber, Projekt: Interaktion der Phosphokinase Csk mit VE-Cadherin

HOCHSCHULAUSBILDUNG

11.11.2002	**DIPLOM (SEHR GUT)** Angefertigt am Max-Planck-Institut für molekulare Physiologie in Dortmund; Abteilung Strukturelle Biologie (Prof. A. Wittinghofer), Arbeitsgruppe Uhrenproteine (Dr. Eva Wolf), Thema: Biochemische Charakterisierung von Uhrenproteinen
07.10.2002	Diplom-Hauptprüfung (Zoologie 1,3 ; Botanik 1, 7; Biochemie 2,0)
1997 -2002	**STUDIUM** der Biologie an der Westfälischen Wilhelms-Universität Münster

SCHULDATEN

1988 -1997	**ABITUR** am Gymnasium St. Mauritz in Münster-Handorf
1984 -1988	Marienschule in Telgte

10.7 Danksagung

Zuallererst möchte ich meinem Freund und meiner Familie danken:

- Meinem Freund, weil er mich immer zum Lachen bringen kann - und weil er mich so gut bekocht, dass ich anschließend mindestens gefühlte 2 Kilo schwerer bin.
- Meiner Mutter und meiner Schwester für die Shopping-Touren in Köln, die Biokost- und die Schokoladen-Versorgungspakete.
- Meinem Vater, weil er sich trotz stressiger Arbeitswoche immer wieder die Zeit genommen hat, mich samstags für ein paar Stunden zusammen mit den anderen zu besuchen.
- Meinem Bruder für das Harry-Dresden Buch, das schwere Entzugserscheinungen durch Büchermangel verhindert hat.

Ausserdem bedanke ich mich herzlich bei:

- Prof. Offenhäusser für die Bereitstellung des Arbeitsplatzes und das abschliessende Korrekturlesen meiner Doktorarbeit.
- Prof. Wagner für die Übernahme der Betreuung im Fachbereich Biologie an der RWTH Aachen.
- Dr. Simone Meffert für die Betreuung und Korrektur meiner Doktorarbeit.
- Dr. Petra Schulte für Tipps und lange Gespräche über Elektrophysiologie und die optimale Auswertung meiner Ephys.-Daten.
- Rita Helpenstein für die ausgezeichnete Cortex-Zellkultur.

....sowie allen Kolleginnen und Kollegen im IBN-2 für die gute Arbeitsatmosphäre.

Diese Arbeit wurde finanziell von SONY Deutschland gefördert. Besonders danke ich Dr. Yasuda und Dr. Nelles, die das Projekt betreut haben.

Eidesstattliche Erklärung

Hiermit versichere ich, daß ich die vorliegende Dissertation selbstständig und nur unter Verwendung der angegebenen Quellen erstellt habe.

Jülich, den 16.03.08